Advances and Applications of Multiple Scale Methods in Complex Dynamical Systems

Armand Issam Awad

A dissertation
submitted in partial fulfillment of the
requirements for the degree of

Doctor of Philosophy

University of Washington

2017

Reading Committee:

Anshu Narang-Siddarth, Chair

Mehran Mesbahi

Robert O'Malley

Program Authorized to Offer Degree:
Aeronautics & Astronautics

University of Washington

Abstract

Advances and Applications of Multiple Scale Methods in Complex Dynamical Systems

Armand Issam Awad

Chair of the Supervisory Committee:
Assistant Professor Anshu Narang-Siddarth
Aeronautics & Astronautics

High dimensionality, numerical stiffness, and complex subsystem interactions pose fundamental challenges for the design, analysis, and certification of modern aerospace systems. This dissertation addresses these issues by leveraging multiple timescale behaviour to formulate mathematically rigorous reduced-order models that are then used to simplify design, treat numerical stiffness, and provide conditions under which desired behaviour is guaranteed for the original system. The approach is based on concepts of asymptoticity and singular perturbation theory.

First, classical multiple scale methods are generalized to analyze classes of systems that depend on a combination of continuous time and/or discrete clocks. It is shown how discrete clock rates cause multiple timescale behaviour to occur in these systems, and corresponding reduced-order models are developed along with asymptotic error bounds on the resulting approximations.

Next, a new technique is developed for efficiently and accurately propagating the trajectories of satellites that are subject to non-conservative forces such as atmospheric drag and solar radiation pressure. Importantly, the approach gives explicit insight into the effects of parametric uncertainties in these non-conservative forces on the resulting trajectory solution.

Finally, reduced-order design and analysis is investigated for several problems in networked dynamics systems. In particular, conditions are provided under which the dynamics

of the agents can be designed separately from the dynamics of the network process. Further, quantitative bounds are established on the underlying graph topology and on the agents' communication rate that guarantee desirable behaviour when these separately designed dynamics are coupled together.

TABLE OF CONTENTS

LIST OF FIGURES

LIST OF TABLES

ACKNOWLEDGMENTS

I am indebted to the many people who helped me grow as a researcher over the years that I have spent developing this dissertation.

First, I would like to recognize the guidance and support of my advisor, Professor Anshu Narang-Siddarth. She has been an unfailing advocate and mentor, and I would not be where I am now without her. I am grateful as well towards the rest of my supervisory committee for their insight and guidance during the PhD process.

I would like to thank Professor Mehran Mesbahi, Dr. Airlie Chapman, Dr. Eric Schoof, and Dr. Ryan Weisman for their unique perspectives and helpful insights during our various collaborations. Thanks also to everyone in the Advanced Dynamics, Validation, and Control Research Lab. I learned a lot from all of them, and their camaraderie helped make graduate school enjoyable. In particular, I want to thank Dr. Max Spetzler for all of the numerous discussions we've had over the years, and for his countless helpful comments and insights along the way.

Last, but certainly not least, I could not have reached this point without the support of my friends and family. So thanks to my father for his guidance and wisdom in helping me navigate both academia and life. Thanks to my mother for her never-ending optimism and belief in me. And thanks to Abby, whose love has supported me in so many essential ways.

Chapter 1

INTRODUCTION

1.1 Motivating Challenges

Rising levels of complexity in aerospace systems lead to high dimensionality and numerical stiffness, as well as complex interconnections between computer algorithms and the physical components they control. These characteristics pose fundamental challenges to accurately modeling, analyzing, and verifying such systems, and can lead to unmodeled and undesirable behaviour [1]. Analysis methods and approximation techniques are therefore required that can rigorously meet these challenges and give insight into the conditions under which desired behaviour is guaranteed [2].

Consider the problem of propagating satellite trajectories for space situational awareness. In this context, tens of ground-based sensors must keep track of tens of thousands of space objects. Efficient propagation methods that are accurate over known time domains are therefore required to keep custody of these objects in between sensor measurements [3]. However, these objects are acted upon by non-conservative perturbing forces such as atmospheric drag and solar radiation pressure that cause the dynamics to be numerically stiff, making direct numerical approaches infeasible. Further complicating these efforts is the fact that the perturbing forces are subject to parametric uncertainties. While it is known that these perturbation effects manifest on a much slower timescale than the fast two-body motion, the structure of these effects on satellite position and velocity under changes in the perturbing forces remains unclear. A need therefore exists for new trajectory propagation methods that give rigorous insight into these effects so that space objects can be more effectively tracked with only sparse measurements.

Heterogeneous time systems, where evolution of the system states depends on a combination of continuous time and/or discrete clocks, arise naturally in distributed robotics problems. Here, autonomous agents move continuously about their environment while communicating with each other over a network to make decisions. One approach to analyzing these types of complex systems is to assume that the agents' network communication occurs very quickly, leading to a purely continuous-time set of dynamics [4]. However, designs based on this continuous behaviour can break down as the time between communication updates becomes too large, leading to instability [5, 6]. An alternative approach is then to view the updates over the network as occurring only intermittently, producing an inherently hybrid-time character in the dynamics. Intuitively, if the robots move quickly relative to the slow discrete updates over the network, then the robots will reach their goal and the network dynamics will evolve as if the robots are always at their state dependent equilibrium. This implies a decoupling between the continuous-time robot dynamics and the discrete-time network dynamics that is based on the different characteristic timescales over which the subsystems evolve. Such a separation between the subsystem dynamics is useful because it decreases the complexity of analyzing the composite system by allowing the formulation of reduced-order models based on the isolated subsystems. However, current approaches do not give the necessary mathematical rigour on what conditions are required for such a separation to hold nor on what behaviour is induced by coupling two subsystems with different time dependencies.

In both the orbit propagation problem and the networked robotics problem, the evolution of the system states occurs in both slow and fast layers. This *multiple timescale* behaviour appears in many natural and engineering applications. In physical chemistry, for example, reactions can oscillate around a chemical equilibrium for long period of time before quickly transitioning to a different equilibrium [7]. Another example is hierarchical control schemes, where reference commands change much slower than the fast tracking dynamics [8]. A third example occurs in power grids, where fast dynamics occur within densely connected areas while slow dynamics occur between sparsely connected regions [9].

Concepts from singular perturbation theory provide an effective approach for dealing with such multiple timescale systems [10]. Singular perturbation theory, discussed in Chapter 2, allows mathematically rigorous and uniformly valid approximate solutions to be found for complex differential equations and difference equations. The approximate solutions are simpler to find than exact solutions because they are based on solutions to reduced order models that describe the system's behaviour over individual timescales, applying mathematical rigour to the intuitive notion of timescale separation. These reduced order models can be used for analysis, estimation, and control, while aiding in the search for conditions where higher-order dynamics can no longer be ignored [11]. However, the characteristic of heterogeneous time dependency places this class of systems outside the current body of singular perturbation theory. A need therefore exists to extend multi-scale methods to systems that depend on a combination of continuous time and/or discrete clocks, and to apply singular perturbation approaches to problems in orbit propagation and networked dynamical systems.

1.2 Summary of Contributions

This dissertation addresses the challenges discussed above, and provides the following contributions.

In Chapter 3, a new mathematical framework is developed for reduced-order modeling of systems where multiple timescales arise due to heterogeneous time dependency. In particular, this approach provides the necessary qualitative and quantitative insight for heterogeneous time systems by: 1) demonstrating how timescales manifest in these complex systems and how they are related to discrete clock rates; and 2) generalizing asymptotic techniques for reduced-order modeling, and in particular multi-scale methods, to these systems. With this generalized multiple timescale framework in place, the developed approach is then applied to two particular classes of heterogeneous-time systems. The first is a class of discrete-time systems whose evolution depends on multiple discrete-time clocks with different update rates. The second is a class of hybrid-time systems which evolve continuously in between impulsive

updates that are governed by a discrete-time clock. In both cases, the singularly perturbed structure of the problem is made clear, reduced-order models are found, and corresponding asymptotic error bounds are proven to be correct in terms of the discrete clock rates.

A new orbit propagation technique is developed in Chapter 4 for propagating the trajectories of satellites subject to non-conservative perturbing forces. Based on the classical method of multiple scales, the resulting trajectory approximations have known error properties that are dependent on the nominal parameters of the perturbation. Unlike other approaches, this method of multiple scales approach is shown to give direct insight into the trajectory's sensitivity to different perturbation parameters. These tools allow direct insight into how parametric uncertainty affect a satellite's trajectory and are expected to be particularly useful for the specific problem of object tracking and catalog maintenance.

Chapter 5 examines interactions across multiple timescales that occur in networked dynamic systems. Three scenarios are explored: 1) a state-dependent graph problem where fast consensus dynamics are paired with slowly-varying edge weights; 2) a continuous-communication consensus tracking problem where slowly-evolving consensus dynamics are tracked by fast agents; and 3) an intermittent-communication consensus tracking problem where the agents can only communicate over the network intermittently to reach consensus. For each scenario, singular perturbation theory is first used to develop mathematically rigorous reduced-order models based on the timescale separation that naturally arises between the network layer and the agent layer. Stability properties of these reduced-order models are then used to establish quantitative bounds on the underlying graph topology and on the communication rate which guarantee stability of the full system. These bounds provide verification tools which are necessary for certification of these complex networked systems.

Chapter 2

BACKGROUND ON SINGULAR PERTURBATION THEORY

Timescales exist in many systems, but in certain systems these timescales induce singular perturbations in the dynamics of the system [12]. In particular, these systems are called singularly perturbed when the presence of a small parasitic parameter changes the order of the system. Multiple timescale methods based on asymptotics and singular perturbation theory were first applied to flight dynamics by Ashley [13], while Lagerstrom and Kevorkian used these approaches in the area of orbital mechanics to find patched conics solutions to the planar restricted three-body problem [14].

The importance of multiple timescale methods is emphasized by two main advantages. The first advantage is that these approaches allow reduced-order equations to be formed, aiding in the design of simple control laws that are amenable to implementation on embedded hardware. The second advantage is that, importantly, the solutions obtained using these simplifications come with *a priori* asymptotic bounds on their error.

2.1 Asymptotics and Singularly Perturbed Problems

Often, systems contain a small parasitic parameter ε, known as the *perturbation parameter.* The presence of this perturbation can complicate system analysis, for example by changing the system's dynamic order or by adding non-linearities. In this case questions arise about when it is permissible to ignore the presence of the perturbation and deal with only the simplified problem, and how the presence of the perturbation changes the behaviour of the solution.

Asymptotic analysis addresses these questions by examining the limiting behaviour of functions as the perturbation parameter approaches a particular value. In this document,

the perturbation parameter will usually (though not always) be denoted by ε, and the limiting value will often be taken to be zero. A basic idea in asymptotic analysis is whether or not a particular function is negligible with respect to another function in this limit. The Landau asymptotic order relationships formalize this notion as follows (see [15, Chapter 1] for a detailed discussion).

Definition 2.1. A function $a(t;\varepsilon)$ is said to be asymptotically smaller than, or "small-Oh" of, a function $b(t;\varepsilon)$ in the limit of $\varepsilon \to \delta$ if over a given domain D_t

$$\lim_{\varepsilon \to \delta} \frac{a(t;\varepsilon)}{b(t;\varepsilon)} = 0$$

for all $t \in D_t$. This relationship is then denoted by $a(t;\varepsilon) = o(b(t;\varepsilon))$.

A simple example of this "small-Oh" relationship is given by the functions $a(t;\varepsilon) = \varepsilon$ and $b(t;\varepsilon) = 1$ in the limit of $\varepsilon \to 0^+$. Then $\varepsilon = o(1)$ holds because

$$\begin{aligned} \lim_{\varepsilon \to 0^+} \frac{a(t;\varepsilon)}{b(t;\varepsilon)} &= \lim_{\varepsilon \to 0^+} \frac{\varepsilon}{1} \\ &= 0 \end{aligned}$$

for all t.

Definition 2.2. Over a given domain D_t, a function $a(t;\varepsilon)$ is said to be of the same order as, or "big-Oh" of, a function $b(t;\varepsilon)$ in the limit of $\varepsilon \to \delta$ if

$$\lim_{\varepsilon \to \delta} \frac{a(t;\varepsilon)}{b(t;\varepsilon)} = k$$

for some $k \in (0, \infty)$ and all $t \in D_t$. This relationship is then denoted by $a(t;\varepsilon) = \mathcal{O}(b(t;\varepsilon))$.

As an illustration of the "big-Oh" relationship, consider $a(t;\varepsilon) = 1 + t$ and $b(t;\varepsilon) = \frac{3}{1+\varepsilon}$ in the limit of $\varepsilon \to 0^+$. Over a fixed and finite domain for t, $D_t = \{t \in \mathbb{R} \,|\, 0 \leq t \leq T\}$, then

$$\begin{aligned} \lim_{\varepsilon \to 0^+} \frac{a(t;\varepsilon)}{b(t;\varepsilon)} &= \lim_{\varepsilon \to 0^+} \frac{1+t}{\frac{3}{1+\varepsilon}} \\ &= \frac{1+t}{3}, \end{aligned}$$

and thus $1+t=\mathcal{O}(\frac{3}{1+\varepsilon})$ over this domain. However, over larger domains this relationship does *not* hold. If $t=1/\varepsilon$, for example, then

$$\begin{aligned}\lim_{\varepsilon\to 0^+}\frac{a(1/\varepsilon;\varepsilon)}{b(1/\varepsilon;\varepsilon)} &= \lim_{\varepsilon\to 0^+}\frac{1+1/\varepsilon}{\frac{3}{1+\varepsilon}}\\ &= \infty\end{aligned}$$

so that $1+t\neq\mathcal{O}(\frac{3}{1+\varepsilon})$. As this example shows, the domain of interest is integral to whether or not a particular asymptotic relationship holds.

Definition 2.3. Over a given domain D_t, a function $a(t;\varepsilon)$ is said to be asymptotically equivalent to a function $b(t;\varepsilon)$ in the limit of $\varepsilon\to\delta$ if

$$\lim_{\varepsilon\to\delta}\frac{a(t;\varepsilon)}{b(t;\varepsilon)}=1$$

for all $t\in D_t$. This relationship is then denoted by $a(t;\varepsilon)\sim b(t;\varepsilon)$.

The notion of asymptotic equivalence is essential to defining a simpler approximation to a complex function when the perturbation parameter is close to its limiting value. For example, $a(t;\varepsilon)=\cos t$ is asymptotically equivalent to $b(t;\varepsilon)=\{1+\ln(1+\varepsilon)\}\cos t$ in the limit of $\varepsilon\to 0^+$ for all t because

$$\lim_{\varepsilon\to 0^+}\frac{\cos t}{\{1+\ln(1+\varepsilon)\}\cos t}=1.$$

Therefore, the simpler $a(t;\varepsilon)$ can be taken as a uniformly valid approximation to $b(t;\varepsilon)$ in the limit of $\varepsilon\to 0^+$. Of course, such an approximation is not unique (*e.g.,* the function $c(t;\varepsilon)=\cos(t+\varepsilon^3)$ is also asymptotically equivalent to $b(t;\varepsilon)$).

To obtain simple approximations for a perturbed dynamical system, it is therefore natural to seek a solution $x_\varepsilon(t;\varepsilon)$, dependent on the time t as well as perturbation parameter ε, in the form of an *asymptotic series expansion*

$$x_\varepsilon(t;\varepsilon)=\sum_i a_i\left(t;\varepsilon\right), \tag{2.1}$$

where $a_i(t;\varepsilon)=o\left(a_{i-1}(t;\varepsilon)\right)$. Such a form is attractive because it means that higher-order terms in (2.1) are well-behaved for small enough ε and do not dominate the overall solution.

If such an expansion is separable for all t in the domain of interest so that

$$a_i(t;\varepsilon) = \delta_i(\varepsilon)\alpha_i(t)$$

for $\alpha_i = \mathcal{O}(1)$, it is called *regularly perturbed*. In this case the perturbation may be ignored for small enough values of ε. Otherwise, the problem is called *singularly perturbed*. This means that, in the limit of ε approaching zero, any uniformly valid approximation over the given domain must incorporate effects of the perturbation parameter. While these perturbation-dependent effects may manifest in many different forms, two of the most common are the *boundary layer* type singularity and the *secular* type singularity. Systems that exhibit these singularities, and approaches to finding uniformly valid approximations for them, are examined in the following sections.

2.2 Boundary Layer Singularities and Standard Form

Boundary layer singularities have historically been very important in the analysis and control of dynamical systems [12]. This type of singularity is especially apparent in the class of dynamic systems given by

$$\begin{aligned} \dot{x}(t) &= f\left(t, x(t), z(t); \varepsilon\right) \\ \varepsilon\dot{z}(t) &= g(t, x(t), z(t); \varepsilon), \end{aligned} \tag{2.2}$$

where $x(t) \in D_x \subset \mathbb{R}^{n_x}$ and $z(t) \in D_z \subset \mathbb{R}^{n_z}$, and subject to the initial conditions $x(0) = x_0$ and $z(0) = z_0$. A system of this type is said to be in *standard singularly perturbed form* [10] if

1. The vector fields are bounded and continuously differentiable in their arguments.

2. Each root $z(t) = h_i\left(t, x(t)\right)$ of the algebraic equation $0 = g(t, x(t), z(t); 0)$, found by setting $\varepsilon = 0$ in (2.2), are isolated.

The states x are then called the *slow states* and z the *fast states*. These conditions ensure that intuitive reduced-order dynamics, the *Reduced Slow System* and *Reduced Fast System*, are well-defined.

To illustrate how a singularity arises in this class of problem, first assume a solution in the form

$$\begin{aligned} x(t) &= \sum_{i\geq 0} \varepsilon^i x^{(i)}(t) \\ z(t) &= \sum_{i\geq 0} \varepsilon^i z^{(i)}(t). \end{aligned}$$

Substituting the assumed form of the solution into (2.2) and equating orders of ε then yields the zeroth order equation

$$\begin{aligned} \dot{x}^{(0)}(t) &= f\left(t, x^{(0)}(t), z^{(0)}(t); 0\right) \\ 0 &= g(t, x^{(0)}(t), z^{(0)}(t); 0), \end{aligned}$$

subject to $x^{(0)}(0) = x_0$. This implies that the fast state $z^{(0)}$ is always at one of the isolated roots $z^{(0)}(t) = h\left(t, x^{(0)}(t)\right)$ of the algebraic equation $0 = g(t, x^{(0)}(t), z^{(0)}(t); 0)$. Substituting this state-dependent equilibrium trajectory into the equation for $\dot{x}^{(0)}$ then gives the Reduced Slow System as

$$\dot{x}^{(0)}(t) = f\left(t, x^{(0)}(t), h\left(t, x^{(0)}(t)\right); 0\right). \tag{2.3}$$

These reduced-order dynamics describe the behaviour of the slow states $x^{(0)}$ as if the fast states $z^{(0)}$ are always at their state-dependent equilibrium $h\left(t, x^{(0)}(t)\right)$. By doing so, however, this reduced-order model ignores the initial conditions and behaviour of $z^{(0)}$ as these states evolve towards the equilibrium trajectory, and is therefore valid for $t = \mathcal{O}(1)$ but not for $t = \mathcal{O}(\varepsilon)$. Intuitively, then, singularities in boundary layer-type problems are seen to occur because any separable asymptotic expansion must ignore some of the initial conditions. However, progress can still be made in finding a uniformly valid solution.

To obtain a set of reduced-order dynamics that accounts for the fast z behaviour, instead

rewrite the original dynamics (2.2) in terms of a scaled time $\tau = t/\varepsilon$ as

$$\begin{aligned} x'(\tau) &= \varepsilon f\left(\varepsilon\tau, x(\tau), z(\tau); \varepsilon\right) \\ z'(\tau) &= g(\varepsilon\tau, x(\tau), z(\tau); \varepsilon), \end{aligned}$$

where the prime denotes the derivative with respect to τ. Again, assume a solution of the form

$$\begin{aligned} x(\tau) &= \sum_{i\geq 0} \varepsilon^i x^{(i)}(\tau) \\ z(\tau) &= \sum_{i\geq 0} \varepsilon^i z^{(i)}(\tau) \end{aligned}$$

in the rescaled dynamics and equate orders of ε in the result. The zeroth-order equation then defines the Reduced Fast Model as

$$\begin{aligned} x^{(0)\prime}(\tau) &= 0 \\ z^{(0)\prime}(\tau) &= g(0, x^{(0)}(\tau), z^{(0)}(\tau); 0), \end{aligned} \tag{2.4}$$

subject to $z^{(0)}(0) = z_0$ and $x^{(0)}(0) = x_0$. This model describes the evolution of the fast states $z^{(0)}$ over a stretched timescale for which the slow states $x^{(0)}$ are constant, but breaks down when $\tau = \mathcal{O}(1/\varepsilon)$.

While individually neither (2.3) nor (2.4) are valid approximations of the original dynamics (2.2) over the whole time domain, together they provide the possibility of such an approximation. The validity of these *combined* reduced-order models to the full dynamics are described by Tikonov-Levinson theory, which yields mathematical rigor and justifies the use of these reduced-order models in analysis and controller design.

Theorem 2.1. *[10, Theorem 2.1] Consider the standard singularly perturbed system defined by (2.2), and assume that:*

1. *The functions f and g are continuous in open sets D_x and D_z of the variables x and z, respectively.*

2. *There is a root* $z^{(0)}(t) = h\left(t, x^{(0)}(t)\right)$ *of the algebraic equation*

$$0 = g(t, x^{(0)}(t), z^{(0)}(t); 0)$$

which is isolated in the domain D_x.

3. *For all* $x^{(0)} \in D_x$, *the isolated root* $z^{(0)}(t) = h\left(t, x^{(0)}(t)\right)$ *is the asymptotically stable equilibrium point of the boundary-layer equation*

$$z^{(0)\prime} = g(t, x^{(0)}, z^{(0)}; 0)$$

in which $x^{(0)}$ *and* t *are fixed parameters.*

4. *The region of influence of the asymptotic equilibrium point* $z^{(0)}(t) = h\left(t, x^{(0)}(t)\right)$ *in the boundary-layer equation includes the initial values.*

Then, for any finite T *there exists an* $\varepsilon_0 > 0$ *such that, for* $0 < \varepsilon < \varepsilon_0$, *the approximations given by the Reduced Slow System (2.3) and the Reduced Fast System (2.4) satisfy*

$$\begin{aligned} x(t) &= x^{(0)}(t) + \mathcal{O}(\epsilon) \\ z(t) &= z^{(0)}(t/\epsilon) + \mathcal{O}(\epsilon) \end{aligned}$$

for all $t \in [0, T]$. *Further, there exists a* $t_1 > 0$ *such that the approximation*

$$z(t) = h\left(t, x^{(0)}(t)\right) + \mathcal{O}(\epsilon)$$

holds for $t \in [t_1, T]$.

Importantly, higher order approximations can also be found for boundary layer singularity dynamics such as (2.2) using *the method of composite asymptotic expansions* [15, 16]. In particular, this approach constructs higher-order expansions valid for $\tau = \mathcal{O}(1)$ and $t = \mathcal{O}(1)$ and that each satisfy a relevant subset of the initial conditions. The individual asymptotic expansions can then be matched to form a composite asymptotic expansion that meets all of

the initial conditions and that is uniformly valid on bounded t intervals. In this context then, Theorem 2.1 certifies that these zeroth order regular expansions, described by the Reduced Slow and Reduced Fast systems, together form an asymptotically valid approximation if the reduced dynamics satisfy the relevant conditions. These results can also be extended analogously for nested, multi-layer systems [10, Chapter 2].

Given the powerful results for systems in standard form, there has been a significant focus on formulating problems in this way. For example, non-dimensionalization has been used to identify the perturbation parameter in aerospace systems [12]. Work has also been done on finding coordinate transforms that yield a system in standard form [17, 18]. Unfortunately, this involves solving partial differential equations in the general case which can make the coordinate transform approach intractable. The results for standard form systems in continuous-time have also been analogously formulated for discrete-time systems with similar structure [19, 20].

To this point in time, the majority of singular perturbation theory has focused on either strictly continuous-time or strictly (single-clock) discrete-time systems. However, practical control systems are often dependent on a mix of possibly multiple discrete clocks and/or continuous-time components. These heterogenous-time systems are a subset of hybrid systems [21], for which there has recently been significant interest. Much of the focus in this area has been on certifying stability of hybrid systems, and the work on singularly perturbed hybrid systems has mirrored this interest. Of particular note is the extension of Tikonov-Levinson theory to singularly perturbed hybrid systems [22] of the form

$$\left.\begin{aligned} \dot{z} &= \psi\left(z, y; \varepsilon\right) \\ \varepsilon\dot{y} &= f\left(z, y; \varepsilon\right) \end{aligned}\right\} \quad (z, y) \in C \times \Psi$$
$$\left.(z, y)^{+} \in G(z, y)\right\} \quad (z, y) \in D \times \Psi, \tag{2.5}$$

where Ψ must be a compact set and the notation $(z, y)^{+} \in G(z, y),\ (z, y) \in D \times \Psi$ means a discrete jump to a point in the set $G(z, y)$ when (z, y) is in the set $D \times \Psi$. Results are given in terms of an averaged hybrid system, and the closeness of solutions to the full system to

solutions of the averaged system. Conditions are also given under which global asymptotic stability of the averaged system implies semi-global practical asymptotic stability of the full system. Singularly perturbed impulsive differential equations have been investigated where the continuous-time subsystem is assumed to be exponentially stable and the discrete updates occur at fixed times [23, 24]. There has also been some work that focuses on the limit of very fast discrete updates [4, 25]. In this regime, hybrid systems are approximated by continuous-time systems in an approach called *dehybridization*. Timescale separation due to slow discrete updates has only been applied conceptually to particular systems and classes of systems, for example in creating a hybrid-time control for certain under-actuated systems where purely continuous-time control approaches cannot yield controllability [26, 27]. However, a more systematic approach has not been formulated that yields insight into the role of the discrete clock rates and that can give higher-order approximations.

2.3 Secular Singularities and the Method of Multiple Scales (MMS)

Secular singularities arise when trying to find asymptotic approximations valid over a long time domain to systems with small disturbances [28, 16]. Intuitively, such singularities occur because the effects of a small disturbance can build up to have non-negligible effects over sufficient time. A simple example illustrates the issue.

Example 2.1. Consider the Duffing oscillator described by

$$\ddot{x} + x = \varepsilon x^3, \tag{2.6}$$

and search for a solution in the form of the asymptotic series

$$x(t) = \sum_{i \geq 0} \varepsilon^i x^{(i)}(t). \tag{2.7}$$

Substituting the expansion (2.7) into the dynamics (2.6) and equating powers of ε yields ordered dynamic equations that must be satisfied. The zeroth order equation describes a

simple harmonic oscillator and has the solution

$$x^{(0)}(t) = a_0 \cos(t + b_0), \tag{2.8}$$

with a_0 and b_0 constants that satisfy the initial values. Using (2.8), the first order equation is then written as

$$\ddot{x}^{(1)} + x^{(1)} = \frac{a_0^3}{4}\left\{3\cos(t+b_0) + \cos(3(t+b_0))\right\}, \tag{2.9}$$

subject to the initial conditions $x^{(1)}(0) = \dot{x}^{(1)}(0) = 0$. The first order solution is therefore

$$x^{(1)}(t) = a_1 \cos(t + b_1) - \frac{1}{32}a_0 \cos(t + b_0) + \frac{3}{8}a_0 t \sin(t + b_0), \tag{2.10}$$

where a_1 and b_1 are constants that satisfy the initial conditions. The solution, however, is only valid for $t = \mathcal{O}(1)$. This is because when $t = \mathcal{O}(\varepsilon^{-1})$,

$$\begin{aligned}
\lim_{\varepsilon\to 0} \frac{\varepsilon x^{(1)}(\varepsilon^{-1})}{x^{(0)}(\varepsilon^{-1})} &= \lim_{\varepsilon\to 0} \frac{\varepsilon\left\{a_1\cos(\varepsilon^{-1}+b_1) - \frac{1}{32}a_0\cos(\varepsilon^{-1}+b_0) + \frac{3}{8}a_0 t\sin(\varepsilon^{-1}+b_0)\right\}}{a_0\cos(\varepsilon^{-1}+b_0)} \\
&= \lim_{\varepsilon\to 0} \frac{\frac{3}{8}a_0\sin(\varepsilon^{-1}+b_0)}{a_0\cos(\varepsilon^{-1}+b_0)} \\
&\neq 0.
\end{aligned}$$

Therefore the validity of the asymptotic series expansion (2.7) breaks down on long time spans due to the term $\frac{3}{8}a_0 t\sin(t+b_0)$ in the first order solution (2.10) which grows unbounded with time. This is an example of what is called a *secular* term in the literature, and occurs due to resonant forcing in the first order equation (2.9) acting over time of order $1/\varepsilon$.

More generally, secular singularities often occur when seeking approximations over large time domains for systems of the form

$$\begin{aligned}
\dot{r} &= \varepsilon f(r,\theta,t) \\
\dot{\theta} &= w(r) + \varepsilon g(r,\theta,t),
\end{aligned}$$

where both r and θ can be vector-valued. Many techniques have been developed to deal with such secular problems, such as averaging, renormalization, amplitude equations, and

multiple scales, and which may be asymptotically equivalent. A good comparison of these approaches may be found, for example, in [29]. While these techniques all have their benefits and drawbacks, only the method of multiple scales (MMS) will be described in detail here. In simplest form, MMS explicitly searches for a solution that is allowed to evolve not only on the usual fast time but also on a slow time where a small disturbance can have non-negligible effects. By assuming a form that is dependent on multiple independent parameters, an approximation can then be found that satisfies both the dynamics and the asymptotic validity of successive terms in the approximation. MMS is appealing due to its intuitive interpretation as well as its additional applicability to both boundary layer type problems and singularly perturbed partial differential equations [28]. The method is now demonstrated on the Duffing oscillator.

Example 2.2. To find a solution valid on a larger domain (longer period of time), search for a solution in a two-time series

$$x(t) = \sum_{i \geq 0} \varepsilon^i x^{(i)}(\eta, \tau), \tag{2.11}$$

where the fast time, $\eta = t$, and the slow time, $\tau = \varepsilon t$, are considered to be independent. The first derivative is then expanded as

$$\begin{aligned} \dot{x}^{(i)} &= \frac{\partial x^{(i)}}{\partial \eta}\frac{d\eta}{dt} + \frac{\partial x^{(i)}}{\partial \tau}\frac{\partial \tau}{\partial t} \\ &= \frac{\partial x^{(i)}}{\partial \eta} + \varepsilon \frac{\partial x^{(i)}}{\partial \tau}, \end{aligned}$$

and the second derivative as

$$\begin{aligned} \ddot{x}^{(i)} &= \frac{d}{dt}\left(\dot{x}^{(i)}\right) \\ &= \frac{\partial}{\partial \eta}\left(\dot{x}^{(i)}\right)\frac{d\eta}{dt} + \frac{\partial}{\partial \tau}\left(\dot{x}^{(i)}\right)\frac{\partial \tau}{\partial t} \\ &= \frac{\partial^2 x^{(i)}}{\partial \eta^2} + \varepsilon 2\frac{\partial^2 x^{(i)}}{\partial \eta \partial \tau} + \varepsilon^2 \frac{\partial^2 x^{(i)}}{\partial \tau^2}. \end{aligned}$$

Substituting (2.11) into the dynamics (2.6) and equating powers of ε yields the ordered

dynamic equations. The zeroth order equation is

$$\frac{\partial^2 x^{(0)}}{\partial \eta^2} + x^{(0)} = 0,$$

the solution to which is again the simple harmonic oscillator

$$x^{(0)} = a_0(\tau)\cos(\eta + b_0(\tau)). \tag{2.12}$$

where now a_0 and b_0 are (as yet unspecified) functions of the slow time, τ, and must satisfy the initial conditions when $\tau = 0$. The first order equation is

$$\frac{\partial^2 x^{(1)}}{\partial \eta^2} + 2\frac{\partial^2 x^{(0)}}{\partial \eta \partial \tau} + x^{(1)} = x^{(0)^3}.$$

Using (2.12), this equation is then rewritten as

$$\frac{\partial^2 x^{(1)}}{\partial \eta^2} + x^{(1)} = \left\{\frac{3a_0^3}{4} + 2a_0\frac{\partial b_0}{\partial \tau}\right\}\cos(\eta + b_0) + \frac{a_0^3}{4}\cos(3(\eta + b_0)) + 2\frac{\partial a_0}{\partial \tau}\sin(\eta + b_0),$$

where the dependence of a_0, b_0 on τ has been made implicit. To avoid the resonant forcing that caused non-uniformity in (2.10), set

$$\frac{\partial a_0}{\partial \tau} = 0; \text{ and } \frac{3a_0^3}{4} + 2a_0\frac{\partial b_0}{\partial \tau} = 0.$$

This choice of the parameters a_0 and b_0 is called the Fredholm alternative, which is a solvability condition for the corresponding differential equations. In this case, the corresponding solutions are

$$a_0(\tau) = a_0(0) \tag{2.13}$$

and

$$b_0(\tau) = b_0(0) - \frac{3a_0^2(0)}{8}\tau. \tag{2.14}$$

Therefore, the full zeroth order solution is found as

$$x^{(0)}(\eta, \tau) = a_0(0)\cos\left(\eta + b_0(0) - \frac{3a_0^2(0)}{8}\tau\right);$$

it can be written in terms of t as

$$x^{(0)}(t) = a_0(0)\cos\left(\left(1 - \varepsilon\frac{3a_0^2(0)}{8}\right)t + b_0(0)\right). \tag{2.15}$$

By construction, the zeroth order solution (2.15) is now valid for time up to order $1/\varepsilon$; by introducing an even slower time $\varepsilon^2 t$, one may obtain an approximation valid for $t = \mathcal{O}(1/\varepsilon)$.

Such secular singularities can also arise in discrete-time systems, and several approaches to formulating a discrete-time MMS are documented in the literature. Denote the fast timescale by $m = k$ and the slow timescale by $s = \varepsilon k$, where k is the discrete-time update counter. In the Taylor expansion approach initially proposed in [30], the forward time-shift operator is Taylor-expanded in the slow timescale as

$$x(k+1) = x(m+1,\, s) + \varepsilon \frac{\partial x}{\partial s}\bigg|_{(m+1,s)} + \mathcal{O}(\varepsilon^2).$$

The resulting mixed difference-differential equations are then solved to maintain asymptoticity of the assumed series solution as in the continuous-time MMS. Alternatively, in [31] the authors instead propose a partial difference operator approach where the total difference operator $\triangle$ is expanded in the independent timescales as

$$\triangle x(k) = \triangle_m x(m,s) + \varepsilon \triangle_s x(m,s), \tag{2.16}$$

and where

$$\begin{aligned} \triangle x(k) &= x(k+1) - x(k) \\ \triangle_m x(m,s) &= x(m+1,s) - x(m,s) \\ \triangle_s x(m,s) &= x(m,s+\varepsilon) - x(m,s). \end{aligned}$$

The resulting partial difference equations are then solved, as usual, to maintain asymptoticity of the assumed series solution. A more rigorous version of this partial difference operator approach is proposed in [32, 33, 34]. Using a multi-dimensional lattice interpretation of the independent timescales, indexing forward in the absolute time k is interpreted as cumulative forward hops along each of the timescale axes. For two timescales, the total difference operator is therefore expanded as

$$\triangle x(k) = \triangle_m x(m,s) + \triangle_s x(m,s) + \triangle_k \triangle_s x(m,s).$$

However, it should be noted that an additional assumption that $\triangle_m x = \mathcal{O}(1)$ and $\triangle_s x = \mathcal{O}(\varepsilon)$ must be explicitly made. Further, using more than two timescales in this approach leads to an accumulation of higher-order coupling terms (analogous to the $\triangle_k \triangle_s$ term in the two-term expansion) that must be dealt with when solving the resulting ordered equations.

Chapter 3

GENERALIZED MULTI-SCALE METHOD

This chapter proposes a new framework for multi-scale analysis. As documented in Chapter 2, differential calculus-based tools like the chain rule are an integral part of classical multi-scale methods for asymptotic analysis. However, it has not been clear to this point how extend these tools to analyze heterogeneous time dynamics, which evolve based on a mix of differential and difference equations with different clock rates. To this end, this chapter proposes using the the time scales calculus, a mathematical framework which unifies and extends the differential and finite-difference calculi, to generalize multi-scale methods to heterogeneous time systems. By doing so, it is shown how multiple timescale dynamics arise in these systems due to discrete clock rates and how this behaviour can be exploited to develop mathematically rigorous reduced-order models.

The structure of the chapter, which is based in part on the author's work [35], is as follows. Section 3.1 provides some background on the time scales calculus. Next, Section 3.2 describes the generic multi-scale approach and demonstrates through several examples how this framework results in classical results for both purely continuous-time dynamics and purely single-rate, discrete-time dynamics. Finally, the generalized multi-scale analysis is applied to two classes of systems. The first class, in Section 3.3, are discrete, multirate systems whose evolution depends on multiple discrete-time clocks with different update rates. The second class, in Section 3.4, are hybrid-time systems which involve both continuous-time evolution as well as impulsive updates that are governed by a discrete-time clock. In both cases, the singularly perturbed structure of the problem is made clear, reduced-order models are found, and corresponding asymptotic error bounds are proven in terms of the discrete clock rates.

3.1 Time Scales Calculus Preliminaries

Both continuous-time and discrete-time dynamic systems are generally well understood. Continuous-time systems are governed by differential equations and analyzed using differential calculus. Likewise, discrete-time systems are governed by finite-difference equations and are studied using finite-difference calculus. The intriguing similarities and differences between continuous-time and discrete-time equations motivates the desire for a unified framework for analyzing these dynamical systems. The time scales calculus, first proposed in [36], provides such a framework by unifying and extending the differential and finite-difference calculi.

Note. This use of the term "time scale" is different from the concept of "timescales" discussed in Chapter 2 and elsewhere in this dissertation. To prevent confusion, the term "time scale" as used in this chapter refers to the time scales calculus and will be denoted by $\mathbb{T}$, *e.g.,* the $\mathbb{T}$ calculus.

In this context, a *time scale* $\mathbb{T}$ is a (non-empty) closed subset of $\mathbb{R}$. So choosing $\mathbb{T} = \mathbb{R}$ leads to differential calculus results, while choosing $\mathbb{T} = \mathbb{Z}$ leads to finite-difference calculus results. However, $\mathbb{T}$ can also be chosen as in Figure 3.1. In the $\mathbb{T}$ calculus, many of the properties (such as differentiability) have to do with the behaviour of the particular $\mathbb{T}$ at the point of interest t. In particular, the concept of *graininess* becomes important, where the graininess function $\mu : \mathbb{T} \to [0, \infty)$ at t is defined as

$$\mu(t) = \sigma(t) - t,$$

and $\sigma : \mathbb{T} \to \mathbb{T}$ is the *forward jump operator* at t defined as

$$\sigma(t) = \inf \left\{ v \in \mathbb{T} \,\middle|\, v > t \right\}.$$

The *delta derivative* of a function $f : \mathbb{T} \to \mathbb{R}$ at $t \in \mathbb{T}^\kappa$, where $\mathbb{T}^\kappa = \mathbb{T} \backslash \{M\}$ if $\mathbb{T}$ has a left-scattered maximum M and $\mathbb{T}^\kappa = \mathbb{T}$ otherwise, may then be defined as

$$\frac{df}{\Delta t}(t) = \lim_{s \to t,\, s \neq \sigma(t)} \frac{f(\sigma(t)) - f(s)}{\sigma(t) - s}.$$

This delta derivative behaves like the classical derivative when $\mathbb{T} = \mathbb{R}$, *i.e.,*

$$\frac{df}{\Delta t} = \frac{df}{dt},$$

and like the classical finite-difference operator when $\mathbb{T} = \mathbb{Z}$, *i.e.,*

$$\frac{df}{\Delta t} = \triangle f(t).$$

For the analogoulsy defined backwards jump operator ρ, a *nabla derivative* is similarly defined.

Figure 3.1: An arbitrary $\mathbb{T}$

More recently, the $\mathbb{T}$ calculus has been expanded to consider multiple variables in [37, 38]. For a function $f : \mathbb{T}_1 \times \cdots \times \mathbb{T}_n \to \mathbb{R}$ and $t = \{t_1, \ldots, t_n\} \in \mathbb{T}_1^\kappa \times \cdots \times \mathbb{T}_n^\kappa$, the *partial delta derivative* of f with respect to $t_i \in \mathbb{T}_i^\kappa$ is defined as

$$\frac{\partial f}{\Delta t_i}(t) = \lim_{s \to t_i,\, s \neq \sigma_i(t_i)} \frac{f\left(t_1, \ldots, t_{i-1}, \sigma_i(t_i), t_{i+1}, \ldots, t_n\right) - \left(t_1, \ldots, t_{i-1}, s, t_{i+1}, \ldots, t_n\right)}{\sigma_i(t_i) - s}.$$

A chain rule and the corresponding total derivative for functions dependent on two $\mathbb{T}$s was also first proposed in [37]. In [39], [40], and [38] these ideas were extended to functions defined on n $\mathbb{T}$s in different ways. The main difference concerns the differentiability assumptions made when defining the total derivative; that is, the approaches differ in where they assume you can hop in a multi-dimensional $\mathbb{T}$ lattice. These differences are inconsequential for functions on $\mathbb{T}$s with zero graininess (*e.g.,* $\mathbb{R}$, $38\mathbb{R}$, $\exp(\mathbb{R})$, etc.) and yield the usual chain rule and total derivative from the differential calculus. For functions on purely discrete $\mathbb{T}$s (that is, with $\mu_i(t_i) > 0$ for all t_i), however, different results are possible based on where a function is partially delta-differentiable. A new expansion for discrete $\mathbb{T}$s is now therefore proposed which expands the total delta derivative sequentialy over each $\mathbb{T}$, and is particularly useful for approaches such as MMS.

Theorem 3.1. *If $f : \mathbb{T}_1 \times \cdots \times \mathbb{T}_n \to \mathbb{R}$ is partially delta-differentiable at $\{t_1, t_2, \ldots, t_n\}$, $\{\sigma_1(t_1), t_2, \ldots, t_n\}$, $\{\sigma_1(t_1), \sigma_2(t_2), t_3 \ldots, t_n\}$, ..., $\{\sigma_1(t_1), \ldots, \sigma_n(t_n)\}$, and if each $\mathbb{T}_i$ is a discrete time scale so that $\sigma_i(t_i) \neq t_i$ for all $t_i \in \mathbb{T}_i$, then the total delta derivative is*

$$\frac{df}{\Delta t}(t) = \sum_{i=1}^{n} \frac{\partial f}{\Delta t_i}(\sigma_1(t_1), \ldots, \sigma_{i-1}(t_{i-1}), t_i, t_{i+1}, \ldots, t_n)\, \mu_i(t_i)$$

where $\mu_i(t_i) = \sigma_i(t_i) - t_i$ is the graininess of the ith time scale at the point t_i.

Proof. Expand the total derivative as

$$\begin{aligned}
\frac{df}{\Delta t}(t_1, \ldots, t_n) &= f(\sigma_1(t_1), \ldots, \sigma_n(t_n)) - f(t_1, \ldots, t_n) \\
&= [f(\sigma_1(t_1), \ldots, \sigma_n(t_n)) - f(\sigma_n(t_1), \ldots, \sigma_{n-1}(t_{n-1}), t_n)] \\
&\quad + [f(\sigma_n(t_1), \ldots, \sigma_{n-1}(t_{n-1}), t_n) - f(\sigma_n(t_1), \ldots, \sigma_{n-2}(t_{n-2}), t_{n-1}, t_n)] \\
&\quad + \cdots + [f(\sigma_1(t_1), t_2, \ldots, t_{n-1}, t_n) - f(t_1, \ldots, t_n)].
\end{aligned}$$

Now, since f is partial delta-differentiable at $(t_1, t_2, \ldots, t_n)$, $(\sigma_1(t_1), t_2, \ldots, t_n)$, $(\sigma_1(t_1), \sigma_2(t_2), t_3 \ldots, t_n)$, ..., $(\sigma_1(t_1), \ldots, \sigma_n(t_n))$, and since each $\mathbb{T}_i$ is a discrete time scale, then

$$\begin{aligned}
&f(\sigma_1(t_1), \ldots, \sigma_{i-1}(t_{i-1}), \sigma_i(t_i), t_{i+1}, \ldots, t_n) \\
&\quad - f(\sigma_1(t_1), \ldots, \sigma_{i-1}(t_{i-1}), t_i, t_{i+1}, \ldots, t_n) \\
&\qquad = \frac{\partial f}{\Delta t_i}(\sigma_1(t_1), \ldots, \sigma_{i-1}(t_{i-1}), t_i, t_{i+1}, \ldots, t_n)\, \mu_i(t_i)
\end{aligned}$$

holds for each i. Therefore,

$$\begin{aligned}
\triangle f(t_1, \ldots, t_n) &= \frac{\partial f}{\Delta t_n}(\sigma_n(t_1), \ldots, \sigma_{n-2}(t_{n-2}), \sigma_{n-1}(t_{n-1}), t_n)\, \mu_n(t_n) \\
&\quad + \frac{\partial f}{\Delta t_{n-1}}(\sigma_n(t_1), \ldots, \sigma_{n-2}(t_{n-2}), t_{n-1}, t_n)\, \mu_{n-1}(t_{n-1}) \\
&\quad + \cdots + \frac{\partial f}{\Delta t_1}(t_1, \ldots, t_{n-2}, t_{n-1}, t_n)\, \mu_1(t_1) \\
&= \sum_{i=1}^{n} \frac{\partial f}{\Delta t_i}(\sigma_1(t_1), \ldots, \sigma_{i-1}(t_{i-1}), t_i, t_{i+1}, \ldots, t_n)\, \mu_i(t_i)
\end{aligned}$$

as claimed. □

With some of the ideas of calculus in place, dynamic equations can be investigated. For example, consider the first order, linear, initial value problem

$$\frac{dy}{\Delta t} = p(t)y,\ y(0) = y_0,$$

defined on some $\mathbb{T}$. This has a unique solution given by

$$y(t) = e_p(t, t_0)y_0,$$

where $e_p(t, s)$ is called the *generalized exponential function* and has many of the familiar properties of the exponential function. It should also be noted that this solution hold under a technical assumption on $p(t)$ called *regressivity*, which in the scalar case is equivalent to the condition $\mu(t)p(t) \neq -1$. Now consider the special case $p(t) = \alpha$. Then if $\mathbb{T} = \mathbb{R}$ the solution is

$$y(t) = e^{\alpha(t-t_0)}y_0,$$

while for $\mathbb{T} = h\mathbb{Z}$ with $h \in \mathbb{R}$ the solution is

$$y(t) = (1 + \alpha h)^{(t-t_0)/h}\, y_0.$$

Thus, the $\mathbb{T}$ dynamics provides a unified way of approaching dynamic systems. More information may be found in a reference such as [41].

As understanding of the $\mathbb{T}$ calculus has matured, the framework has recently been applied to a variety of dynamical systems. For instance, in [42] a class of hybrid systems where the continuous dynamics switch at discrete intervals was posed in terms of $\mathbb{T}$, and sufficient conditions for practical stability in terms of a comparison principle were given. When these switched dynamics are linear, Lyapunov's second (direct) method was developed in [43] in terms of $\mathbb{T}$. For linear impulsive dynamic systems, on the other hand, the analysis in [44] presented the dynamics in a $\mathbb{T}$ framework and explored solution properties, including state transition matrices and notions of stability.

3.2 Description of the Method

With the background on the $\mathbb{T}$ calculus in place, the generalized multi-scale analysis method can now be described. Given a set of dynamics involving some combination of differential equations and difference equations, the approach is as follows.

Step 1: Identify the relevant base $\mathbb{T}$s for the problem, noting that there will be several if the system is described by a combination of differential and difference equations or if different difference equations depend on their own discrete clocks. For instance, a differential equation gives rise to dependence on $\mathbb{T} = \mathbb{R}$ while a difference equation that updates every 7 seconds gives rise to dependence on $\mathbb{T} = 7\mathbb{Z}$.

Step 2: Rewrite the differential and discrete dynamic equations in terms of the corresponding delta derivatives as dynamic equations on $\mathbb{T}$s. Any discrete update rates now show up explicitly in the dynamics and can be used as the perturbation parameter if desired.

Step 3: Assume a series solution that is dependent on appropriately scaled fast and slow versions of the relevant timescales. The set of fast timescales will be assumed to be independent of the set of slow timescales. For example, assume $x(t) = x_f(\eta) + x_s(\tau)$ or $x(t) = x(\eta, \tau)$ where $\eta = t \in \mathbb{T}$ and $\tau = \varepsilon t \in \mathbb{T}$.

Step 4: Expand each delta derivative of a base $\mathbb{T}$ in its scaled versions using the chain rule for the calculus on $\mathbb{T}$s. For example, with $x(t) = x(\eta, \tau)$, and η and τ defined as above the total derivative is

$$\frac{dx}{\Delta t}(t) = \frac{\partial x}{\Delta \eta}(\eta, \tau) + \varepsilon \frac{\partial x}{\Delta \tau}(\sigma(\eta), \tau),$$

where σ is the appropriate forward jump operator.

Step 5: Substitute assumed expressions into the $\mathbb{T}$ dynamics and equate orders of the perturbation parameter to find the ordered dynamic equations on $\mathbb{T}$s.

Step 6: Sequentially solve the ordered equations to ensure that the resulting approximation is asymptotic and uniform for all t in the desired domain.

The following example shows how this generalized multi-scale approach is consistent with classical results in the purely continuous-time case.

Example 3.1. Consider the continuous-time dynamics given by the differential equation

$$\begin{aligned} \dot{x}(t) &= f\left(t, x(t), z(t); \varepsilon\right) \\ \varepsilon \dot{z}(t) &= g(t, x(t), z(t); \varepsilon) \end{aligned} \tag{3.1}$$

and subject to the initial conditions $x(0) = x_0$ and $z(0) = z_0$. These dynamics evolve on $\mathbb{T} = \mathbb{R}$, so (3.1) can be equivalently written as the $\mathbb{T}$ dynamics

$$\begin{aligned} \frac{dx}{\Delta t} &= f\left(t, x, z; \varepsilon\right) \\ \varepsilon \frac{dz}{\Delta t} &= g(t, x, z; \varepsilon). \end{aligned} \tag{3.2}$$

Assume solutions in the form of a composite asymptotic expansion

$$\begin{aligned} x(t;\varepsilon) &= \sum_{i \geq 0} \varepsilon^i \left\{ x_f^{(i)}(\eta) + x_s^{(i)}(\tau) \right\} \\ z(t;\varepsilon) &= \sum_{i \geq 0} \varepsilon^i \left\{ z_f^{(i)}(\eta) + z_s^{(i)}(\tau) \right\}, \end{aligned} \tag{3.3}$$

where $\eta = t/\varepsilon \in \mathbb{T}/\varepsilon$ is the fast time and $\tau = t \in \mathbb{T}$ is the slow time. The delta derivative is then expanded as

$$\frac{dx^{(i)}}{\Delta t}(t) = \frac{1}{\varepsilon} \frac{\partial x_f^{(i)}}{\Delta \eta}(\eta) + \frac{\partial x_s^{(i)}}{\Delta \tau}(\tau),$$

and similarly for $z^{(i)}$. Substituting into the original $\mathbb{T}$ dynamics (3.2) yields

$$\begin{aligned} \sum_{i \geq 0} \varepsilon^i \left\{ \frac{1}{\varepsilon} \frac{\partial x_f^{(i)}}{\Delta \eta} + \frac{\partial x_s^{(i)}}{\Delta \tau} \right\} &= f\left(\tau, \sum_{i \geq 0} \varepsilon^i \left\{ x_f^{(i)} + x_s^{(i)} \right\}, \sum_{i \geq 0} \varepsilon^i \left\{ z_f^{(i)} + z_s^{(i)} \right\}; \varepsilon \right) \\ \sum_{i \geq 0} \varepsilon^i \left\{ \frac{\partial z_f^{(i)}}{\Delta \eta} + \varepsilon \frac{\partial z_s^{(i)}}{\Delta \tau} \right\} &= g\left(\tau, \sum_{i \geq 0} \varepsilon^i \left\{ x_f^{(i)} + x_s^{(i)} \right\}, \sum_{i \geq 0} \varepsilon^i \left\{ z_f^{(i)} + z_s^{(i)} \right\}; \varepsilon \right). \end{aligned} \tag{3.4}$$

The slow dynamics should satisfy the original dynamics, so enforce

$$\begin{aligned}\sum_{i\geq 0}\varepsilon^i\frac{\partial x_s^{(i)}}{\Delta\tau} &= f\left(\tau,\sum_{i\geq 0}\varepsilon^i x_s^{(i)},\sum_{i\geq 0}\varepsilon^i z_s^{(i)};\varepsilon\right)\\ \varepsilon\sum_{i\geq 0}\varepsilon^i\frac{\partial z_s^{(i)}}{\Delta\tau} &= g\left(\tau,\sum_{i\geq 0}\varepsilon^i x_s^{(i)},\sum_{i\geq 0}\varepsilon^i z_s^{(i)};\varepsilon\right).\end{aligned} \tag{3.5}$$

The fast dynamics are then written from (3.4) and (3.5) as

$$\begin{aligned}\sum_{i\geq 0}\varepsilon^i\frac{\partial x_f^{(i)}}{\Delta\eta} &= \varepsilon f\left(\tau,\sum_{i\geq 0}\varepsilon^i\left\{x_f^{(i)}+x_s^{(i)}\right\},\sum_{i\geq 0}\varepsilon^i\left\{z_f^{(i)}+z_s^{(i)}\right\};\varepsilon\right)-\varepsilon f\left(\tau,\sum_{i\geq 0}\varepsilon^i x_s^{(i)},\sum_{i\geq 0}\varepsilon^i z_s^{(i)};\varepsilon\right)\\ \sum_{i\geq 0}\varepsilon^i\frac{\partial z_f^{(i)}}{\Delta\eta} &= g\left(\tau,\sum_{i\geq 0}\varepsilon^i\left\{x_f^{(i)}+x_s^{(i)}\right\},\sum_{i\geq 0}\varepsilon^i\left\{z_f^{(i)}+z_s^{(i)}\right\};\varepsilon\right)-g\left(\tau,\sum_{i\geq 0}\varepsilon^i x_s^{(i)},\sum_{i\geq 0}\varepsilon^i z_s^{(i)};\varepsilon\right).\end{aligned} \tag{3.6}$$

Equating orders of ε then gives the zeroth order slow equation

$$\begin{aligned}\frac{\partial x_s^{(0)}}{\Delta\tau} &= f\left(\tau,x_s^{(0)},z_s^{(0)};0\right)\\ 0 &= g\left(\tau,x_s^{(i)},z_s^{(i)};0\right)\end{aligned} \tag{3.7}$$

and the zeroth order fast equation

$$\begin{aligned}\frac{\partial x_f^{(0)}}{\Delta\eta} &= 0\\ \frac{\partial z_f^{(0)}}{\Delta\eta} &= g\left(\tau,x_f^{(0)}+x_s^{(0)},z_f^{(0)}+z_s^{(0)};0\right)-g\left(\tau,x_s^{(0)},z_s^{(0)};0\right),\end{aligned} \tag{3.8}$$

subject to the initial conditions $x_s^{(0)}(0)+x_f^{(0)}(0)=x_0$ and $z_s^{(0)}(0)+z_f^{(0)}(0)=x_0$. The ansatz (3.3) and its corresponding reduced-order models (3.7) and (3.8) are those found by using the classical method of composite expansions approach (*e.g.,* [45, Chapter 4]), and are solved identically.

The generalized multi-scale approach can also be applied in a straightforward manner to singularly perturbed discrete-time systems, as the next example shows.

Example 3.2. Consider the discrete-time dynamics given by the difference equation

$$\begin{aligned} x(k+1) &= x(k) + \varepsilon f(x(k), z(k)) \\ z(k+1) &= z(k) + g(x(k), z(k)), \end{aligned} \tag{3.9}$$

where $k \in \mathbb{Z}$ is the discrete-time index. These dynamics evolve on $\mathbb{T} = \mathbb{Z}$, so (3.9) can be equivalently written as the $\mathbb{T}$ dynamics

$$\begin{aligned} \frac{dx}{\Delta k} &= \varepsilon f(x, z; \varepsilon) \\ \frac{dx}{\Delta k} &= g(x, z; \varepsilon), \end{aligned} \tag{3.10}$$

since $\mu(k) = 1$ for $k \in \mathbb{Z}$. Assume solutions of the form

$$\begin{aligned} x(t;\varepsilon) &= \sum_{i \geq 0} \varepsilon^i x^{(i)}(\eta, \tau) \\ z(t;\varepsilon) &= \sum_{i \geq 0} \varepsilon^i z^{(i)}(\eta, \tau), \end{aligned}$$

where the fast time, $\eta = k \in \mathbb{T}$, and the slow time, $\tau = \varepsilon k \in \varepsilon\mathbb{T}$, are assumed to be independent. The delta derivative is then expanded as

$$\begin{aligned} \frac{dx}{\Delta t}(k) &= \frac{\partial x}{\Delta \eta}(\eta, \tau) + \varepsilon \frac{\partial x}{\Delta \tau}(\sigma(\eta), \tau) \\ &= \frac{\partial x}{\Delta \eta}(\eta, \tau) + \varepsilon \frac{\partial x}{\Delta \tau}(\eta + 1, \tau) \end{aligned}$$

and similarly for z. Substituting into (3.10) yields

$$\begin{aligned} \sum_{i \geq 0} \varepsilon^i \left\{ \frac{\partial x^{(i)}}{\Delta \eta}(\eta, \tau) + \varepsilon \frac{\partial x^{(i)}}{\Delta \tau}(\eta + 1, \tau) \right\} &= \varepsilon f \left(\sum_{i \geq 0} \varepsilon^i x^{(i)}(\eta, \tau), \sum_{i \geq 0} \varepsilon^i z^{(i)}(\eta, \tau); \varepsilon \right) \\ \sum_{i \geq 0} \varepsilon^i \left\{ \frac{\partial z^{(i)}}{\Delta \eta}(\eta, \tau) + \varepsilon \frac{\partial z^{(i)}}{\Delta \tau}(\eta + 1, \tau) \right\} &= g \left(\sum_{i \geq 0} \varepsilon^i x^{(i)}(\eta, \tau), \sum_{i \geq 0} \varepsilon^i z^{(i)}(\eta, \tau); \varepsilon \right). \end{aligned}$$

Equating orders of ε then gives the zeroth order equation

$$\begin{aligned} \frac{\partial x^{(0)}}{\Delta \eta}(\eta, \tau) &= 0 \\ \frac{\partial z^{(0)}}{\Delta \eta}(\eta, \tau) &= g\left(x^{(0)}(\eta, \tau), z^{(0)}(\eta, \tau); 0 \right), \end{aligned} \tag{3.11}$$

and the first order equation

$$\frac{\partial x^{(1)}}{\Delta\eta}(\eta,\tau)+\frac{\partial x^{(0)}}{\Delta\tau}(\eta+1,\tau)=f\left(x^{(0)}(\eta,\tau),z^{(0)}(\eta,\tau);0\right)$$
$$\frac{\partial z^{(1)}}{\Delta\eta}(\eta,\tau)+\frac{\partial z^{(0)}}{\Delta\tau}(\eta+1,\tau)=\left.\frac{\partial g}{\partial\varepsilon}\right|_{x^{(0)},z^{(0)}}+\left.\frac{\partial g}{\partial x}\right|_{x^{(0)},z^{(0)}}x^{(1)}+\left.\frac{\partial g}{\partial z}\right|_{x^{(0)},z^{(0)}}z^{(1)}. \tag{3.12}$$

The approach outlined here is functionally similar to the discrete-time MMS approach outlined in [31] as well as the partial difference operator approach proposed in [32, 33, 34], except that the expansion of the discrete-time difference is rigorously justified here by the $\mathbb{T}$ calculus and simplifies the analysis by not leading to an accumulation of higher-order cross-coupling partial derivative terms as described in Chapter 2. The resulting reduced-order solutions, specialized to linear f and g, are also asymptotically equivalent to those developed for discrete-time linear systems in [19].

These examples have shown how the generalized multi-scale approach agrees with the classical approaches for both continuous-time as well as discrete-time systems. Again, this should be expected since it is based on the $\mathbb{T}$ calculus which unifies the differential and finite-difference calculi. With the general technique now established, the following sections show how this method can be applied to analyze a wider set of dynamical systems with multi-scale behaviour.

3.3 Analysis of Discrete, Multirate Systems

This section investigates the multiple timescale behaviour that can occur due to coupling between two discrete-time subsystems with different update rates. Understanding the behaviour of multirate systems is essential to ensure reliability of the complex systems that naturally arise during the integration of individual discrete-time subsystems. Important applications of multirate systems include: (i) identifying time constraints for run time assurance of complex cyber physical systems [46]; (ii) accommodating for both digitally implemented controllers as well as digital structural mode filters implemented at faster update frequencies for the Space Shuttle Orbiter autopilot [47]; and (iii) safely combining the high frequency

stability augmentation and low frequency gain-scheduling on a digital fly-by-wire system [48]. A fundamental design variable in many of these systems is the clock speed of an individual subsystem. Therefore, a natural question when the subsystems are designed separately is how close the behaviour of the composite system will be to the individual subsystem behaviours, as well as how changes in the clock rates will effect this behaviour. However, analyzing the behaviour of multirate systems with different update rates is particularly challenging due to a lack of adequate techniques [1].

Analysis techniques for multirate systems have traditionally focused on the system's behaviour around a particular set of subsystem update rates. The main challenge for typical frequency-domain based stability criteria is that they require numerical methods such as the Nyquist criterion for studying the effect of the individual clock periods on the overall system [49, 50]. This limit arises because the characteristic equation cannot be obtained in closed-form for general multirate systems. Consequently, repeated numerical computation of the Nyquist plot is required for each combination of subsystem frequencies. Alternatively, time-domain based stability criteria of multirate systems approximately describe the system's behaviour through construction of state transition matrices over different sub-intervals [51, 52, 53, 54]. Current results, however, only study the stability effects of small differences in a particular set of update rates without a way to analyze the role of significantly changing update rates. This challenge is overcome by applying the generalized multi-scale analysis proposed in this chapter.

3.3.1 General Case

Consider the dynamics

$$\begin{aligned} x^+ &= f(x,z), & t &= t_{k_1} \\ z^+ &= g(x,z), & t &= t_{k_2} \end{aligned} \tag{3.13}$$

for $x \in D_x \subseteq \mathbb{R}^{n_x}$ and $z \in D_z \subseteq \mathbb{R}^{n_z}$ subject to the initial conditions $x(0) = x_0 \in D_x$ and $z(0) = z_0 \in D_z$, and where $t_{k_i} \in k_i\mathbb{Z}$ with corresponding update periods $k_i \in \mathbb{R}^+$. It will be

assumed that the vector fields f and g are Lipschitz and that g has a Lipschitz derivative in its second argument for $x \in D_x$ and $z \in D_z$. Without loss of generality, let $k_1 \geq k_2$ so that the x state does not update more often than the z states. The choice of the update periods directly effects the event sequences of the dynamics; for example, Figure 3.2 shows a sequence of updates of the x and z subsystems when $k_1 = 5$ and $k_2 = 2$. Different sets of update periods can therefore lead to very different responses of the system. This section examines the multiscale behaviour that arises in (3.13) as the update periods become separated.

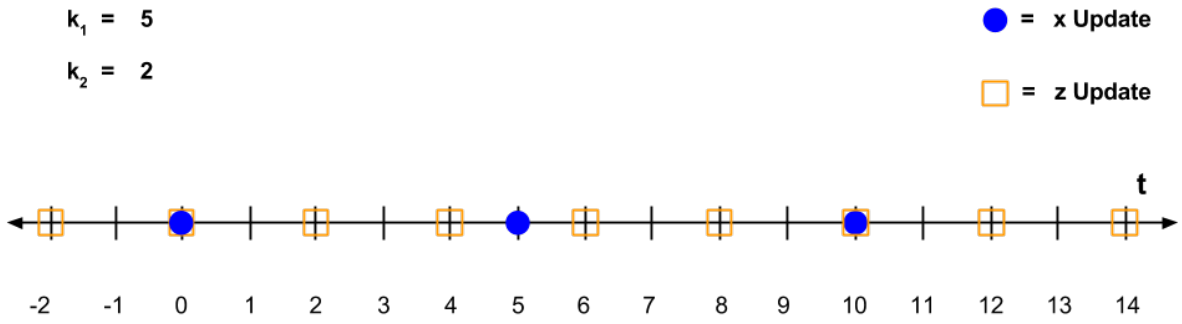

Figure 3.2: Event sequences in a discrete, multirate system

3.3.1.1 Asymptotic Analysis

To analyze the discrete, multirate dynamics (3.13), begin by noting that there are two base $\mathbb{T}$s for this problem: $\mathbb{T}_1 = k_1\mathbb{Z}$ and $\mathbb{T}_2 = k_2\mathbb{Z}$. Rewriting (3.13) in terms of the corresponding delta derivatives then leads to the $\mathbb{T}$ dynamics

$$\begin{aligned} \frac{\partial x}{\Delta t_{k_1}} &= \frac{1}{k_1}\left\{f(x,z) - x\right\} \\ \frac{\partial z}{\Delta t_{k_1}} &= \frac{1}{k_2}\left\{g(x,z) - z\right\}, \end{aligned}$$

since $\mu_1 = k_1$ and $\mu_2 = k_2$. Now, define $\kappa = k_1/k_2$ as the multirate system's update ratio so that the the update periods of the x and z subsystems become separated as κ grows larger. The dynamics are then equivalently written as

$$\begin{aligned}\frac{\partial x}{\Delta t_{k_1}} &= \frac{1}{k_1}\left\{f(x,z) - x\right\} \\ \frac{1}{\kappa}\frac{\partial z}{\Delta t_{k_2}} &= \frac{1}{k_1}\left\{g(x,z) - z\right\}.\end{aligned}$$

Setting $k_1 = 1$ for simplicity and without loss of generality then yields

$$\begin{aligned}\frac{\partial x}{\Delta t_{k_1}} &= f(x,z) - x \\ \frac{1}{\kappa}\frac{\partial z}{\Delta t_{k_2}} &= g(x,z) - z\end{aligned} \tag{3.14}$$

in standard singular perturbation form.

Now, begin by assuming a straightforward asymptotic series solution in the limit of $\kappa \to \infty$ and expanding x and z as

$$\begin{aligned}x(t_{k_1}, t_{k_2}) &= \sum_{i\geq 0} \kappa^{-i} x^{(i)}(t_{k_1}, t_{k_2}) \\ z(t_{k_1}, t_{k_2}) &= \sum_{i\geq 0} \kappa^{-i} z^{(i)}(t_{k_1}, t_{k_2}).\end{aligned} \tag{3.15}$$

Substituting (3.15) in (3.14) and equating orders of κ then leads to the zeroth order problem

$$\begin{aligned}\frac{\partial x^{(0)}}{\Delta t_{k_1}} &= f(x^{(0)}, z^{(0)}) - x^{(0)} \\ 0 &= g(x^{(0)}, z^{(0)}) - z^{(0)}.\end{aligned} \tag{3.16}$$

These dynamics assumes that $z^{(0)}$ is always at an $x^{(0)}$-dependent equilibrium value that satisfies the algebraic equation $0 = g(x^{(0)}, z^{(0)}) - z^{(0)}$, ignoring the $z^{(0)}$ initial conditions. This implies that there is a boundary layer degeneracy if the $z^{(0)}$ subsystem is separately stable.

To obtain a different model that retains the initial $z^{(0)}$ behaviour, rescale the original dynamics (3.14) in terms of $\eta_{k_i} = \kappa t_{k_i}$ so that the delta derivatives are rewritten as

$$\frac{\partial}{\Delta t_{k_i}} = \kappa \frac{\partial}{\Delta \eta_{k_i}},$$

and (3.14) becomes

$$\begin{aligned}\frac{\partial x}{\Delta\eta_{k_1}} &= \frac{1}{\kappa}\left\{f(x,z)-x\right\}\\ \frac{\partial z}{\Delta\eta_{k_2}} &= g(x,z)-z.\end{aligned} \tag{3.17}$$

Assuming an asymptotic series solution based on the rescaled times

$$\begin{aligned}x(t_{k_1},t_{k_2}) &= \sum_{i\geq 0}\kappa^{-i}x^{(i)}(\eta_{k_1},\eta_{k_2})\\ z(t_{k_1},t_{k_2}) &= \sum_{i\geq 0}\kappa^{-i}z^{(i)}(\eta_{k_1},\eta_{k_2})\end{aligned}$$

in (3.17) and equating orders of κ then yields the new zeroth order dynamics

$$\begin{aligned}\frac{\partial x^{(0)}}{\Delta\eta_{k_1}} &= 0\\ \frac{\partial z^{(0)}}{\Delta\eta_{k_2}} &= g(x^{(0)},z^{(0)})-z^{(0)}.\end{aligned} \tag{3.18}$$

These new dynamics describes the fast z behaviour over a stretched timescale for which x is fixed; that is, the z behaviour in-between the slow x updates.

Similarly to the continuous-time boundary layer singularities described in Chapter 2, neither (3.16) nor (3.18) individually provides a uniformly valid approximation over the entire time domain. Based on these investigations, however, such an approximation can be found by combining these models and is formalized as follows.

Multirate Outer System Define the equilibrium trajectory of the isolated z dynamics as a known function $h:\ D_x \to D_z$ which satisfies the algebraic equation $0 = g(p,h(p))-h(p)$ for $p \in D_x$. The outer system is then defined as

$$x^{(0)}(\sigma_1(t_{k_1})) = f\left(x^{(0)}(t_{k_1}), h(x^{(0)}(t_{k_1}))\right), \tag{3.19}$$

subject to $x^{(0)}(0) = x_0$.

Multirate Inner System Define each interval between x updates as $\mathcal{I}(t_{k_1}) \triangleq \left\{ t \in \mathbb{R} \,\middle|\, t_{k_1} \leq t < \sigma(t_{k_1}) \right\}$. The inner system is then defined separately for each interval as

$$z^{(0)}(\sigma_2(t_{k_2})) = g\left(x^{(0)}(t_{k_1}), z^{(0)}(t_{k_2})\right), \tag{3.20}$$

subject to $z^{(0)}(0) = z_0$ for the first interval and $z^{(0)}(t_{k_1}) = h\left(x^{(0)}(\rho(t_{k_1}))\right)$ otherwise, where ρ is the backwards jump operator and $x^{(0)}$ is the state vector of the decision system defined in (3.19).

The outer system (3.19) describes the reduced-order behaviour of the isolated x dynamics with the z dynamics always at their state-dependent equilibrium. The inner system (3.20) then describes the evolution of the more frequent z dynamics between each set of consecutive x updates. The initial conditions for the inner system are based on the state vector $x^{(0)}$ of the outer system alone. They are independent of the state of the inner system on any previous intervals. While the original dynamics are fully coupled, the reduced-order models (3.19) and (3.20) obtain their triangular structure by exploiting the equilibrium trajectory $h(x^{(0)})$.

Together, (3.19) and (3.20) provide reduced-order descriptions of the original dynamics (3.85). They mirror the classical Reduced Fast and Reduced Slow models for continuous-time dynamics in standard singularly perturbed form described in Section 2.2. The validity of these models is investigated next.

3.3.1.2 Bounds on the Reduced-Order Approximation

In this subsection, asymptotic bounds are proven for the reduced-order models (3.16) and (3.18) developed in the previous subsection. The analysis consists of two parts. In the first part, bounds are proven for the quickly updating z state between updates of the x state assuming certain assumptions hold for the initial conditions. The second part then uses these bounds on z to find corresponding bounds for the evolution of x.

As Figure 3.2 shows, there is not necessarily a consistent number of updates of the fast z subsystem between the less frequent updates of the x subsystem. It is therefore necessary to

understand these sequences to be able to understand the trajectories of z and x. To simplify the analysis, decompose the general, complex sequence of updates into simple sequences where the ith simple sequence has κ_i updates of the fast subsystem for every update of the slow subsystem. To do so, define a *building block sub-sequence* as the sequence of updates that begins with an update of x and ends the instant before the next update of x. The ith building block sequences has an *update ratio* κ_i, which is the number of z updates in the sequence, and a *phase* ϕ_i, which is defined as the time from the initial x update until the first z update. Furthermore, if $\phi_i = 0$ then the ith sub-sequence is said to be *synchronous*. Otherwise, the sub-sequence is *asynchronous*. This concept is illustrated in Figure 3.3.

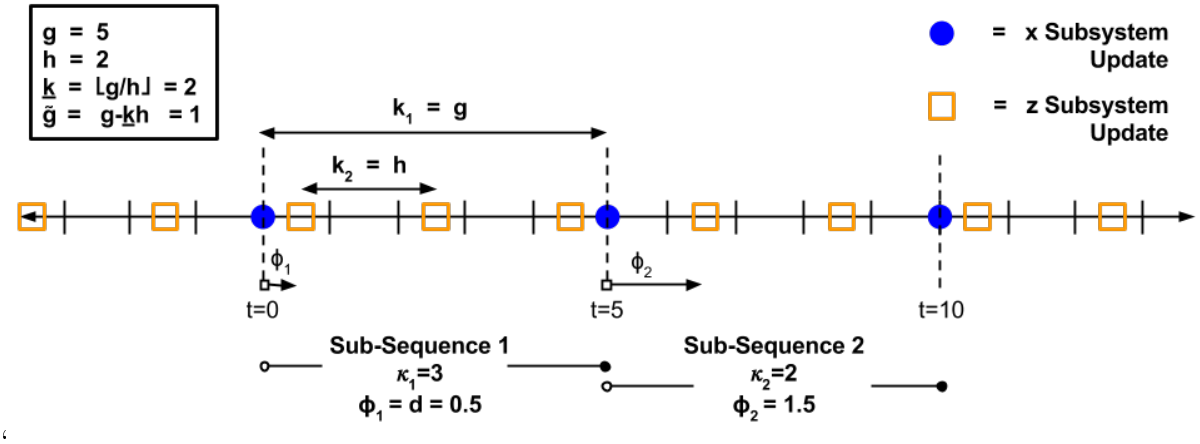

Figure 3.3: Decomposition of a multirate system into building block sub-sequences when $k_1 = 5$ and $k_2 = 2$.

In order to relate the behaviour of the multirate system to the properties of the building block sequence systems, knowledge of the range of building block update ratios, κ_i, is necessary. The following proposition captures this information.

Proposition 3.1. *For a multirate system decomposed into building block sub-sequences, define* $\underline{k} = \lfloor k_1/k_2 \rfloor$ *with* $\lfloor k_1/k_2 \rfloor$ *the integer value of* k_1/k_2. *Then the update ratios* κ_i *only take on the values* $\underline{k}$ *or* $\underline{k}+1$.

Proof. For any given building block sub-sequence, by definition there are k_1 seconds within the interval and the first update occurs at time ϕ_i. There are at least $\underline{k}$ updates of z in this interval so that the $\underline{k}$th occurs at time $\phi_i + (\underline{k}-1)k_2$. Now, if $\phi_i > k_1 - \underline{k}k_2$ then the $(\underline{k}+1)$st update will occur after the end of the interval. But, if $\phi_i < k_1 - \underline{k}k_2$ then the $(\underline{k}+1)$st update occurs at time $\phi_i + \underline{k}k_2 < k_1 - \underline{k}k_2 + \underline{k}k_2 = k_1$ which is within the interval. □

When the update periods k_1 and k_2 form a rational ratio, that is $k_1/k_2 = g/h$ with $g, h \in \mathbb{N}$, the multirate system is said to be *periodic.* This is because the sequence of subsystem updates, and thus the sequence of building block sub-sequences, eventually repeat themselves. In this case, more can be said about the structure of the building block sequences, and in particular how frequently each value of κ_i will appear.

Theorem 3.2. *For a periodic, multirate system where $k_1/k_2 = g/h$ with $g, h \in \mathbb{N}$, define $\underline{k} = \lfloor g/h \rfloor$ and $\tilde{g} = g - \underline{k}h$. Further, define d for $d \in \mathbb{R}$ with $0 \leq d < h$ as an initial offset of the subsystem updates. Then, if $d \in \{0, 1, 2, \ldots, h-1\}$, the system can be decomposed into one synchronous sequence with $\kappa_i = \underline{k}+1$, $\tilde{g}-1$ asynchronous sequences with $\kappa_i = \underline{k}+1$, and $h - \tilde{g}$ asynchronous sequences with update ratio $\underline{k}$. Otherwise, the system can be decomposed into $\tilde{g}$ asynchronous sequences with $\kappa_i = \underline{k}+1$, and $h-\tilde{g}$ asynchronous sequences with update ratio $\underline{k}$.*

Proof. The proof begins by constructing the sequence of phases, $\{\phi_i\}$,of the building block sequences from the update ratio of the original system. The building block sequences are then partitioned into distinct congruence classes based on their phase, with known frequency of occurrence. Finally, an explicit relationship is derived between the congruence class and the corresponding update ratio of the building block sequences in that class, completing the proof.

To begin, some definitions are beneficial. For $k_1/k_2 = g/h$ with $g > h$ and g and h

relatively prime, define $\underline{k} = \lfloor g/h \rfloor$ and $\tilde{g} = g - \underline{k}h$. Then

$$\begin{aligned} \frac{k_1}{k_2} &= \frac{g}{h} \\ &= \lfloor g/h \rfloor + \frac{g - \lfloor g/h \rfloor h}{h} \\ &= \underline{k} + \frac{\tilde{g}}{h}, \end{aligned}$$

and $\tilde{g} < h$ with $\tilde{g}$ and h relatively prime. Without loss of generality, take $k_2 = h$ and $k_1 = g$. Further, define time $t = 0$ by an update of Subsystem 1 so that for $i \in \mathbb{N}$, updates of x occur at times ig; for $j \in \mathbb{N}$ and $d \in \mathbb{R}$ with $0 \leq d < h$, updates of z occur at times $jh + d$. See Figure 3.3 for an illustration of these definitions. Finally, define an indicator function

$$\delta(\phi_i) = \begin{cases} 1, & \phi_i < \tilde{g} \\ 0, & \text{otherwise} \end{cases}.$$

With this setup in mind, the first building block sequence has phase $\phi_1 = d$ and update ratio

$$\begin{aligned} \kappa_1 &= \underline{k} + \delta(\phi_1) \\ &= \underline{k} + \delta(d), \end{aligned}$$

since the next update of x occurs at $t = g = \underline{k}h + \tilde{g}$ and if $d < \tilde{g}$ then the $(k+1)$st z update occurs at $\underline{k}h + d < \underline{k}h + \tilde{g}$. The second building block sequence then has the first z update at time $t = d + \kappa_1 h$. The phase is therefore

$$\begin{aligned} \phi_2 &= (d + \kappa_1 h) - g \\ &= \{d + (\underline{k}h + \delta(\phi_1))\, h\} - \{\underline{k}g + \tilde{g}\} \\ &= d - \tilde{g} + \delta(d)h \\ &= \begin{cases} d - \tilde{g}, & d \geq \tilde{g} \\ d - \tilde{g} + h, & \text{otherwise} \end{cases} \\ &= (d - \tilde{g}) \mod h \\ &\triangleq [d - \tilde{g}]_h, \end{aligned}$$

and the update ratio is $\kappa_2 = \underline{k} + \delta(\phi_2)$ by the same arguments as for the case of the first building block sequence. The third building block sequence has phase

$$\begin{aligned}
\phi_3 &= (d + (\kappa_1 + \kappa_2)\, h) - 2\tilde{g} \\
&= \{d + (2\underline{k} + \delta(d) + \delta(\phi_2))\, h\} - 2\,\{\underline{k}h + \tilde{g}\} \\
&= (d - 2\tilde{g}) + (\delta(d) + \delta(\phi_2))\, h \\
&= (d - 2\tilde{g}) \mod h \\
&= [d - 2\tilde{g}]_h\,,
\end{aligned}$$

and similarly $\kappa_3 = \underline{k} + \delta(\phi_3)$. In general, then, the update ratio of the ith building block sequence can be found by its phase from the relationship $\kappa_i = \underline{k} + \delta\,(\phi_i)$ where the phase is

$$\phi_i = [d - (i-1)\tilde{g}]_h\,.$$

Consider the zero-offset case, that is, $d = 0$. Then

$$\phi_i = [-(i-1)\tilde{g}]_h\,.$$

Now, there are h unique elements in

$$\left\{ [r\tilde{g}]_h \;\middle|\; r \in \mathbb{Z} \right\},$$

since $\tilde{g}h$ is the least common multiple of $\tilde{g}$ and h. Further, the congruence classes induced by $r \in \{0, -1, -2, \ldots, -(h-1)\}$ are distinct. Therefore, there are h distinct sets of building block sequence phases. Further, $\tilde{g}$ of them will have $\kappa_i = \underline{k} + 1$ since there are $\tilde{g}$ congruence classes such that $\delta(\phi_i) = 1$. The rest necessarily have $\kappa_i = \underline{k}$. Since only the case $\phi_i = [0]_h$ corresponds to a synchronous update, there will be one synchronous sequence with $\kappa_i = \underline{k}+1$, $\tilde{g}-1$ asynchronous sequences with $\kappa_i = \underline{k}+1$, and $h-\tilde{g}$ asynchronous sequences with update ratio $\kappa_i = \underline{k}$. This can be extended analogously for $d \neq 0$ by defining a one-to-one mapping ϕ between the $d \neq 0$ updates and the congruence classes $[-(i-1)\tilde{g}]_h$ by

$$[d - (i-1)\tilde{g}]_h = [\lfloor d \rfloor - (i-1)\tilde{g}]_h\,.$$

In this case, if $d \in \{0, 1, 2, \ldots, h-1\}$ then there is still a synchronous update; otherwise, instead of a synchronous update with $\kappa_i = \underline{k} + 1$ there will be an additional asynchronous update with $\kappa_i = \underline{k} + 1$. □

Together, Theorems 3.1 and 3.2 show how, as $\kappa = k_1/k_2 \to \infty$, the building block sequences have correspondingly growing update ratios κ_i. The evolution of z in between updates of x can now be described. Bounds on the trajectories of z are described in the following lemma.

Lemma 3.1. *Consider the multirate dynamics (3.13). Assume that $z - h(x^{(0)}) = \mathcal{O}(1)$ just before the last x update and that $x - x^{(0)} = \mathcal{O}(1)$ just after the last update. If the reduced $z^{(0)}$ dynamics defined in (3.20) are individually asymptotically stable to $h(x^{(0)})$, then κ can be chosen large enough that trajectories of the true z state satisfy*

$$z - z^{(0)} = \mathcal{O}(1)$$

in between x updates. Further, the approximation

$$z - h(x^{(0)}) = \mathcal{O}(1)$$

holds at the time of the next x update.

Proof. Define the error vector as $e_z = z - z^{(0)}$. Then the dynamics of e_z can be written as

$$\begin{aligned}
e_z^+ &= g(x,z) - g(x^{(0)}, z^{(0)}) \\
&= g(x^{(0)}, z) - g(x^{(0)}, z^{(0)}) + \big\{g(x,z) - g(x^{(0)}, z)\big\} \\
&= \big\{g(x^{(0)}, h(x^{(0)})) - h(z^{(0)})\big\} + g(x^{(0)}, z) - g(x^{(0)}, z^{(0)}) + \big\{g(x,z) - g(x^{(0)}, z)\big\} \\
&= \big\{g(x^{(0)}, e_z + h(x^{(0)})) - g(x^{(0)}, e_z + h(x^{(0)}))\big\} + \big\{g(x^{(0)}, h(x^{(0)})) - h(x^{(0)})\big\} \\
&\quad + g(x^{(0)}, z) - g(x^{(0)}, z^{(0)}) + \big\{g(x,z) - g(x^{(0)}, z)\big\} \\
&= \big\{g(x^{(0)}, e_z + h(x^{(0)})) - h(x^{(0)})\big\} \\
&\quad + \underbrace{\big\{g(x^{(0)}, e_z + z^{(0)}) - g(x^{(0)}, e_z + h(x^{(0)})) - g(x^{(0)}, z^{(0)}) + g(x^{(0)}, h(x^{(0)}))\big\}}_{\Delta_1} \\
&\quad + \underbrace{\big\{g(x,z) - g(x^{(0)}, z)\big\}}_{\Delta_2}.
\end{aligned}$$

Further, the Δ_i have the norm bounds

$$\begin{aligned}
\|\Delta_1\| &= \left\|g(x^{(0)}, e_z + z^{(0)}) - g(x^{(0)}, e_z + h(x^{(0)})) - g(x^{(0)}, z^{(0)}) + g(x^{(0)}, h(x^{(0)}))\right\| \\
&= \left\| \int_0^{z^{(0)} - h(x^{(0)})} \left\{ g_z(x^{(0)}, s + e_z + h(x^{(0)})) - g_z(x^{(0)}, s + h(x^{(0)})) \right\} ds \right\| \\
&\leq \int_0^{z^{(0)} - h(x^{(0)})} \left\| \left\{ g_z(x^{(0)}, s + e_z + h(x^{(0)})) - g_z(x^{(0)}, s + h(x^{(0)})) \right\} \right\| ds \\
&\leq \int_0^{z^{(0)} - h(x^{(0)})} c_z \|e_z\| \, ds \\
&\leq c_z \|e_z\| \left\| z^{(0)} - h(x^{(0)}) \right\|
\end{aligned}$$

where c_z is the Lipschitz constant of g_z, and

$$\begin{aligned}
\|\Delta_2\| &= \left\| g(x, z) - g(x^{(0)}, z) \right\| \\
&\leq c_1 \left\| x - x^{(0)} \right\|
\end{aligned}$$

where c_1 is the Lipschitz constant of g in its first argument. Therefore, the error can be written as a perturbed version of the reduced-order $z^{(0)}$ dynamics:

$$e_z^+ = g(x^{(0)}, e_z + h(x^{(0)})) - h(x^{(0)}) + \Delta_1 + \Delta_2. \tag{3.21}$$

Now, from [55, Theorem 3], uniform asymptotic stability of the reduced dynamics implies that $\exists$ a locally Lipschitz, positive definite function V with $V(h(x^{(0)})) = 0$ such that

$$V(g(x^{(0)}, z^{(0)})) - V(z^{(0)}) < 0$$

on some finite norm ball centered around $h(x^{(0)})$. Use V as a Lyapunov candidate for the perturbed dynamics (3.21). Then

$$V(e_z^+ + h(x^{(0)})) - V(e_z + h(x^{(0)}))$$

$$
\begin{aligned}
&= V\left(g(x^{(0)}, e_z + h(x^{(0)})) + \Delta_1 + \Delta_2\right) - V\left(e_z + h(x^{(0)})\right) \\
&= \left\{V\left(g(x^{(0)}, e_z + h(x^{(0)})) + \Delta_1 + \Delta_2\right) - V\left(g(x^{(0)}, e_z + h(x^{(0)}))\right)\right\} \\
&+ \left\{V\left(g(x^{(0)}, e_z + h(x^{(0)}))\right) - V\left(e_z + h(x^{(0)})\right)\right\} \\
&\leq c_v \left\|\Delta_1\right\| + c_v \left\|\Delta_2\right\| \\
&+ \left\{V\left(g(x^{(0)}, e_z + h(x^{(0)}))\right) - V\left(e_z + h(x^{(0)})\right)\right\} \\
&\leq c_v c_z \left\|e_z\right\| \left\|z^{(0)} - h(x^{(0)})\right\| + c_v c_1 \left\|x - x^{(0)}\right\| \\
&+ \left\{V\left(g(x^{(0)}, e_z + h(x^{(0)}))\right) - V\left(e_z + h(x^{(0)})\right)\right\},
\end{aligned}
$$

where c_v is the Lipschitz constant of V. Now,

$$V(g(x, e_z + h(x^{(0)}))) - V(e_z + h(x^{(0)})) < 0$$

by definition of V, and $\left\|x - x^{(0)}\right\| = \mathcal{O}(1)$ and $\left\|e_z(0)\right\| = \mathcal{O}(1)$ from the assumptions. Since $\left\|z^{(0)} - h(x^{(0)})\right\|$ is asymptotically stable by assumption, κ can therefore be chosen large enough that

$$V(e_z^+ + h(x^{(0)})) - V(e_z + h(x^{(0)})) < 0,$$

so that e_z is bounded for all time in the interval with a decreasing upper bound as $\kappa \to \infty$. Therefore $z - z^{(0)} = \mathcal{O}(1)$ at each point in the interval.

From the definition of asymptotic stability (e.g., [56, page 765]), asymptotic stability of the reduced-order model implies that

$$\left\|z^{(0)} - h(x^{(0)})\right\| \to 0$$

as the number of iterations increases. Similarly,

$$\left\|z - z^{(0)}\right\| \to 0$$

due to the $\mathcal{O}(1)$ bound on the error dynamics. Therefore, just before the next x update,

$$
\begin{aligned}
\left\|z - h(x^{(0)})\right\| &= \left\|z - z^{(0)} + z^{(0)} - h(x^{(0)})\right\| \\
&\leq \left\|z - z^{(0)}\right\| + \left\|z^{(0)} - h(x^{(0)})\right\| \\
&= \mathcal{O}(1)
\end{aligned}
$$

in the limit of $\kappa \to \infty$, as desired. $\square$

With this information in place, the following theorem establishes asymptotic bounds on the reduced-order models for both x and z.

Theorem 3.3. *Consider the multirate dynamics (3.13). If the reduced $z^{(0)}$ dynamics defined in (3.20) are individually asymptotically stable to $h(x^{(0)})$, then κ can be chosen large enough that, for any finite number of iterations of x, the reduced-order models (3.19) and (3.20) satisfy*

$$\begin{aligned} x - x^{(0)} &= \mathcal{O}(1) \\ z - z^{(0)} &= \mathcal{O}(1) \end{aligned}$$

in the limit of $\kappa \to \infty$.

Proof. Just before the first iteration of x, $z(t_{k_1}) - h(x^{(0)}(0)) = \mathcal{O}(1)$ by Lemma 3.1 and $x(0) - x^{(0)}(0) = 0$ by definition of the reduced-order model initial conditions. So

$$\begin{aligned} \left\| x(t_{k_1}) - x^{(0)}(t_{k_1}) \right\| &= \left\| f(x(0), z(t_{k_1})) - f(x^{(0)}(0), h(x^{(0)}(0))) \right\| \\ &\leq c_2 \left\| z(t_{k_1}) - h(x^{(0)}(0)) \right\| \\ &= \mathcal{O}(1) \end{aligned}$$

holds, where c_2 is the Lipschitz constant with respect to the second argument of $f(x, z)$. Now assume for some iteration of x that $x - x^{(0)} = \mathcal{O}(1)$ and $z - h(x) = \mathcal{O}(1)$. Then trajectories of $\left\| x - x^{(0)} \right\|$ are bounded by

$$\begin{aligned} \left\| x - x^{(0)} \right\|^+ &= \left\| f(x, z) - f(x^{(0)}, h(x^{(0)})) \right\| \\ &= \left\| f(x, z) - f(x^{(0)}, z) + f(x^{(0)}, z) - f(x^{(0)}, h(x^{(0)})) \right\| \\ &\leq \left\| f(x, z) - f(x^{(0)}, z) \right\| + \left\| f(x^{(0)}, z) - f(x^{(0)}, h(x^{(0)})) \right\| \\ &\leq c_1 \left\| x - x^{(0)} \right\| + c_2 \left\| z - h(x^{(0)}) \right\| \\ &= \mathcal{O}(1), \end{aligned}$$

where c_i is the Lipschitz constant with respect to the ith argument of $f(x,z)$, and the conditions of Lemma 3.1 hold between iterations so that $z - z^{(0)} = \mathcal{O}(1)$ in this interval. It therefore follows by induction that the asymptotic bounds $x - x^{(0)} = \mathcal{O}(1)$ and $z - z^{(0)} = \mathcal{O}(1)$ hold for any fixed, finite number of iterations of x. □

As expected, the results of Theorem 3.3 give results only for *finite* iterations of x as $\kappa \to \infty$. This is because the bound for x in the induction step is based only on the Lipschitz properties of f and may therefore grow secularly in the number of x iterations. Further stability information for the x subsystem would therefore be required to extend the validity of the reduced-order models.

3.3.1.3 Example

Consider the dynamics

$$\begin{aligned} x^+ &= z(1-x), & t &= t_{k_1} \\ z^+ &= \frac{1}{2}z + \frac{7}{4}x, & t &= t_{k_2}, \end{aligned} \tag{3.22}$$

where $k_1 = 1$ and $k_2 = \kappa$ and subject to $x(0) = 0.5$ and $z(0) = 0$. Applying the results of Section 3.3.1.1, the inner system is defined for each interval $\mathcal{I}(t_{k_1})$ as

$$z^{(0)}(\sigma(t_{k_2})) = \frac{1}{2}z^{(0)}(t_{k_2}) + \frac{7}{4}x^{(0)}(t_{k_1}), \tag{3.23}$$

which is exponentially stable. The corresponding algebraic equation

$$0 = -\frac{1}{2}z^{(0)} + \frac{7}{4}x^{(0)}$$

has the solution $z^{(0)} = h(x^{(0)}) = \frac{7}{2}x^{(0)}$, so the outer system is found to be

$$x^{(0)}(\sigma(t_{k_1})) = \frac{7}{2}x^{(0)}(1 - x^{(0)}). \tag{3.24}$$

This the well-studied logistic map with an intrinsic growth rate of 7/2. These dynamics satisfy the assumptions of Theorem 3.3, so $x^{(0)}$ is therefore expected to exhibit a stable period-4 cycle for large enough κ [57, Chapter 10].

Trajectories of x and z for various values of κ are compared to the reduced-order models $x^{(0)}$ and $z^{(0)}$ in Figure 3.4. As expected, the true states remain close to the states of the reduced-order models for large enough κ, with the x states exhibiting the expected period-4 cycle. This behaviour is lost for smaller κ.

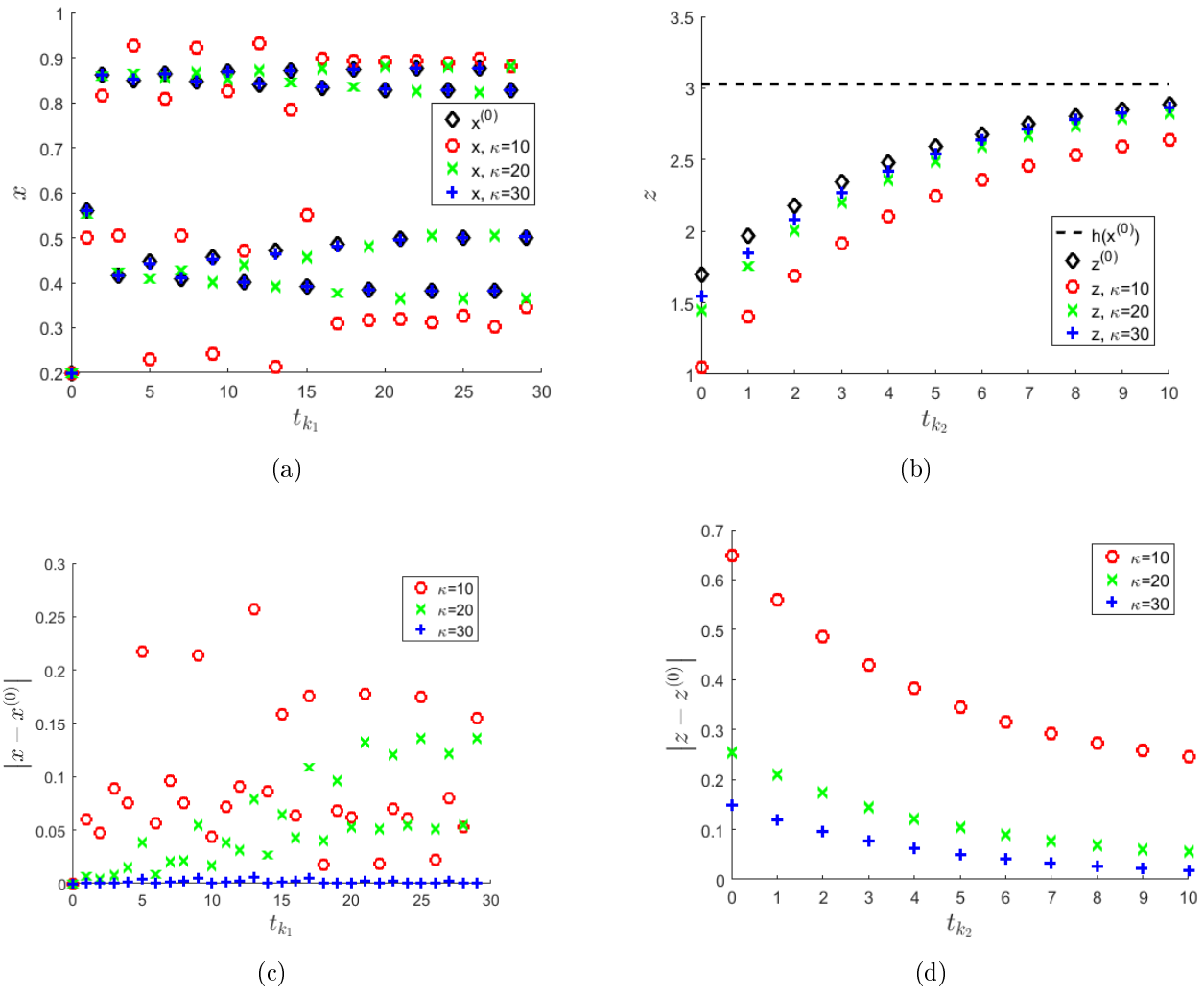

Figure 3.4: Comparison of state evolution for different κ values in the example of Section 3.3.1.3. (a) x trajectories. (b) z trajectories between updates of the x subsystem. (c) $\left|x - x^{(0)}\right|$ trajectories. (d) $\left|z - z^{(0)}\right|$ trajectories.

3.3.2 Linear Subsystems Case

More precise results can be found, for example, if each of the subsystems are linear:

$$\begin{aligned} x^+ &= A_{11}x + A_{12}z, & t &= t_{k_1} \\ z^+ &= A_{21}x + A_{22}z, & t &= t_{k_2}. \end{aligned} \tag{3.25}$$

In this case, dynamics can be can be explicitly constructed over a building block sub-sequence as

$$\begin{aligned} \begin{bmatrix} x(\sigma_1(t_{k_1})) \\ z(\sigma_1(t_{k_1})) \end{bmatrix} &= \begin{bmatrix} A_{11} & A_{12} \\ \mathbf{0} & I \end{bmatrix} \underbrace{\begin{bmatrix} I & \mathbf{0} \\ A_{21} & A_{22} \end{bmatrix} \cdots \begin{bmatrix} I & \mathbf{0} \\ A_{21} & A_{22} \end{bmatrix}}_{\kappa_i \text{ times}} \begin{bmatrix} x(t_{k_1}) \\ z(t_{k_1}) \end{bmatrix} \\ &= \underbrace{\begin{bmatrix} A_{11} + A_{12}\sum_{j=0}^{\kappa_i - 1} A_{22}^j A_{21} & A_{12}A_{22}^{\kappa_i} \\ \sum_{j=0}^{\kappa_i - 1} A_{22}^j A_{21} & A_{22}^{\kappa_i} \end{bmatrix}}_{\Phi_{asynch}(\kappa_i)} \begin{bmatrix} x(t_{k_1}) \\ z(t_{k_1}) \end{bmatrix}, \end{aligned} \tag{3.26}$$

where κ_i is the update ratio and it is assumed that the sub-sequence is asynchronous. The dynamics (3.26) can be seen as the evolution of the composite system from the perspective of the x dynamics.

Now define a new state $q(m) = [x(\sigma_1^m(t_{k_1}))^T,\ z(\sigma_1^m(t_{k_1}))^T]^T$, where m counts the number of x updates that have occurred, so that the amalgamated sequence system over a period is obtained as

$$q(m+1) = \Phi_{asynch}(\kappa_i)q(m) \tag{3.27}$$

with initial conditions

$$q(0) = \begin{bmatrix} x(0) \\ z(0) \end{bmatrix}. \tag{3.28}$$

The following analyzes (3.27) in the particular case where $\kappa_i = \kappa_{i+1} = \cdots = \kappa$; that is, when $k_1/k_2 \in \mathbb{N}$.

3.3.2.1 Initial Asymptotic Analysis

To begin the analysis, first define ε as the spectral radius of A_{22},

$$\varepsilon = \max\left\{\left|\lambda_i\left(A_{22}\right)\right|\right\},$$

and rewrite A_{22} as $A_{22} = \varepsilon\hat{A}_{22}$. Note that for all eigenvalues λ and eigenvectors v of A_{22},

$$\begin{aligned}\hat{A}_{22}v &= \frac{1}{\varepsilon}\left(A_{22}v\right)\\ &= \frac{1}{\varepsilon}\left(\lambda v\right)\\ &= \frac{\lambda}{\varepsilon}v\end{aligned}$$

so that λ/ε is an eigenvalue of $\hat{A}_{22}$ associated with the eigenvector v. Since ε is the spectral radius of A_{22}, all the eigenvalues of $\hat{A}_{22}$ have absolute value less than or equal to one. In terms of $\hat{A}_{22}$ and ε, the asynchronous amalgamated system (3.27) is now rewritten as the perturbed system

$$q(m+1) = \underbrace{\begin{bmatrix} A_{11} + A_{12}\sum_{j=0}^{\kappa-1}\varepsilon^j\hat{A}_{22}^jA_{21} & A_{12}\varepsilon^\kappa\hat{A}_{22}^\kappa \\ \sum_{j=0}^{\kappa-1}\varepsilon^j\hat{A}_{22}^jA_{21} & \varepsilon^\kappa\hat{A}_{22}^\kappa \end{bmatrix}}_{\Phi_{asynch}(\varepsilon,\kappa)} q(m). \tag{3.29}$$

Notice that the state transition matrix becomes degenerate as the ratio of subsystem updates, κ, grows in (3.29):

$$\lim_{\kappa\to\infty;\,\varepsilon\,\text{fixed}}\Phi_{asynch}(\varepsilon,\kappa) = \begin{bmatrix} A_{11} + A_{12}\left(1-\varepsilon\hat{A}_{22}\right)^{-1}A_{21} & \mathbf{0} \\ \left(1-\varepsilon\hat{A}_{22}\right)^{-1}A_{21} & \mathbf{0} \end{bmatrix}.$$

In this limit case, the solution of (3.29) then depends solely on $q_1(0)$ and does not require iterative matrix multiplications of size $n_x + n_z$ when determining the response of the system. This is because the second subsystem is allowed to approach equilibrium as κ grows large, and the equilibrium is itself directly dependent on the solution of the first subsystem. A similar degeneracy also occurs in (3.29) when the second subsystem is highly stable:

$$\lim_{\varepsilon\to 0^+;\,\kappa\,\text{fixed}}\Phi_{asynch}(\varepsilon,\kappa) = \begin{bmatrix} A_{11} + A_{12}A_{21} & \mathbf{0} \\ A_{21} & \mathbf{0} \end{bmatrix}.$$

This time, the degeneracy occurs even when the subsystem update ratio is not large. Once again, the degeneracy leads to solutions that are dependent only on $q_1(0)$. As described in Chapter 2, this dependence of a system's solution on a subset of the initial conditions is known as a boundary-layer-type degeneracy. The approximations developed in the rest of this section will quantify the effects of changes in ε and κ on the system's behaviour.

To account for the boundary-layer degeneracy, seek an approximation to the true solution of the form

$$\begin{aligned} q_1(m) &= \tilde{q}_1(m) + \varepsilon^{\kappa m+\kappa} p_1(m) \\ q_2(m) &= \tilde{q}_2(m) + \varepsilon^{\kappa m} p_2(m), \end{aligned} \tag{3.30}$$

where $\tilde{q}$ represents the outer solution that captures the limit case and p the inner solution that captures the transients and is valid for smaller m. This is a standard form for discrete-time boundary layer systems [19], and accounts for the fact that effects of the inner solution should decay with $\varepsilon^{\kappa m}$ as m increases. Substituting (3.30) into (3.29) gives

$$\tilde{q}_1(m+1) + \varepsilon^{\kappa(m+1)+\kappa} p_1(m+1) =$$

$$\left(A_{11} + A_{12} \sum_{j=0}^{\kappa-1} \varepsilon^j \hat{A}_{22}^j A_{21} \right) \left[\tilde{q}_1(m) + \varepsilon^{\kappa m+\kappa} p_1(m) \right] + \varepsilon^{\kappa} A_{12} \hat{A}_{22}^{\kappa} \left[\tilde{q}_2(m) + \varepsilon^{\kappa m} p_2(m) \right]$$

$$\tilde{q}_2(m+1) + \varepsilon^{\kappa(m+1)} p_2(m+1) =$$

$$\left(\sum_{j=0}^{\kappa-1} \varepsilon^j \hat{A}_{22}^j A_{21} \right) \left[\tilde{q}_1(m) + \varepsilon^{\kappa m+\kappa} p_1(m) \right] + \varepsilon^{\kappa} \hat{A}_{22}^{\kappa} \left[\tilde{q}_2(m) + \varepsilon^{\kappa m} p_2(m) \right]. \tag{3.31}$$

The outer problem should satisfy the original (outer) problem, so enforce

$$\begin{aligned} \tilde{q}_1(m+1) &= \left(A_{11} + A_{12} \sum_{j=0}^{\kappa-1} \varepsilon^j \hat{A}_{22}^j A_{21} \right) \tilde{q}_1(m) + \varepsilon^{\kappa} A_{12} \hat{A}_{22}^{\kappa} \tilde{q}_2(m) \\ \tilde{q}_2(m+1) &= \left(\sum_{j=0}^{\kappa-1} \varepsilon^j \hat{A}_{22}^j A_{21} \right) \tilde{q}_1(m) + \varepsilon^{\kappa} \hat{A}_{22}^{\kappa} \tilde{q}_2(m). \end{aligned} \tag{3.32}$$

Using (3.32) in (3.31) and simplifying then yields the inner problem,

$$\begin{aligned} \varepsilon^{\kappa} p_1(m+1) &= \left(A_{11} + A_{12} \sum_{j=0}^{\kappa-1} \varepsilon^j \hat{A}_{22}^j A_{21} \right) p_1(m) + A_{12} \hat{A}_{22}^{\kappa} p_2(m) \\ p_2(m+1) &= \left(\sum_{j=0}^{\kappa-1} \varepsilon^j \hat{A}_{22}^j A_{21} \right) p_1(m) + \hat{A}_{22}^{\kappa} p_2(m). \end{aligned} \tag{3.33}$$

Solutions to (3.32) and (3.33) will be sought in the form of a generalized asymptotic series

$$\tilde{q}_i(m;\varepsilon) = \sum_{r=0}^{\infty} \varepsilon^r \tilde{q}_i^{(r)}(m;\varepsilon), \; p_i(m;\varepsilon) = \sum_{r=0}^{\infty} \varepsilon^r p_i^{(r)}(m;\varepsilon) \tag{3.34}$$

for $i = 1, 2$, and where $\varepsilon \tilde{q}_i^{(r+1)} = \mathcal{O}\left(\tilde{q}_i^{(r)}\right)$ and $\varepsilon p_i^{(r+1)} = \mathcal{O}\left(p_i^{(r)}\right)$. Substituting the initial conditions (3.28) into (3.34) and equating like orders of ε yields the zeroth order initial conditions as

$$\begin{aligned} \tilde{q}_1^{(0)}(0;\varepsilon) &= q_1(0) \\ p_2^{(0)}(0;\varepsilon) &= q_2(0) - \tilde{q}_2^{(0)}(0;\varepsilon), \end{aligned} \tag{3.35}$$

and the rth order initial conditions, $1 \leq r \leq \kappa - 1$, as

$$\begin{aligned} \tilde{q}_1^{(r)}(0;\varepsilon) &= 0 \\ p_2^{(r)}(0;\varepsilon) &= -\tilde{q}_2^{(r)}(0;\varepsilon). \end{aligned} \tag{3.36}$$

Thus, the outer solutions $\tilde{q}_i^{(r)}$ depend only on the initial condition $\tilde{q}_1^{(r)}(0;\varepsilon)$ while the inner solutions $p_i^{(r)}$ depend only on the initial condition $p_2^{(r)}(0;\varepsilon)$. Together with (3.32) and (3.33), the outer and inner problems are now well-defined and will be solved next.

3.3.2.2 Outer Problem

In the following, solutions to the outer problem are first developed for the special case of one-dimensional subsystems. It is shown that a straightforward asymptotic expansion cannot produce uniformly valid solutions to the outer problem over long time intervals. To this end, solutions valid over long time intervals are developed using the generalized MMS approach. These solutions are then extended to the general case of multidimensional subsystems.

One-Dimensional Subsystem Case The outer problem (3.32) is written in the one-dimensional subsystem case as

$$\tilde{q}(m+1) = \begin{bmatrix} a_{11} + a_{12}\sum_{j=0}^{\kappa-1}\varepsilon^j \hat{a}_{22}^j a_{21} & a_{12}\varepsilon^\kappa \hat{a}_{22}^\kappa \\ \sum_{j=0}^{\kappa-1}\varepsilon^j \hat{a}_{22}^j a_{21} & \varepsilon^\kappa \hat{a}_{22}^\kappa \end{bmatrix} \tilde{q}(m), \tag{3.37}$$

where $\hat{a}_{22}, a_{ij} \in \mathbb{R}$ and $\hat{a}_{22} = \text{sign}(a_{22})$. As is shown below, a straightforward asymptotic series expansion, where the ordered solutions $\tilde{q}_i(r)$ are not dependent on ε, fails for the outer problem over large numbers of iterations. To remedy this issue, a solution is found using the generalized MMS approach.

To begin, assume a straightforward asymptotic series solution by expanding the outer solution $\tilde{q}(m;\varepsilon)$ as

$$\tilde{q}_i(m;\varepsilon) = \sum_{r\geq 0} \varepsilon^r \tilde{q}_i^{(r)}(m) \tag{3.38}$$

for $i = 1, 2$. This is a restriction on the more general expansion in (3.34) as it eliminates the dependence of $\tilde{q}_i^{(r)}$ on ε. The ordered solutions are then found by substituting the expansion (3.38) into the outer problem (3.37), equating orders of ε, and solving the resulting ordered equations. The zeroth order solution is then found as

$$\begin{aligned} \tilde{q}_1^{(0)}(m) &= (a_{11} + a_{12}a_{21})^m \, q_1(0) \\ \tilde{q}_2^{(0)}(m) &= a_{21}\,(a_{11} + a_{12}a_{21})^{m-1} \, q_1(0), \end{aligned} \tag{3.39}$$

while the first order solution is found as

$$\begin{aligned} \tilde{q}_1^{(1)}(m) &= m\,(a_{11} + a_{12}a_{21})^m \, \frac{a_{12}\hat{a}_{22}a_{21}}{(a_{11} + a_{12}a_{21})} q_1(0) \\ \tilde{q}_2^{(1)}(m) &= (a_{11} + a_{12}a_{21})^m \left\{ \frac{a_{12}\hat{a}_{22}a_{21}^2}{(a_{11} + a_{12}a_{21})^2}(m-1) + \frac{\hat{a}_{22}a_{21}}{(a_{11} + a_{12}a_{21})} \right\} q_1(0). \end{aligned} \tag{3.40}$$

When $m = \mathcal{O}(1/\varepsilon)$, however, these solutions cease to be asymptotically valid. This can be seen by setting $m = 1/\varepsilon$ and looking at the ratio of the zeroth and first order terms in the assumed asymptotic series expansion ($\tilde{q}_i^{(0)}(m)$ and $\varepsilon\tilde{q}_i^{(1)}(m)$, respectively) in the limit of ε

approaching zero,

$$\begin{aligned}\lim_{\varepsilon\to 0^+}\frac{\varepsilon\tilde{q}_1^{(1)}(1/\varepsilon)}{\tilde{q}_1^{(0)}(1/\varepsilon)} &= \lim_{\varepsilon\to 0^+}\frac{\varepsilon\,(1/\varepsilon)\,(a_{11}+a_{12}a_{21})^{1/\varepsilon}\,\frac{a_{12}\hat{a}_{22}a_{21}}{(a_{11}+a_{12}a_{21})}q_1(0)}{(a_{11}+a_{12}a_{21})^{1/\varepsilon}\,q_1(0)}\\ &= \frac{a_{12}\hat{a}_{22}a_{21}}{(a_{11}+a_{12}a_{21})}\end{aligned}$$

and

$$\begin{aligned}\lim_{\varepsilon\to 0^+}\frac{\varepsilon\tilde{q}_2^{(1)}(1/\varepsilon)}{\tilde{q}_2^{(0)}(1/\varepsilon)} &= \lim_{\varepsilon\to 0^+}\frac{\varepsilon\left\{a_{21}\tilde{q}_1^{(1)}(\varepsilon^{-1}-1)+\hat{a}_{22}a_{21}\tilde{q}_1^{(0)}(\varepsilon^{-1}-1)\right\}}{a_{21}\tilde{q}_1^{(0)}(\varepsilon^{-1}-1)}\\ &= \lim_{\varepsilon\to 0^+}\frac{\varepsilon\tilde{q}_1^{(1)}\,(\varepsilon^{-1}-1)}{\tilde{q}_1^{(0)}\,(\varepsilon^{-1}-1)}\\ &= \frac{a_{12}\hat{a}_{22}a_{21}}{(a_{11}+a_{12}a_{21})}.\end{aligned}$$

Here, the $\tilde{q}_2^{(r)}$ terms have been written explicitly in terms of their dependence on $\tilde{q}_1^{(r)}$. A valid asymptotic expansion must be zero in the limit of ε approaching zero, while the straightforward expansions (3.38) are not. For both $\tilde{q}_1$ and $\tilde{q}_2$ this is due to resonant forcing terms in the ordered outer equations for $\tilde{q}_1(m)$ and, as noted in Chapter 2, is evidence of multiple time scale behaviour in the outer solution.

To obtain solutions that are asymptotically valid for longer time spans, first note that the outer problem (3.37) is defined in terms of a single base $\mathbb{T}$, namely $\mathbb{Z}$. Rewriting (3.37) in terms of the corresponding delta derivatives then leads to the $\mathbb{T}$ dynamics

$$\frac{d\tilde{q}}{\Delta m}(m)=\begin{bmatrix}(a_{11}-1)+a_{12}\sum_{j=0}^{\kappa-1}\varepsilon^j\hat{a}_{22}^j a_{21} & \varepsilon^\kappa\hat{a}_{22}^\kappa a_{12}\\ \sum_{j=0}^{\kappa-1}\varepsilon^j\hat{a}_{22}^j a_{21} & \varepsilon^\kappa\hat{a}_{22}^\kappa-1\end{bmatrix}\tilde{q}(m). \tag{3.41}$$

Now, assume a solution of the form

$$\tilde{q}_1(m)=\sum_{r\geq 0}\varepsilon^r\tilde{q}_1^{(r)}(s_0,s_1,\ldots,s_{\kappa-1}), \tag{3.42}$$

where each discrete time scale

$$s_i=\varepsilon^i m \tag{3.43}$$

will be treated as independent. Further assume that each $\tilde{q}_1^{(r)}(s_0, s_1, \ldots, s_{\kappa-1})$ is partially delta-differentiable for all $(s_0, \ldots, s_{\kappa-1}) \in \mathbb{N} \times \varepsilon\mathbb{N} \times \cdots \times \varepsilon^{\kappa-1}\mathbb{N}$. By Theorem 3.1, the total delta difference of each ordered solution, $\tilde{q}_1^{(r)}$, is therefore expanded as

$$\frac{d\tilde{q}_1^{(r)}}{\Delta m}(s_0, s_1, \ldots, s_{\kappa-1}) = \sum_{i=0}^{\kappa} \varepsilon^i \frac{\partial \tilde{q}_1^{(r)}}{\Delta s_i}(\sigma_0(s_0), \ldots, \sigma_{i-1}(s_{i-1}), s_i, s_{i+1}, \ldots, s_{\kappa-1}), \tag{3.44}$$

where the forward jump operator for the ith timescale is defined by

$$\sigma_i(s_i) = s_i + \varepsilon^i.$$

The resulting solutions, which will be constructed to both satisfy the dynamics and maintain asymptoticity for large m, are generalized asymptotic expansions where every ordered solution depend on ε. Note that this multiple time scale form is only explicitly used for $\tilde{q}_1$. A similar assumption is not necessary for $\tilde{q}_2$ because each ordered solution $\tilde{q}_2^{(r)}$ is algebraically dependent on the ordered solutions of $\tilde{q}_1$.

Substituting the multiple-scale expansion (3.42) along with the total delta difference expression (3.44) into (3.41) and equating orders of ε then gives the zeroth order problem as

$$\begin{aligned} \frac{\partial \tilde{q}_1^{(0)}}{\Delta s_0}(s_0, s_1, \ldots, s_{k-1}) &= (\bar{a}_{11} - 1)\,\tilde{q}_1^{(r)}(s_0, s_1, \ldots, s_{\kappa-1}) \\ \triangle \tilde{q}_2^{(0)}(m) &= a_{21}\tilde{q}_1^{(0)}(s_0, s_1, \ldots, s_{\kappa-1}) - \tilde{q}_2^{(0)}(m), \end{aligned} \tag{3.45}$$

subject to $\tilde{q}_1^{(0)}(0) = q_1(0)$ (from (3.35)) and where $\bar{a}_{11} \triangleq a_{11} + a_{12}a_{21}$. The rth order problem for $1 \leq r \leq \kappa - 1$ is found as

$$\sum_{l=0}^{r} \frac{\partial \tilde{q}_1^{(r-l)}}{\Delta s_l}(\sigma_0(s_0), \ldots, \sigma_{l-1}(s_{l-1}), s_l, s_{l+1}, \ldots, s_{\kappa-1}) =$$

$$(\bar{a}_{11} - 1)\,\tilde{q}_1^{(r)}(s_0, s_1, \ldots, s_{k-1}) + a_{12}\sum_{l=1}^{r} \hat{a}_{22}^l a_{21}\tilde{q}_1^{(r-l)}(s_0, s_1, \ldots, s_{\kappa-1})$$

$$\triangle \tilde{q}_2^{(r)}(m) = a_{21}\sum_{l=0}^{r} \hat{a}_{22}^l \tilde{q}_1^{(r-l)}(s_0, s_1, \ldots, s_{\kappa-1}) - \tilde{q}_2^{(r)}(m), \tag{3.46}$$

subject to the initial condition $\tilde{q}_1^{(r)}(0) = 0$ (from (3.36)). Here the total difference operator Δ has been used for $\tilde{q}_2^{(r)}$ to emphasize that a multiple-scale solution is not being explicitly sought for $\tilde{q}_2$. These ordered dynamic equations are now solved to maintain asymptoticity of the ordered solutions in terms of the time scales s_i.

From the zeroth order equation, (3.45), solutions for $\tilde{q}_1^{(0)}$ have the form

$$\tilde{q}_1^{(0)}\left(s_0, s_1, \ldots, s_{k-1}\right) = \bar{a}_{11}^{s_0} C_1\left(s_1, \ldots, s_{\kappa-1}\right), \tag{3.47}$$

where C_1 is a function of the slow timescales s_1–$s_{\kappa-1}$ and subject to $C_1\left(0, \ldots, 0\right) = q_1(0)$. From (3.46), the first order equation for $\tilde{q}_1$ is then

$$\frac{\partial \tilde{q}_1^{(1)}}{\Delta s_0}\left(s_0, \ldots, s_{\kappa-1}\right) - \left(\bar{a}_{11} - 1\right)\tilde{q}_1^{(1)}\left(s_0, s_1, \ldots, s_{\kappa-1}\right) =$$

$$- \left[\bar{a}_{11} C_1^{\triangle_{s_1}}\left(s_1, \ldots, s_{\kappa-1}\right) - a_{12}\hat{a}_{22}a_{21} C_1\left(s_1, \ldots, s_{\kappa-1}\right)\right]\bar{a}_{11}^{s_0}. \tag{3.48}$$

Now, if the right-hand side of (3.48) is not zero then $\tilde{q}_1^{(1)}$ will be subject to resonant forcing and $\varepsilon\tilde{q}_1^{(1)}$ will become non-asymptotic to $\tilde{q}_1^{(0)}$ when $m = \mathcal{O}\left(\varepsilon^{-1}\right)$ as in the straightforward expansion (3.38). Therefore, enforce

$$\bar{a}_{11}\frac{\partial C_1}{\Delta s_1}\left(s_1, \ldots, s_{\kappa-1}\right) - a_{12}\hat{a}_{22}a_{21} C_1\left(s_1, \ldots, s_{\kappa-1}\right) = 0, \tag{3.49}$$

which has the solution (see [41])

$$C_1\left(s_1, \ldots, s_{\kappa-1}\right) = \left(1 + \varepsilon\frac{a_{12}\hat{a}_{22}a_{21}}{\bar{a}_{11}}\right)^{s_1/\varepsilon} C_2\left(s_2, \ldots, s_{\kappa-1}\right)$$

subject to $C_2\left(0, \ldots, 0\right) = q_1(0)$.

By similar arguments on the equations of order up to $\kappa - 1$, the resulting solution is

$$\tilde{q}_1^{(0)}\left(s_0, s_1, \ldots, s_{\kappa-1}\right) = \bar{a}_{11}^{s_0}\left(1 + \varepsilon\frac{a_{12}\hat{a}_{22}a_{21}}{\bar{a}_{11}}\right)^{s_1/\varepsilon}\left(1 + \varepsilon^2\frac{a_{12}\hat{a}_{22}^2 a_{21}}{\bar{a}_{11} + \varepsilon a_{12}\hat{a}_{22}a_{21}}\right)^{s_2/\varepsilon^2}$$

$$\cdots\left(1 + \varepsilon^{\kappa-1}\frac{a_{12}\hat{a}_{22}^{\kappa-1}a_{21}}{\bar{a}_{11} + \varepsilon a_{12}\hat{a}_{22}a_{21} + \cdots + \varepsilon^{\kappa-2}a_{12}\hat{a}_{22}^{\kappa-2}a_{21}}\right)^{s_{\kappa-1}/\varepsilon^{\kappa-1}} q_1(0). \tag{3.50}$$

Using (3.43) to write (3.50) in terms of m then yields

$$\begin{aligned}\tilde{q}_1^{(0)}(m) = \quad & \bar{a}_{11}^m \left(1+\varepsilon\frac{a_{12}\hat{a}_{22}a_{21}}{\bar{a}_{11}}\right)^{\varepsilon m/\varepsilon} \left(1+\varepsilon^2\frac{a_{12}\hat{a}_{22}^2a_{21}}{\bar{a}_{11}+\varepsilon a_{12}\hat{a}_{22}a_{21}}\right)^{\varepsilon^2 m/\varepsilon^2} \\ & \cdots \left(1+\varepsilon^{\kappa-1}\frac{a_{12}\hat{a}_{22}^{\kappa-1}a_{21}}{\bar{a}_{11}+\varepsilon a_{12}\hat{a}_{22}a_{21}+\cdots+\varepsilon^{\kappa-2}a_{12}\hat{a}_{22}^{\kappa-2}a_{21}}\right)^{\varepsilon^{\kappa-1}m/\varepsilon^{\kappa-1}} q_1(0) \\ = \quad & \left(\bar{a}_{11}+\varepsilon a_{12}a_{21}+\cdots+\varepsilon^{\kappa-2}a_{12}a_{21}+\varepsilon^{\kappa-1}a_{12}a_{21}\right)^m q_1(0),\end{aligned}$$

which simplifies to

$$\tilde{q}_1^{(0)}(m) = \left(a_{11}+a_{12}\left(\frac{\varepsilon^\kappa\hat{a}_{22}^\kappa-1}{\varepsilon\hat{a}_{22}-1}\right)a_{21}\right)^m q_1(0). \tag{3.51}$$

From (3.45), this leads to the solution

$$\tilde{q}_2^{(0)}(m) = a_{21}\left(a_{11}+a_{12}\left(\frac{\varepsilon^\kappa\hat{a}_{22}^\kappa-1}{\varepsilon\hat{a}_{22}-1}\right)a_{21}\right)^{m-1} q_1(0) \tag{3.52}$$

for $\tilde{q}_2^{(0)}(m)$. Note that even though these solutions contain ε terms in accordance with the initial assumption of a generalized asymptotic series solution (3.34), they are both of $\mathcal{O}(1)$. By construction, this solution is asymptotically valid up to $m = \mathcal{O}(1/\varepsilon^{\kappa-1})$.

Multidimensional Subsystem Case Inspired by the form of (3.51) and (3.54), assume the zeroth order solution

$$\begin{aligned}\tilde{q}_1^{(0)}(m) &= \left(A_{11}+A_{12}\sum_{j=0}^{\kappa-1}\varepsilon^j\hat{A}_{22}^jA_{21}\right)^m q_1(0) \\ \tilde{q}_2^{(0)}(m) &= A_{21}\left(A_{11}+A_{12}\sum_{j=0}^{\kappa-1}\varepsilon^j\hat{A}_{22}^jA_{21}\right)^{m-1} q_1(0)\end{aligned} \tag{3.53}$$

in the generalized asymptotic series (3.34). Now, (3.53) satisfies

$$\begin{aligned}\tilde{q}_1^{(0)}(m+1) &= \left(A_{11}+A_{12}\sum_{j=0}^{\kappa-1}\varepsilon^j\hat{A}_{22}^jA_{21}\right)^{m+1} q_1(0) \\ &= \left(A_{11}+A_{12}\sum_{j=0}^{\kappa-1}\varepsilon^j\hat{A}_{22}^jA_{21}\right)\tilde{q}_1^{(0)}(m)\end{aligned} \tag{3.54}$$

and

$$\tilde{q}_2^{(0)}(m+1) = A_{21}\tilde{q}_1^{(0)}(m), \tag{3.55}$$

so that the outer problem (3.32) is satisfied to zeroth order.

Substituting (3.53) and (3.34) into the outer problem (3.32) and equating orders of ε then yields the rth order outer equation for $0 < r \leq \kappa - 1$ as

$$\begin{aligned} \tilde{q}_1^{(r)}(m+1) - (A_{11} + A_{12}A_{21})\,\tilde{q}_1^{(r)}(m) &= A_{12}\sum_{j=1}^{r-1} \hat{A}_{22}^{r-j} A_{21}\tilde{q}_1^{(j)}(m) \\ \tilde{q}_2^{(r)}(m+1) &= \sum_{j=0}^{r} \hat{A}_{22}^{r-j} A_{21}\tilde{q}_1^{(j)}(m). \end{aligned} \tag{3.56}$$

Since $\tilde{q}_1^{(r)}(0) = 0$ from the initial conditions, the solution for $\tilde{q}_1^{(r)}(m)$ is then found as

$$\tilde{q}_1^{(r)}(m) = 0,$$

and therefore

$$\tilde{q}_2^{(r)}(m) = \hat{A}_{22}^{r} A_{21}\left(A_{11} + A_{12}\sum_{j=0}^{\kappa-1} \varepsilon^j \hat{A}_{22}^{j} A_{21}\right)^{m-1} q_1(0)$$

for $1 \leq r \leq \kappa - 1$.

While the expansion (3.34) is in some ways a "straightforward" expansion, the assumed solution (3.53) correctly incorporates the multiple time scale behaviour of the outer solution that was examined in the one-dimensional subsystem case. By including appropriate terms of order ε and higher in the zeroth order solution $\tilde{q}_1^{(0)}$, the terms that cause resonance in the higher order solutions are eliminated. The resulting approximations therefore remain asymptotic over long time spans, as desired. This can be seen by evaluating the asymptoticity of the zeroth and first order solutions:

$$\begin{aligned} \lim_{\varepsilon\to 0^+} \frac{\left\|\varepsilon\tilde{q}_1^{(1)}(m)\right\|}{\left\|\tilde{q}_1^{(0)}(m)\right\|} &= \lim_{\varepsilon\to 0^+} \frac{0}{\left\|\left(A_{11} + A_{12}\sum_{j=0}^{\kappa-1}\varepsilon^j\hat{A}_{22}^{j}A_{21}\right)^{m} q_1(0)\right\|} \\ &= 0, \end{aligned}$$

and

$$\begin{aligned}\lim_{\varepsilon\to 0^+}\frac{\left\|\varepsilon\tilde{q}_2^{(1)}(m)\right\|}{\left\|\tilde{q}_2^{(0)}(m)\right\|} &= \lim_{\varepsilon\to 0^+}\frac{\left\|\varepsilon\hat{A}_{22}A_{21}\left(A_{11}+A_{12}\sum_{j=0}^{\kappa-1}\varepsilon^j\hat{A}_{22}^jA_{21}\right)^{m-1}q_1(0)\right\|}{\left\|A_{21}\left(A_{11}+A_{12}\sum_{j=0}^{\kappa-1}\varepsilon^j\hat{A}_{22}^jA_{21}\right)^{m-1}q_1(0)\right\|}\\ &= 0.\end{aligned}$$

The asymptoticity of further terms in the series up to $(\kappa-1)$st order follows since they are all either zero or algebraic combinations of lower-order solutions.

This concludes the search for a solution to the outer problem (3.32).

3.3.2.3 Inner Problem

In the following, solutions to the inner problem are first developed for the special case of one-dimensional subsystems. As in the outer problem, the solutions are derived using the generalized MMS approach so that the results are valid over long time intervals. These solutions are then extended to the general case of multidimensional subsystems.

One-Dimensional Subsystem Case The inner problem (3.33) is written in the one-dimensional subsystem case as

$$\begin{aligned}\varepsilon^\kappa p_1(m+1) &= \left(a_{11}+a_{12}\sum_{j=0}^{\kappa-1}\varepsilon^j\hat{a}_{22}^ja_{21}\right)p_1(m)+a_{12}\hat{a}_{22}^\kappa p_2(m)\\ p_2(m+1) &= \left(\sum_{j=0}^{\kappa-1}\varepsilon^j\hat{a}_{22}^jA_{21}\right)p_1(m)+\hat{a}_{22}^\kappa p_2(m),\end{aligned}\tag{3.57}$$

where once again $\hat{a}_{22}$, $a_{ij}\in\mathbb{R}$ and $\hat{a}_{22}=\text{sign}(a_{22})$. As in the outer solution, a straightforward expansion yields solutions that are only valid for $m=\mathcal{O}(1)$. In this case, the ordered solutions of $p_1(m)$ directly depend on the ordered solutions of $p_2(m)$ (due to the ε^κ term that multiplies $p_1(m+1)$ in (3.57)), and the expansion fails due to resonant forcing terms in the ordered equations for $p_2(m)$.

Therefore, rewrite the inner problem (3.57) in terms of $\mathbb{T} = \mathbb{Z}$ as the $\mathbb{T}$ dynamics

$$\begin{aligned} \varepsilon^{\kappa} \frac{dp_1}{\Delta m}(m) &= \left(a_{11} + a_{12} \sum_{j=0}^{\kappa-1} \varepsilon^j \hat{a}_{22}^j a_{21} - \varepsilon^{\kappa} \right) p_1(m) + a_{12} \hat{a}_{22}^{\kappa} p_2(m) \\ \frac{dp_2}{\Delta m}(m) &= \left(\sum_{j=0}^{\kappa-1} \varepsilon^j \hat{a}_{22}^j A_{21} \right) p_1(m) + (\hat{a}_{22}^{\kappa} - 1)\, p_2(m). \end{aligned} \tag{3.58}$$

Assume a multiple scales solution of the form

$$p_2(m) = \sum_{r \geq 0} \varepsilon^r p_2^{(r)}(s_0, s_1, \ldots, s_{\kappa-1}) \tag{3.59}$$

to treat the resonance, where each discrete time scale

$$s_i = \varepsilon^i m \tag{3.60}$$

will be treated as independent. Once more, assume that each $p_2^{(r)}(s_0, s_1, \ldots, s_{\kappa-1})$ is partially delta-differentiable for all $(s_0, \ldots, s_{\kappa-1}) \in \mathbb{N} \times \varepsilon\mathbb{N} \times \cdots \times \varepsilon^{\kappa-1}\mathbb{N}$. By Theorem 3.1, the total delta difference of each order solution, $p_2^{(r)}$, is then expanded as

$$\frac{dp_2^{(r)}}{\Delta m}(s_0, s_1, \ldots, s_{\kappa-1}) = \sum_{i=0}^{\kappa} \varepsilon^i \frac{\partial p_2^{(r)}}{\Delta s_i}(\sigma_0(s_0), \ldots, \sigma_{i-1}(s_{i-1}), s_i, s_{i+1}, \ldots, s_{\kappa-1}). \tag{3.61}$$

A similar assumption is not necessary for p_1 because each ordered solution $p_1^{(r)}$ is algebraically dependent on the ordered solutions of p_2.

Substituting (3.59) and (3.61) in (3.58) and equating orders of ε then gives the zeroth order inner problem as

$$\begin{aligned} 0 &= \bar{a}_{11} p_1^{(0)}(m) + a_{12} \hat{a}_{22}^{\kappa} p_2^{(0)}(s_0, s_1, \ldots, s_{\kappa-1}) \\ \frac{\partial p_2^{(0)}}{\Delta s_0}(s_0, s_1, \ldots, s_{\kappa-1}) &= a_{21} p_1^{(0)}(m) + (\hat{a}_{22}^{\kappa} - 1)\, p_2^{(0)}(s_0, s_1, \ldots, s_{\kappa-1}), \end{aligned} \tag{3.62}$$

subject to $p_2^{(0)}(0) = q_2(0) - \tilde{q}_2^{(0)}(0)$ (from (3.35)), and the rth order inner equation for $1 \leq r \leq \kappa - 1$ as

$$0 = \bar{a}_{11} p_1^{(r)}(m) + a_{12} \sum_{j=1}^{r} \hat{a}_{22}^j a_{21} p_1^{(r-j)}(m) + a_{12} \hat{a}_{22}^{\kappa} p_2^{(r)}(s_0, s_1, \ldots, s_{\kappa-1})$$

$$\sum_{j=0}^{r} \frac{\partial p_2^{(r-j)}}{\Delta s_k} \left(\sigma_0\left(s_0\right), \ldots, \sigma_{j-1}\left(s_{j-1}\right), s_j, s_{j+1}, \ldots, s_{\kappa-1}\right) =$$

$$\sum_{j=0}^{r} \hat{a}_{22}^{j} a_{21} p_1^{(r-j)}(m) + \left(\hat{a}_{22}^{\kappa} - 1\right) p_2^{(r)}(s_0, s_1, \ldots, s_{\kappa-1}), \quad (3.63)$$

subject to $p_2^{(r)}(0) = -\tilde{q}_2^{(r)}(0)$ (from (3.36)).

Solving these ordered dynamic equations to maintain asymptoticity analogous to the approach in Section 3.3.2.2 then yields the ordered solutions in terms of the time scales s_i. Writing each s_i in terms of m and ε, the zeroth order solution is found to be

$$p_1^{(0)}(m) = -\bar{a}_{11}^{-1} a_{12} \hat{a}_{22}^{\kappa} \left[\left\{ 1 - \left(\sum_{i=0}^{\kappa-1} \varepsilon^i \left(1 - \frac{a_{12}a_{21}}{\bar{a}_{11}} \right)^i \hat{a}_{22}^{i} \right) \frac{a_{12}a_{21}}{\bar{a}_{11}} \right\} \hat{a}_{22}^{\kappa} \right]^m \left(q_2(0) - \tilde{q}_2^{(0)}(0) \right)$$

$$p_2^{(0)}(m) = \left[\left\{ 1 - \left(\sum_{i=0}^{\kappa-1} \varepsilon^i \left(1 - \frac{a_{12}a_{21}}{\bar{a}_{11}} \right)^i \hat{a}_{22}^{i} \right) \frac{a_{12}a_{21}}{\bar{a}_{11}} \right\} \hat{a}_{22}^{\kappa} \right]^m \left(q_2(0) - \tilde{q}_2^{(0)}(0) \right). \quad (3.64)$$

If $|(1 - a_{12}a_{21}/\bar{a}_{11})\varepsilon| \geq 1$ then (3.64) is a diverging series and only the first term should be used for numerical computations. As in the outer solution, this solution is asymptotically valid up to $m = \mathcal{O}(1/\varepsilon^{\kappa-1})$ by construction.

Multidimensional Subsystem Case Inspired by the form of (3.64), assume the zeroth order solution

$$p_1^{(0)}(m) = -\bar{A}_{11}^{-1} A_{12} \hat{A}_{22}^{\kappa} \left[\left(I - A_{21}\bar{A}_{11}^{-1}A_{12} \right) \left\{ I \right. \right.$$
$$\left. \left. - \sum_{i=1}^{\kappa-1} \varepsilon^i \left(\hat{A}_{22} - \hat{A}_{22}\left(A_{21}\bar{A}_{11}^{-1}A_{12}\right) \right)^{i-1} \hat{A}_{22}\left(A_{21}\bar{A}_{11}^{-1}A_{12}\right) \right\} \hat{A}_{22}^{\kappa} \right]^m \cdot \left(q_2(0) - \tilde{q}_2^{(0)}(0) \right)$$

$$p_2^{(0)}(m) = \left[\left(I - A_{21}\bar{A}_{11}^{-1}A_{12} \right) \left\{ I \right. \right.$$
$$\left. \left. - \sum_{i=1}^{\kappa-1} \varepsilon^i \left(\hat{A}_{22} - \hat{A}_{22}\left(A_{21}\bar{A}_{11}^{-1}A_{12}\right) \right)^{i-1} \hat{A}_{22}\left(A_{21}\bar{A}_{11}^{-1}A_{12}\right) \right\} \hat{A}_{22}^{\kappa} \right]^m \cdot \left(q_2(0) - \tilde{q}_2^{(0)}(0) \right)$$

(3.65)

in the asymptotic series (3.34). Now, (3.65) satisfies

$$\begin{aligned} p_2^{(0)}(m+1) &= \Big[\big(I - A_{21}\bar{A}_{11}^{-1}A_{12}\big) \\ &\quad \cdot \left\{ I - \sum_{i=1}^{\kappa-1} \varepsilon^i \left(\hat{A}_{22} - \hat{A}_{22}\left(A_{21}\bar{A}_{11}^{-1}A_{12}\right)\right)^{i-1} \hat{A}_{22}\left(A_{21}\bar{A}_{11}^{-1}A_{12}\right) \right\} \hat{A}_{22}^{\kappa} \Big]^{m+1} \\ &\qquad \cdot \Big(q_2(0) - \tilde{q}_2^{(0)}(0) \Big) \\ &= \Big[\big(I - A_{21}\bar{A}_{11}^{-1}A_{12}\big) \\ &\quad \cdot \left\{ I - \sum_{i=1}^{\kappa-1} \varepsilon^i \left(\hat{A}_{22} - \hat{A}_{22}\left(A_{21}\bar{A}_{11}^{-1}A_{12}\right)\right)^{i-1} \hat{A}_{22}\left(A_{21}\bar{A}_{11}^{-1}A_{12}\right) \right\} \hat{A}_{22}^{\kappa} \Big] p_2^{(0)}(m) \end{aligned} \tag{3.66}$$

and

$$p_1^{(0)}(m) = -\bar{A}_{11}^{-1}A_{12}\hat{A}_{22}^{\kappa}p_2^{(0)}(m),$$

so that the inner problem (3.33) is satisfied to zeroth order.

Substituting (3.34) and (3.65) into the inner problem (3.33) and equating orders of ε yields the rth order inner problem, $1 \le r \le \kappa - 1$, as

$$\begin{aligned} 0 &= -A_{12}\hat{A}_{22}^{r}\left(A_{21}\bar{A}_{11}^{-1}A_{12}\right)\hat{A}_{22}^{\kappa}p_2^{(0)}(m) + \bar{A}_{11}p_1^{(r)}(m) \\ &\quad + \sum_{j=1}^{r-1} A_{12}\hat{A}_{22}^{r-j}A_{21}p_1^{(j)}(m) + A_{12}\hat{A}_{22}^{\kappa}p_2^{(r)}(m) \end{aligned}$$

$$\begin{aligned} p_2^{(r)}(m+1) &= -\left\{ \hat{A}_{22}^{r-1} - \big(I - A_{21}\bar{A}_{11}^{-1}A_{12}\big)\left(\hat{A}_{22} - \hat{A}_{22}\left(A_{21}\bar{A}_{11}^{-1}A_{12}\right)\right)^{r-1} \right\} \\ &\quad \cdot \hat{A}_{22}\left(A_{21}\bar{A}_{11}^{-1}A_{12}\right)\hat{A}_{22}^{\kappa}p_2^{(0)}(m) + \sum_{j=1}^{r}\hat{A}_{22}^{r-j}A_{21}p_1^{(j)}(m) + \hat{A}_{22}^{\kappa}p_2^{(r)}(m). \end{aligned}$$

In particular, the first order inner problem is

$$\begin{aligned} 0 &= -A_{12}\hat{A}_{22}\left(A_{21}\bar{A}_{11}^{-1}A_{12}\right)\hat{A}_{22}^{\kappa}p_2^{(0)}(m) + \bar{A}_{11}p_1^{(1)}(m) + A_{12}\hat{A}_{22}^{\kappa}p_2^{(1)}(m) \\ p_2^{(1)}(m+1) &= -\left(A_{21}\bar{A}_{11}^{-1}A_{12}\right)\hat{A}_{22}\left(A_{21}\bar{A}_{11}^{-1}A_{12}\right)\hat{A}_{22}^{\kappa}p_2^{(0)}(m) + A_{21}p_1^{(1)}(m) + \hat{A}_{22}^{\kappa}p_2^{(1)}(m). \end{aligned} \tag{3.67}$$

From the first equation,

$$p_1^{(1)}(m) = \bar{A}_{11}^{-1} A_{12} \hat{A}_{22} \left(A_{21} \bar{A}_{11}^{-1} A_{12} \right) \hat{A}_{22}^{\kappa} p_2^{(0)}(m) - \bar{A}_{11}^{-1} A_{12} \hat{A}_{22}^{\kappa} p_2^{(1)}(m)$$

so that $p_2^{(1)}(m+1)$ satisfies

$$p_2^{(1)}(m+1) = \left(I - A_{21} \bar{A}_{11}^{-1} A_{12} \right) \hat{A}_{22}^{\kappa} p_2^{(1)}(m).$$

This equation has the general solution

$$p_2^{(1)}(m) = \left[\left(I - A_{21} \bar{A}_{11}^{-1} A_{12} \right) \hat{A}_{22}^{\kappa} \right]^m p_2^{(1)}(0).$$

Using the initial condition $p_2^{(1)}(0) = -\tilde{q}_2^{(1)}(0)$, the particular solution is then

$$p_2^{(1)}(m) = 0, \tag{3.68}$$

so that

$$p_1^{(1)}(m) = \bar{A}_{11}^{-1} A_{12} \hat{A}_{22} \left(A_{21} \bar{A}_{11}^{-1} A_{12} \right) \hat{A}_{22}^{\kappa} p_2^{(0)}(m). \tag{3.69}$$

As with the assumed solution for the multidimensional outer system, the assumed inner solution (3.65) incorporates the multiple time scale behaviour of the inner solution that was examined in the one-dimensional subsystem case. This can be seen by evaluating the asymptoticity of the zeroth and first order solutions:

$$\begin{aligned} \lim_{\varepsilon \to 0^+} \frac{\left\| \varepsilon p_2^{(1)}(m) \right\|}{\left\| p_2^{(0)}(m) \right\|} &= \lim_{\varepsilon \to 0^+} \frac{0}{\left\| p_2^{(0)}(m) \right\|} \\ &= 0 \end{aligned}$$

and

$$\begin{aligned} \lim_{\varepsilon \to 0^+} \frac{\left\| \varepsilon p_1^{(1)}(m) \right\|}{\left\| p_1^{(0)}(m) \right\|} &= \lim_{\varepsilon \to 0^+} \frac{\left\| \varepsilon \bar{A}_{11}^{-1} A_{12} \hat{A}_{22} \left(A_{21} \bar{A}_{11}^{-1} A_{12} \right) \hat{A}_{22}^{\kappa} p_2^{(0)}(m) \right\|}{\left\| -\bar{A}_{11}^{-1} A_{12} \hat{A}_{22}^{\kappa} p_2^{(0)}(m) \right\|} \\ &= 0, \end{aligned}$$

where $p_1^{(0)}$ and $p_1^{(1)}$ have been written in terms of their dependence on $p_2^{(0)}$ and $p_2^{(1)}$, respectively. The asymptoticity of further terms in the series up to the $(\kappa-1)$st order follows since they are all either zero or algebraic combinations of lower-order solutions.

This concludes the search for a solution to the inner problem (3.33).

3.3.2.4 Overall Approximation and Bounds on Eigenvalues

From (3.30), (3.53), and (3.65), the zeroth order solution to the singularly perturbed amalgamated system (3.29) is

$$q_1(m) \sim \left(A_{11} + A_{12} \sum_{j=0}^{\kappa-1} \varepsilon^j \hat{A}_{22}^j A_{21} \right)^m q_1(0) - \varepsilon^{\kappa m+\kappa} \bar{A}_{11}^{-1} A_{12} \hat{A}_{22}^{\kappa} \left[\left(I - A_{21} \bar{A}_{11}^{-1} A_{12} \right) \left\{ I \right.\right.$$
$$\left.\left. - \sum_{i=1}^{\kappa-1} \varepsilon^i \left(\hat{A}_{22} - \hat{A}_{22} \left(A_{21} \bar{A}_{11}^{-1} A_{12} \right) \right)^{i-1} \hat{A}_{22} \left(A_{21} \bar{A}_{11}^{-1} A_{12} \right) \right\} \hat{A}_{22}^{\kappa} \right]^m$$
$$\cdot \left(q_2(0) - A_{21} \left(A_{11} + A_{12} \sum_{j=0}^{\kappa-1} \varepsilon^j \hat{A}_{22}^j A_{21} \right)^{-1} q_1(0) \right)$$

$$q_2(m) \sim A_{21} \left(A_{11} + A_{12} \sum_{j=0}^{\kappa-1} \varepsilon^j \hat{A}_{22}^j A_{21} \right)^{m-1} q_1(0) + \varepsilon^{\kappa m} \left[\left(I - A_{21} \bar{A}_{11}^{-1} A_{12} \right) \left\{ I \right.\right.$$
$$\left.\left. - \sum_{i=1}^{\kappa-1} \varepsilon^i \left(\hat{A}_{22} - \hat{A}_{22} \left(A_{21} \bar{A}_{11}^{-1} A_{12} \right) \right)^{i-1} \hat{A}_{22} \left(A_{21} \bar{A}_{11}^{-1} A_{12} \right) \right\} \hat{A}_{22}^{\kappa} \right]^m$$
$$\cdot \left(q_2(0) - A_{21} \left(A_{11} + A_{12} \sum_{j=0}^{\kappa-1} \varepsilon^j \hat{A}_{22}^j A_{21} \right)^{-1} q_1(0) \right).$$

This can be written in terms of A_{22} instead of ε and $\hat{A}_{22}$ as

$$q_1(m) \sim \left(A_{11} + A_{12} \sum_{j=0}^{\kappa-1} A_{22}^j A_{21} \right)^m q_1(0) - \bar{A}_{11}^{-1} A_{12} A_{22}^{\kappa}$$
$$\left[\left(I - A_{21} \bar{A}_{11}^{-1} A_{12} \right) \left\{ I - \sum_{i=1}^{\kappa-1} \left(A_{22} - A_{22} \left(A_{21} \bar{A}_{11}^{-1} A_{12} \right) \right)^{i-1} A_{22} \left(A_{21} \bar{A}_{11}^{-1} A_{12} \right) \right\} A_{22}^{\kappa} \right]^m$$
$$\cdot \left(q_2(0) - A_{21} \left(A_{11} + A_{12} \sum_{j=0}^{\kappa-1} A_{22}^j A_{21} \right)^{-1} q_1(0) \right)$$

$$q_2(m) \sim A_{21}\left(A_{11} + A_{12}\sum_{j=0}^{\kappa-1} A_{22}^j A_{21}\right)^{m-1} q_1(0)$$

$$+\left[\left(I - A_{21}\bar{A}_{11}^{-1}A_{12}\right)\left\{I - \sum_{i=1}^{\kappa-1}\left(A_{22} - A_{22}\left(A_{21}\bar{A}_{11}^{-1}A_{12}\right)\right)^{i-1} A_{22}\left(A_{21}\bar{A}_{11}^{-1}A_{12}\right)\right\} A_{22}^{\kappa}\right]^m$$

$$\cdot\left(q_2(0) - A_{21}\left(A_{11} + A_{12}\sum_{j=0}^{\kappa-1} A_{22}^j A_{21}\right)^{-1} q_1(0)\right). \quad (3.70)$$

It can be seen from these solutions that, in the limit of $\varepsilon \to 0$ or $\kappa \to \infty$, the simple sequence system's eigenvalues will have n_x eigenvalues that approach the eigenvalues of $\left(A_{11} + A_{12}\sum_{j=0}^{\kappa-1} A_{22}^j A_{21}\right)$ and n_z eigenvalues that approach the eigenvalues of $\left(I - A_{21}\bar{A}_{11}^{-1}A_{12}\right)A_{22}^{\kappa}$. This property is captured by the following theorem:

Theorem 3.4. *The eigenvalues of $\Phi_{asynch}(\kappa)$ are within $\mathcal{O}(\varepsilon^{\kappa})$ of the eigenvalues of $\left(A_{11} + A_{12}\sum_{j=0}^{\kappa-1} A_{22}^j A_{21}\right)$ and of $\left(I - A_{21}\bar{A}_{11}^{-1}A_{12}\right)A_{22}^{\kappa}$.*

Proof. Define

$$G_1 = \left\{ z \,\middle|\, \left\| \left(\left(A_{11} + A_{12}\sum_{j=0}^{\kappa-1} \varepsilon^j \hat{A}_{22}^j A_{21} \right) - zI_{n_1} \right)^{-1} \right\|^{-1} \le \varepsilon^{\kappa} \left\| A_{12}\hat{A}_{22}^{\kappa} \right\| \right\}$$

$$G_2 = \left\{ z \,\middle|\, \left\| \left(\varepsilon^{\kappa}\hat{A}_{22}^{\kappa} - zI_{n_2} \right)^{-1} \right\|^{-1} \le \varepsilon^{\kappa} \left\| A_{12}\hat{A}_{22}^{\kappa} \right\| \right\}.$$

By the Gershgorin Theorem for block-partitioned matrices [58], all eigenvalues of (3.29) lie within the union of G_1 and G_2. In particular, G_1 contains the eigenvalues of $A_{11} + A_{12}\sum_{j=0}^{\kappa-1} \varepsilon^j \hat{A}_{22}^j A_{21}$ and G_2 contains the eigenvalues of $\varepsilon^{\kappa}\hat{A}_{22}^{\kappa}$. Further, when G_1 and G_2 are disjoint, n_x eigenvalues of 3.29 are contained in G_1 and n_z eigenvalues of (3.29) are contained in G_2. Therefore, since the sets are bounded by a function of $\mathcal{O}(\varepsilon^{\kappa})$, n_x eigenvalues of $\Phi_{asynch}(\kappa)$ are within $\mathcal{O}(\varepsilon^{\kappa})$ of the eigenvalues of $\left(A_{11} + A_{12}\sum_{j=0}^{\kappa-1} A_{22}^j A_{21}\right)$ and n_z eigenvalues are within $\mathcal{O}(\varepsilon^{\kappa-1})$ of both A_{22}^{κ} and $\left(I - A_{21}\bar{A}_{11}^{-1}A_{12}\right)A_{22}^{\kappa}$ in the limit $\varepsilon \to 0$ or $\kappa \to \infty$. □

This theorem implies that the stability of a simple sequence system is asymptotically governed by the dominant eigenvalue of the reduced-order matrix $\left(A_{11} + A_{12}\sum_{j=0}^{\kappa-1} A_{22}^{j} A_{21}\right)$ as the individual clock periods are separated. This captures how the simple sequence system's stability is affected by the κ updates of the fast subsystem.

3.3.2.5 Example

Consider the heat distribution in a thin, homogeneous bar where sensors measure the temperature at n equidistant points on the bar and where heaters apply temperature differentials at each point to control the bar's temperature profile. The discrete-time dynamics of such a bar are described (see [59]) by

$$x^{+} = \begin{bmatrix} (1-2\alpha) & \alpha & 0 & \cdots & 0 \\ \alpha & (1-2\alpha) & \alpha & & \vdots \\ 0 & \alpha & (1-2\alpha) & \ddots & \\ \vdots & \vdots & \vdots & \ddots & \alpha \\ 0 & 0 & 0 & \alpha & (1-2\alpha) \end{bmatrix} x + I_n u,$$

where $x = [x_1, \ldots, x_n]^T$ is a collection of temperatures at the discrete points, α is the heat transfer coefficient of the bar, and u is the vector of control inputs. The dynamics of each sensor z_i, $i = 1, \ldots, n$, are described by discretized versions of a typical temperature sensor model (see [60]) as

$$z_i^{+} = \begin{bmatrix} 0.4777 & -0.1990 \\ 0.2866 & 0.9554 \end{bmatrix} z_i + \begin{bmatrix} 0.1433 \\ 0.0321 \end{bmatrix} x_i.$$

Take $n = 4$. There are therefore $n_2 = 2n_1 = 8$ states in the second subsystem with corresponding state vector $z = \left[z_1^T, \ldots, z_5^T\right]^T$ and spectral radius $\varepsilon = 0.72$. For $\alpha = 0.2$, a control is then chosen independently of the sensor dynamics as

$$u = -Kz,$$

where K is the discrete-time LQR solution with $Q = I_4$ and $R = 5I_4$.

Figure 3.5 shows how the separation in update rates affects the eigenvalues of the amalgamated period system. Intuitively, as this separation approaches infinity the sensors reach steady-state readings and the LQR-based controller is provided with true state-feedback. However, when the update rate separation are finite, the temperature in the bar is affected by the sensor dynamics. This figure illustrates how the reduced-order approximations yield eigenvalues that correctly capture this relationship even though $\varepsilon = 0.72$, a relatively large value for the perturbation parameter. For the particular update rate relationship $\kappa = 10$, Figure 3.6 shows the evolution of the temperatures along the bar along with two boundary-layer-corrected reduced-order solutions. The first reduced-order solution, denoted "No MMS" in the figure, does not incorporate the multiple time scale behaviour identified in Section 3.3.2.2 that is induced by clock period separation. This approximation therefore does not match the true solution well because it not uniformly valid over the domain. The second reduced-order solution, denoted "With MMS" in the figure, uses the uniformly valid approximation summarized in Section 3.3.2.4. This second approximation correctly incorporates the multiple time scale behaviour induced by the clock period separation and therefore matches the exact solution well.

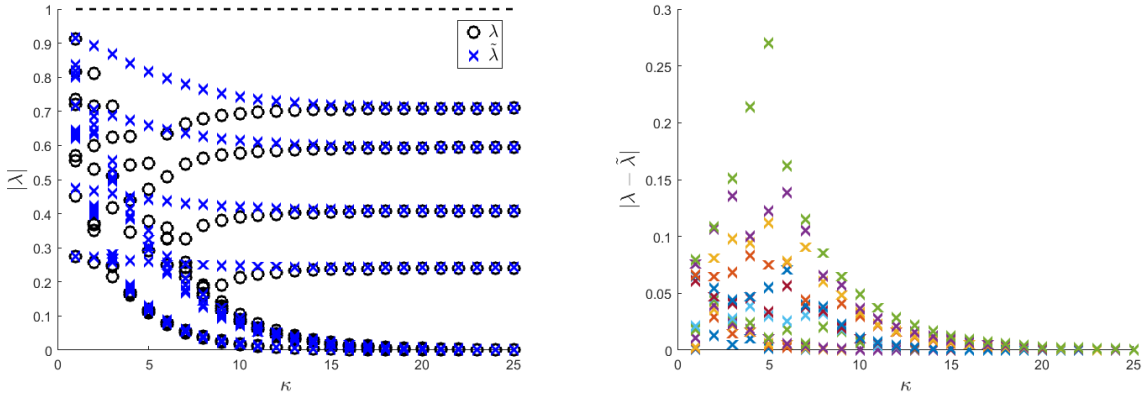

(a) (b)

Figure 3.5: Comparison of eigenvalues in the example of Section 3.3.2.5 for different values of κ. (a) Exact and approximated eigenvalues. (b) Error in eigenvalue approximation.

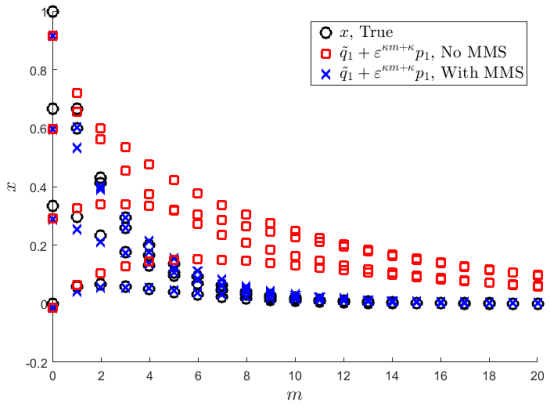

Figure 3.6: Comparison of exact and approximated trajectories in the example of Section 3.3.2.5 when $\kappa = 10$, $\varepsilon = 0.72$

3.4 Analysis of Hybrid-Time Systems

This section investigates the multiple timescale behaviour that can occur when a system updates in both continuous and discrete time. Such behaviour arises naturally, for example, in distributed robotics problems where communication occurs intermittenly between the agents (see Chapter 5 for more details). In this context, approaches are desired that can decrease the complexity of analyzing these systems and give insight into the role of the discrete update rate on the system's behaviour. However, current singular perturbation results are focused on the role of a small parameter which is assumed to exist *a priori* in a subset of the system states and are restricted in the class of systems they analyze. The work on impulsive differential equations, for example, assumes exponentially stable continuous-time subsystems and fixed update rates [23, 24]. Meanwhile, results in the context of hybrid systems allow the update rate to vary by changing the update map but restricts the fast continuous dynamics to evolve on a compact set [61, 22]. These limitations are overcome with generalized multi-scale analysis proposed in this chapter, which gives the desired insight into how the discrete update rate effects the behaviour of the hybrid-time dynamics and provides an approach to systematically construct reduced-order models.

3.4.1 General Case

Consider the dynamics

$$\begin{aligned} x^+ &= f(x, k; \nu), & t &= t_k \\ \dot{x} &= g(x, t; \nu), & t &\neq t_k, \end{aligned} \tag{3.71}$$

for $x \in D_x \subseteq \mathbb{R}^{n_x}$ and $z \in D_z \subseteq \mathbb{R}^{n_z}$ subject to the initial conditions $x(0) = x_0 \in D_x$ and $z(0) = z_0 \in D_z$, and where $t_k \in \{t_0, t_1, \ldots\}$ are the distinct times of discrete updates and $\nu = 1/(t_k - t_{k-1})$ measures the current update rate. The dependence of f and g on ν therefore encodes any changes in the vector fields due to a different update rate. It will be

assumed that the vector fields f and g are bounded, Lipschitz, and sufficiently differentiable in the domains.

3.4.1.1 Asymptotic Analysis

To analyze the hybrid-time dynamics (3.71), note that there are two base $\mathbb{T}$s for this problem: $\mathbb{T} = \mathbb{R}$ for the continuous dynamics and $\mathbb{T}_k = \{t_k\}$ for the discrete dynamics. Rewriting (3.71) in terms of the corresponding delta derivatives then leads to the $\mathbb{T}$ dynamics

$$\begin{aligned} \frac{\partial x}{\Delta t_k} &= \frac{1}{\mu(k)} \left\{ f(x, k; \nu) - x \right\} \\ \frac{\partial x}{\Delta t} &= g(x, t; \nu). \end{aligned} \tag{3.72}$$

where $\mu(k) = t_{k+1} - t_k$ is the graininess of $\mathbb{T}_k$ at the kth discrete update. The following considers the behaviour of (3.72) as the time between updates grows; that is, as $\mu \to \infty$.

Begin by assuming a straightforward asymptotic series solution and expanding x as

$$x(t, t_k) = \sum_{i \geq 0} \mu^{-i} x^{(i)}(t, t_k). \tag{3.73}$$

Next, substitute (3.73) into (3.72) and equate orders of μ. The $\mathcal{O}(1)$ equation is then found to be

$$\begin{aligned} \frac{\partial x^{(0)}}{\Delta t_k} &= 0 \\ \frac{\partial x^{(0)}}{\Delta t} &= g(x^{(0)}, t; 0), \end{aligned} \tag{3.74}$$

subject to $x^{(0)}(0, 0) = x(0)$. This implies that $x^{(0)}$ is continuous. The $\mathcal{O}(\mu^{-1})$ equation is then

$$\begin{aligned} \frac{\partial x^{(1)}}{\Delta t_k} &= \left\{ f(x^{(0)}, k; 0) - x^{(0)} \right\} \\ \frac{\partial x^{(1)}}{\Delta t} &= \frac{\partial g}{\partial \nu}\Big|_{x^{(0)}} + \frac{\partial g}{\partial x}\Big|_{x^{(0)}} x^{(1)}, \end{aligned} \tag{3.75}$$

subject to $x^{(1)}(0, 0) = 0$. Now, over the first interval ($0 \leq t < t_1$), $x^{(1)}$ satisfies

$$x^{(1)} = 0$$

using the initial condition. $x^{(1)}$ is then updated at $t = t_1$ as

$$\begin{aligned} x^{(1)}(t_1, t_1) &= x^{(1)}(t_1, t_0) + \mu \left\{ f(x^{(0)}(t_1, t_0), k; 0) - x^{(0)}(t_1, t_0) \right\} \\ &= \mu \left\{ f(x^{(0)}(t_1, t_0), k; 0) - x^{(0)}(t_1, t_0) \right\}. \end{aligned}$$

Therefore, at time t_1,

$$\begin{aligned} \lim_{\mu \to \infty} \frac{\mu^{-1} x^{(1)}(t_1, t_1)}{x^{(0)}(t_1, t_1)} &= \lim_{\mu \to \infty} \frac{\mu \left\{ f(x^{(0)}(t_1, t_0), k; 0) - x^{(0)}(t_1, t_0) \right\}}{x^{(0)}(t_1, t_1)} \\ &\neq 0 \end{aligned}$$

in general, so that $\mu^{-1} x^{(1)} \neq \mathcal{O}(x^{(0)})$ at the time of the discrete update. The dynamics (3.72) therefore exhibit secular behaviour on this slow timescale, which implies that a MMS based approach can be used here.

To obtain a solution that is valid over discrete updates search for a solution in the form

$$x(t, t_k) = \sum_{i \geq 0} \mu^{-i} x^{(i)}(\eta_t, \eta_k, \tau_t, \tau_k), \tag{3.76}$$

where $\eta_t = t$ and $\eta_k = t_k$ are the fast scales, and $\tau_t = t/\mu$ and $\tau_k = t_k/\mu$ are the slow scales. The delta derivatives are then expanded as

$$\frac{\partial x}{\Delta t_k}(t, t_k) = \frac{\partial x}{\Delta \eta_k}(\eta_t, \eta_k, \tau_t, \tau_k) + \frac{1}{\mu} \frac{\partial x}{\Delta \tau_k}(\eta_t, \sigma(\eta_k), \tau_t, \tau_k)$$

and

$$\frac{\partial x}{\Delta t}(t, t_k) = \frac{\partial x}{\Delta \eta_t}(\eta_t, \eta_k, \tau_t, \tau_k) + \frac{1}{\mu} \frac{\partial x}{\Delta \tau_t}(\eta_t, \eta_k, \tau_t, \tau_k).$$

For compactness, these sets of times will be denoted as $(\eta, \tau) \triangleq (\eta_t, \eta_k, \tau_t, \tau_k)$ and $(\sigma_k(\eta), \tau) \triangleq (\eta_t, \sigma(\eta_k), \tau_t, \tau_k)$. Next, substitute (3.76) into (3.72) along with the delta derivative expansions and equate orders of μ. The $\mathcal{O}(1)$ equation is then found to be

$$\begin{aligned} &\frac{\partial x^{(0)}}{\Delta \eta_k}(\eta, \tau) = 0 \\ &\frac{\partial x^{(0)}}{\Delta \eta_t}(\eta, \tau) = g(x^{(0)}(\eta, \tau), \eta_t; 0), \end{aligned} \tag{3.77}$$

subject to $x^{(0)}(0,0,0,0) = x(0)$. This implies that $x^{(0)}$ is continuous in the fast scales. Dependence on the slow scales will be determined to ensure asymptoticity of $x^{(0)}$ and $\mu x^{(1)}$. To this end, noting that $x^{(0)}\left(\sigma_k(\eta),\tau\right) = x^{(0)}\left(\eta,\tau\right)$, the $\mathcal{O}(\mu^{-1})$ equation is found to be

$$\begin{aligned}
\frac{\partial x^{(1)}}{\Delta\eta_k}\left(\eta,\tau\right) + \frac{\partial x^{(0)}}{\Delta\tau_k}\left(\eta,\tau\right) &= \left\{f\left(x^{(0)}\left(\eta,\tau\right),k;0\right) - x^{(0)}\left(\eta,\tau\right)\right\} \\
\frac{\partial x^{(1)}}{\Delta\eta_t}\left(\eta,\tau\right) + \frac{\partial x^{(0)}}{\Delta\tau_t}\left(\eta,\tau\right) &= \left.\frac{\partial g}{\partial\nu}\right|_{x^{(0)}} + \left.\frac{\partial g}{\partial x}\right|_{x^{(0)}} x^{(1)}\left(\eta,\tau\right),
\end{aligned} \tag{3.78}$$

subject to $x^{(1)}(0,0,0,0) = 0$. Now, if $x^{(1)}\left(\eta,\tau\right) = \mathcal{O}(1)$ and the asymptoticity conditions

$$\begin{aligned}
\frac{\partial x^{(0)}}{\Delta\tau_k}\left(\eta,\tau\right) - f\left(x^{(0)}\left(\eta,\tau\right),k;0\right) + x^{(0)}\left(\eta,\tau\right) &= \mathcal{O}(\mu^{-1}) \\
\frac{\partial x^{(0)}}{\Delta\tau_t}\left(\eta,\tau\right) &= 0
\end{aligned} \tag{3.79}$$

are enforced, then

$$\begin{aligned}
x^{(1)}\left(\sigma_k(\eta),\tau\right) &= x^{(1)}\left(\eta,\tau\right) + \mu\left\{f\left(x^{(0)}\left(\eta,\tau\right),k;0\right) - x^{(0)}\left(\eta,\tau\right) - \frac{\partial x^{(0)}}{\Delta\tau_k}\left(\eta,\tau\right)\right\} \\
&= \mathcal{O}(1)
\end{aligned}$$

as well. Therefore, $\mu^{-1}x^{(1)} = o(x^{(0)})$ holds for a finite number of discrete updates. Higher-order terms may be found similarly.

3.4.1.2 Example

Consider the dynamics

$$\begin{aligned}
\begin{bmatrix} x_1^+ \\ x_2^+ \end{bmatrix} &= \left(1 + x_1^2 + x_2^2\right)\begin{bmatrix} \cos(2\pi k/100) \\ \sin(2\pi k/100) \end{bmatrix}, && t = t_k \\
\begin{bmatrix} \dot{x}_1 \\ \dot{x}_2 \end{bmatrix} &= -\begin{bmatrix} x_1^3 \\ x_2^3 \end{bmatrix}, && t \neq t_k,
\end{aligned} \tag{3.80}$$

subject to $x_1(0) = 1$ and $x_2(0) = 0$. Rewriting (3.80) in terms of $\mathbb{T} = \mathbb{R}$ and $\mathbb{T}_k = \{t_k\}$ leads to the $\mathbb{T}$ dynamics

$$\begin{aligned}\frac{\partial x}{\Delta t_k} &= \frac{1}{\mu}\left\{\left(1+\|x\|^2\right)\begin{bmatrix}\cos(2\pi k/100)\\ \sin(2\pi k/100)\end{bmatrix} - x\right\}\\ \frac{\partial x_i}{\Delta t} &= -x_i^3.\end{aligned} \tag{3.81}$$

Applying the results of Section 3.4.1.1, the $\mathcal{O}(1)$ equation is found from (3.77) as

$$\begin{aligned}\frac{\partial x^{(0)}}{\Delta \eta_k} &= 0\\ \frac{\partial x_i^{(0)}}{\Delta \eta_t} &= -x_i^3.\end{aligned}$$

This has the solution

$$x_i^{(0)} = \frac{\operatorname{sign}\left(A_i(\tau_t,\tau_k)\right)}{\sqrt{\frac{1}{A_i(\tau_t,\tau_k)^2} + 2\left(\eta_t - \tau_k\mu\right)}} \tag{3.82}$$

subject to $A_i(0,0) = x_i(0)$. The asymptoticity conditions are then written from (3.79) as

$$\begin{aligned}\frac{\partial x^{(0)}}{\Delta \tau_k}(\eta_t,\sigma(\eta_k),\tau_t,\tau_k) - \left(1+\left\|x^{(0)}\right\|^2\right)\begin{bmatrix}\cos(2\pi k/100)\\ \sin(2\pi k/100)\end{bmatrix} + x^{(0)} &= \mathcal{O}(\mu^{-1})\\ \frac{\partial x^{(0)}}{\Delta \tau_t}(\eta_t,\eta_k,\tau_t,\tau_k) &= 0\end{aligned}$$

Now, from (3.82),

$$\left\|x^{(0)}\right\|^2 = \frac{1}{\frac{1}{A_1(\tau_t,\tau_k)^2} + 2\left(\eta_t - \tau_k\mu\right)} + \frac{1}{\frac{1}{A_2(\tau_t,\tau_k)^2} + 2\left(\eta_t - \tau_k\mu\right)}$$

Just before the discrete update, $(\eta_t,\eta_k,\tau_t,\tau_k) = (\eta_{k+1},\eta_k,\tau_{k+1},\tau_k)$ so that

$$\begin{aligned}\left\|x^{(0)}\right\|^2 &= \frac{1}{\frac{1}{A_1(\tau_k,\tau_k)^2} + 2\left(\eta_{k+1} - \tau_k\mu\right)} + \frac{1}{\frac{1}{A_2(\tau_k,\tau_k)^2} + 2\left(\eta_{k+1} - \tau_k\mu\right)}\\ &= \frac{1}{\frac{1}{A_1(\tau_k,\tau_k)^2} + 2\mu} + \frac{1}{\frac{1}{A_2(\tau_k,\tau_k)^2} + 2\mu}\\ &= 0 + \mathcal{O}(\mu^{-1})\end{aligned}$$

Therefore,

$$\frac{\partial x^{(0)}}{\Delta\tau_k}(\eta_t, \sigma(\eta_k), \tau_t, \tau_k) = \begin{bmatrix} \cos(2\pi k/100) \\ \sin(2\pi k/100) \end{bmatrix} - x^{(0)}$$
$$\frac{\partial x^{(0)}}{\Delta\tau_t}(\eta_t, \eta_k, \tau_t, \tau_k) = 0$$

satisfies the asymptoticity conditions. This gives the solution

$$A(\tau_t, \tau_k) = \begin{bmatrix} \cos(2\pi k/100) \\ \sin(2\pi k/100) \end{bmatrix}$$

for A. The zeroth order solution (3.82) is then rewritten as

$$x_1^{(0)} = \frac{\text{sign}\left(\cos(2\pi\tau_k/100)\right)}{\sqrt{\frac{1}{\cos(2\pi\tau_k/100)^2} + 2\left(\eta_t - \tau_k\mu\right)}}$$
$$x_2^{(0)} = \frac{\text{sign}\left(\sin(2\pi\tau_k/100)\right)}{\sqrt{\frac{1}{\sin(2\pi\tau_k/100)^2} + 2\left(\eta_t - \tau_k\mu\right)}},$$

or in terms of t and k as

$$x_1^{(0)} = \frac{\text{sign}\left(\cos(2\pi k/100)\right)}{\sqrt{\frac{1}{\cos(2\pi k/100)^2} + 2\left(t - k\mu\right)}}$$
$$x_2^{(0)} = \frac{\text{sign}\left(\sin(2\pi k/100)\right)}{\sqrt{\frac{1}{\sin(2\pi k/100)^2} + 2\left(t - k\mu\right)}}. \tag{3.83}$$

Trajectories of (3.83) are shown in comparison to trajectories of the original dynamics (3.71) in Figure 3.7. As expected, the true states remain close to the states of the reduced-order models for large μ. The error in the approximated solution grows when μ is decreased, both over discrete updates as well as over each continuous interval.

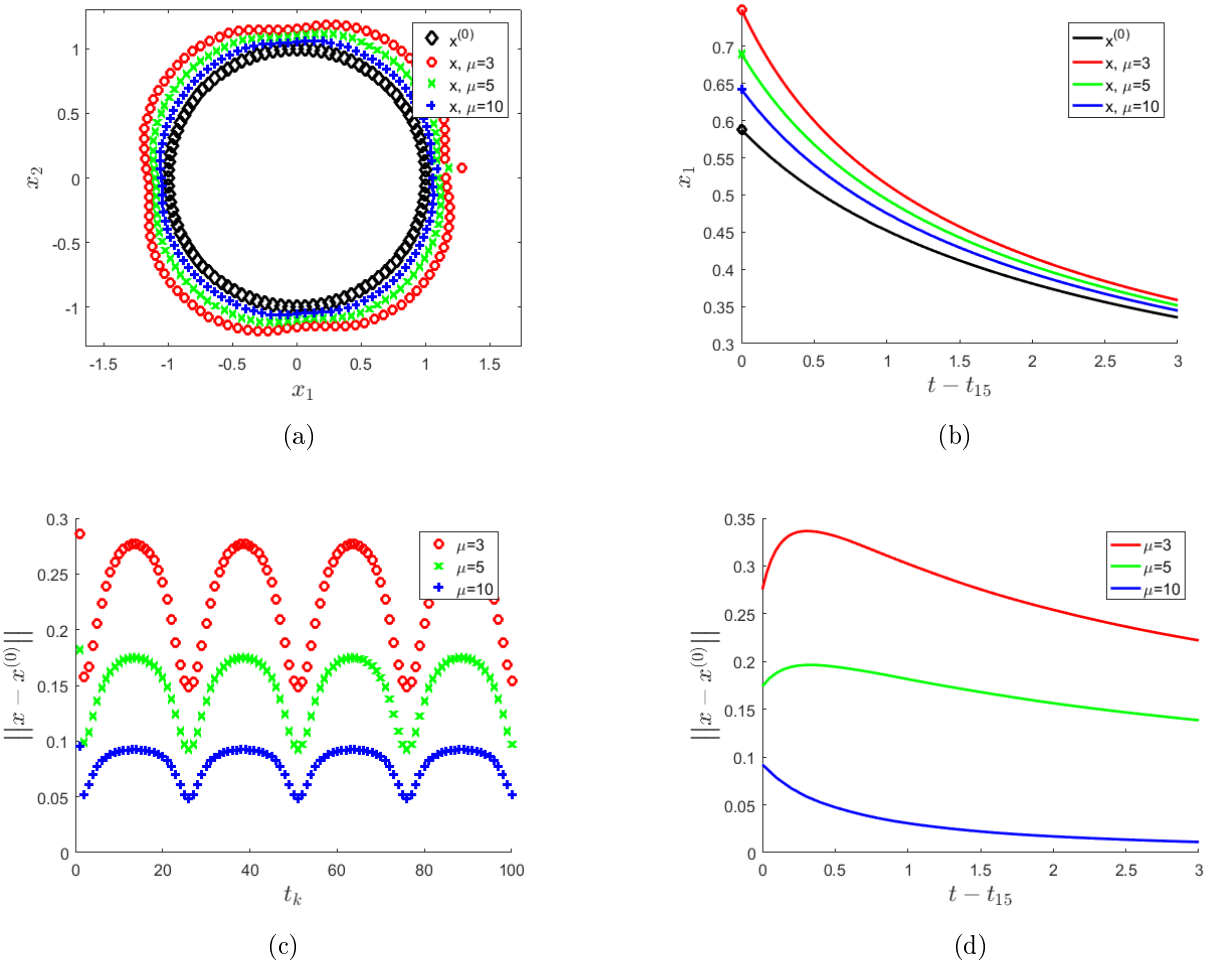

Figure 3.7: Comparison of state evolution for different μ values in the example of Section 3.4.1.2. (a) x trajectories at the discrete update times. (b) x trajectories within a continuous interval. (c) $\left\|x_1 - x_1^{(0)}\right\|$ trajectories at the discrete update times. (d) $\left\|x_1 - x_1^{(0)}\right\|$ trajectories within a continuous interval.

3.4.2 Coupled Discrete-time and Continuous-time System Case

When the continuous and discrete states are separated, more precise results can be found. In this case, the dynamics are of the form

$$\begin{aligned} x^+ &= f(x, z, k; \nu), & t &= t_k \\ \dot{z} &= g(x, z, t; \nu), & t &\neq t_k, \end{aligned} \tag{3.84}$$

so that x is a purely discrete state subject to $x(0) = x_0$ and z is a purely continuous state subject to $z(0) = z_0$. Dynamics in the form (3.84) often arise in hierarchical control schemes where the discrete x subsystem defines a reference command that is carried out by the continuous z subsystem. The dependence on $\nu = 1/(t_k - t_{k-1})$ again encodes any changes in the vector fields due to a different update rate. It will be assumed that the vector fields f and g are bounded, Lipschitz, and sufficiently differentiable in their domains.

See also Chapter 5 for a distributed robotics application involving intermittent communication that makes use of the following results.

3.4.2.1 Asymptotic Analysis and Reduced-Order Models

Similarly to the general case presented in Section 3.4.1, the dynamics (3.84) are rewritten in terms of $\mathbb{T} = \mathbb{R}$ and $\mathbb{T}_k = \{t_k\}$ as

$$\begin{aligned} \frac{\partial x}{\Delta t_k} &= \frac{1}{\mu(k)} \{f(x, z, k; \nu) - x\} \\ \frac{\partial z}{\Delta t} &= g(x, z, t; \nu). \end{aligned} \tag{3.85}$$

with $\mu(k) = t_{k+1} - t_k$ is the graininess of $\mathbb{T}_k$ at the kth update.

Assuming a straightforward asymptotic series solution

$$\begin{aligned} x(t, t_k) &= \sum_{i \geq 0} \mu^{-i} x^{(i)}(t, t_k) \\ z(t, t_k) &= \sum_{i \geq 0} \mu^{-i} z^{(i)}(t, t_k) \end{aligned}$$

in the $\mathbb{T}$ dynamics (3.85) and equating orders of μ then gives the zeroth order dynamics

$$\begin{aligned}\frac{\partial x^{(0)}}{\Delta t_k} &= 0 \\ \frac{\partial z^{(0)}}{\Delta t} &= g(x^{(0)}, z^{(0)}, t; 0).\end{aligned} \tag{3.86}$$

These dynamics describe the evolution of the continuous states on a timescale where there are no updates of the discrete-time subsystem, and are valid for $t = \mathcal{O}(1)$. As in the general case, this model fails to capture the discrete behaviour that occurs when $t = \mathcal{O}(\mu)$. Unlike the general case, however, the distinct discrete and continuous states means that rescaling (3.85) can give further insight into the problem.

To this end, rewrite (3.85) in terms of the slow scales $\tau_t = t/\mu$ and $\tau_k = t_k/\mu$ as

$$\begin{aligned}\frac{\partial x}{\Delta \tau_k} &= \{f(x, z, k; \nu) - x\} \\ \frac{1}{\mu}\frac{\partial z}{\Delta \tau_t} &= g(x, z, t; \nu).\end{aligned}$$

Assuming an asymptotic series solution

$$\begin{aligned}x(t, t_k) &= \sum \mu^{-i} x^{(i)}(\tau_t, \tau_k) \\ z(t, t_k) &= \sum \mu^{-i} z^{(i)}(\tau_t, \tau_k)\end{aligned}$$

and equating orders of μ then yields the new zeroth order dynamics

$$\begin{aligned}\frac{\partial x^{(0)}}{\Delta \tau_k} &= \left\{f(x^{(0)}, z^{(0)}, k; 0) - x^{(0)}\right\} \\ 0 &= g(x^{(0)}, z^{(0)}, t; 0).\end{aligned} \tag{3.87}$$

This reduced model describes the evolution of the discrete state x on a slow scale where the continuous state has reached the solution $z^{(0)} = h(x^{(0)}, t)$ of the algebraic equation $0 = g(x^{(0)}, z^{(0)}, t; 0)$.

As in the continuous-time boundary layer singularities described in Chapter 2, neither (3.86) nor (3.87) individually provide a uniformly valid approximation over the entire time

domain. Together, however, they can provide such an approximation. Based on these investigations, reduced-order models valid both within continuous-time intervals as well as across discrete updates are formally stated as follows.

Decision System Define the equilibrium trajectory of the isolated continuous-time dynamics as a known function $h: D_x \times \mathbb{R}_+ \to D_z$ which satisfies $\dot{h}(p,t) = g(p, h(p,t), t; 0)$ for $p \in D_x$ and $t \in R_+$. The decision system is then defined as

$$x^{(0)}\left(t_k^+\right) = f\left(x^{(0)}(t_k^-), h(x^{(0)}(t_k^-), t_k), k; 0\right), \tag{3.88}$$

subject to $x^{(0)}(t_0) = x_0$.

Interval Correction System Define the kth time interval between discrete-time updates as $\mathcal{I}_k \triangleq \left\{t \in \mathbb{R} \,\middle|\, t_k \leq t < t_{k+1}\right\}$ and the elapsed time within this interval as $\eta \triangleq t - t_k$. The interval correction system is then defined separately for each interval $\mathcal{I}_k$ as

$$\dot{\hat{z}}_k(\eta) = g\left(x^{(0)}(t_k^+), \hat{z}_k(\eta) + h\left(x^{(0)}\left(t_k^+\right), \eta + t_k\right), \eta + t_k; 0\right) - \frac{\partial h\left(x^{(0)}\left(t_k^+\right), \eta + t_k\right)}{\partial t}, \tag{3.89}$$

subject to $\hat{z}_0(0) = z_0 - h\left(x^{(0)}\left(t_0\right), t_0\right)$ for the first interval and $\hat{z}_k(0) = h\left(x^{(0)}\left(t_k^-\right), t_k\right) - h\left(x^{(0)}\left(t_k^+\right), t_k\right)$ otherwise, and where $x^{(0)}$ is the state vector of the decision system defined in (3.88).

The decision system (3.88) describes the reduced-order behaviour of the isolated discrete-time dynamics with the continuous-time dynamics always at their state-dependent equilibrium. Note that the system is purely discrete. The interval correction system (3.89) describes the evolution of the isolated continuous dynamics towards the equilibrium trajectory between each set of consecutive discrete updates. The initial conditions are based on the state vector $x^{(0)}$ of the decision system alone. They are independent of the state of the interval correction system on any previous intervals. Note that the interval correction system describes purely continuous-time dynamics. The new time variable η is introduced here to make clear that

solutions of (3.89) are dependent on the elapsed time and are defined only for a particular interval $\mathcal{I}_k$. While the original dynamics are fully coupled, the reduced-order models (3.88) and (3.89) obtain their triangular structure by exploiting the equilibrium trajectory $h(x^{(0)}, t)$.

Together, (3.88) and (3.89) provide reduced-order descriptions of the original dynamics (3.85). They mirror the classical Reduced Fast and Reduced Slow models for continuous-time dynamics in standard singularly perturbed form described in Section 2.2 as well as the reduced-order models found for discrete, multirate systems in Section 3.3. The validity of these models is investigated next.

3.4.2.2 Bounds on the Reduced-Order Approximation

In this subsection, asymptotic bounds are proven for the reduced-order models (3.86) and (3.87) developed in the previous subsection. The analysis consists of two parts. In the first part, bounds are proven for the fast, continuous z state in between discrete updates of the x state and assuming certain assumptions hold for the initial conditions. The second part then uses these bounds on z to find corresponding bounds for the evolution of the discrete x state.

To this end, the following lemma provides conditions to ensure that the approximation provided by the reduced-order continuous-time $z^{(0)}$ dynamics remains close to the true continuous-time z dynamics between discrete updates, given that the initial conditions of $z^{(0)}$ and $x^{(0)}$ are both close to their corresponding true values at the start of the interval.

Lemma 3.2. *For the dynamics (3.84), further assume that the interval correction system (3.89) is uniformly asymptotically stable for all points $x^{(0)} \in D_x$ and the corresponding known trajectories $h\left(x^{(0)}\left(t_k^+\right), t\right)$. Then, if $z(t_k) - \hat{z}_k(0) - h(x^{(0)}(t_k^+), t_k) = \mathcal{O}(1)$ and $x(t_k^+) - x^{(0)}(t_k^+) = \mathcal{O}(1)$ in the limit $\mu \to \infty$, μ can be chosen large enough that*

$$z(t) - \hat{z}_k(t - t_k) - h(x^{(0)}(t_k^+), t) = \mathcal{O}(1)$$

for all t in the time interval $\mathcal{I}_k = \left\{t \in \mathbb{R} \,\middle|\, t_k \leq t < t_{k+1}\right\}$. Further, there is a t_j with $t_k <$

$t_j \leq t_{k+1}$ *such that*

$$z(t) - h(x^{(0)}(t_k^+), t) = \mathcal{O}(1)$$

holds for all $t \in [t_j, t_{k+1})$.

Proof. The proof of the lemma follows three steps:

1. Formulate the dynamics of the continuous-state approximation error over an interval as a perturbed version of the interval correction dynamics.

2. Use the stability of the interval correction system and a converse Lyapunov theorem to obtain a Lyapunov function with certain desirable bounding properties for the interval correction dynamics.

3. Use the interval correction dynamics' Lyapunov function as well as the form of the perturbation in the dynamics of the continuous-state approximation error to obtain bounds on the norm of this approximation error.

The steps are detailed as follows:

Step 1:

In the following, all instances of $x(t_k^+)$ will be written as x and all instances of $x^{(0)}(t_k^+)$ as $x^{(0)}$ for conciseness since both $x(t_k^+)$ and $x^{(0)}(t_k^+)$ are constant over the interval $\mathcal{I}_k$ where the analysis is performed.

Define the error in the approximation over the interval $\mathcal{I}_k$ as $e_z(\eta) \triangleq z(\eta + t_k) - h(x^{(0)}, \eta + t_k) - \hat{z}_k(\eta)$. The error dynamics within the interval is then written as

$$\begin{aligned} \frac{de_z}{d\eta} &= \frac{d}{d\eta}\left[z(\eta + t_k) - h(x^{(0)}, \eta + t_k) - \hat{z}_k(\eta)\right] \\ &= \dot{z}(\eta + t_k) - \frac{\partial h(x^{(0)}, \eta + t_k)}{\partial t} - \dot{\hat{z}}_k(\eta). \end{aligned}$$

Now, with $\dot{z}$ defined in (3.84) and $\dot{\hat{z}}_k$ defined in (3.89), the error dynamics are

$$\begin{aligned}
\frac{de_z}{d\eta} &= g\left(x, z\left(\eta+t_k\right), \eta+t_k; \nu\right) - \frac{\partial h(x^{(0)}, \eta+t_k)}{\partial t} \\
&\quad - \left\{ g\left(x^{(0)}, \hat{z}_k(\eta) + h\left(x^{(0)}, \eta+t_k\right), \eta+t_k; 0\right) - \frac{\partial h\left(x^{(0)}, \eta+t_k\right)}{\partial t} \right\} \\
&= g\left(x, z, \eta+t_k; \nu\right) - g\left(x^{(0)}, \hat{z}_k + h\left(x^{(0)}, \eta+t_k\right), \eta+t_k; 0\right) \\
&\quad + \left\{ g\left(x^{(0)}, z, \eta+t_k; \nu\right) - g\left(x^{(0)}, z, \eta+t_k; \nu\right) \right\} \\
&\quad + \left\{ g\left(x^{(0)}, z, \eta+t_k; 0\right) - g\left(x^{(0)}, z, \eta+t_k; 0\right) \right\} \\
&\quad + \left\{ g\left(x^{(0)}, e_z + h\left(x^{(0)}, \eta+t_k\right), \eta+t_k; 0\right) - g\left(x^{(0)}, e_z + h\left(x^{(0)}, \eta+t_k\right), \eta+t_k; 0\right) \right\} \\
&\quad + \left\{ g(x^{(0)}, h(x^{(0)}, \eta+t_k), \eta+t_k; 0) - \frac{\partial h(x^{(0)}, \eta+t_k)}{\partial t} \right\} \\
&= g\left(x^{(0)}, e_z + h\left(x^{(0)}, \eta+t_k\right), \eta+t_k; 0\right) - \frac{\partial h(x^{(0)}, \eta+t_k)}{\partial t} \\
&\quad + \underbrace{\left\{ g\left(x^{(0)}, e_z + \hat{z}_k + h\left(x^{(0)}, \eta+t_k\right), \eta+t_k; 0\right) - g\left(x^{(0)}, e_z + h\left(x^{(0)}, \eta+t_k\right), \eta+t_k; 0\right) \right.}_{\Delta_1} \\
&\qquad \underbrace{\left. - g\left(x^{(0)}, \hat{z}_k + h\left(x^{(0)}, \eta+t_k\right), \eta+t_k; 0\right) + g(x^{(0)}, h(x^{(0)}, \eta+t_k), \eta+t_k; 0) \right\}}_{\Delta_1} \\
&\quad + \underbrace{\left\{ g\left(x^{(0)}, z, \eta+t_k; \nu\right) - g\left(x^{(0)}, z, \eta+t_k; 0\right) \right\}}_{\Delta_2} \\
&\quad + \underbrace{\left\{ g\left(x, z, \eta+t_k; \nu\right) - g\left(x^{(0)}, z, \eta+t_k; \nu\right) \right\}}_{\Delta_3},
\end{aligned}$$

using $z(\eta+t_k) = e_z(\eta) + h(x^{(0)}, \eta+t_k) + \hat{z}_k(\eta)$ by definition of the approximation error, and $g\left(p, h(p, \eta+t_k), \eta+t_k; 0\right) - \frac{\partial h(p, \eta+t_k)}{\partial t} = 0$ for $p \in D_x$ by definition of the equilibrium trajectory. That is, the error dynamics may be written as

$$\frac{de_z}{d\eta} = g\left(x^{(0)}, e_z + h\left(x^{(0)}, \eta+t_k\right), \eta+t_k; 0\right) - \frac{\partial h(x^{(0)}, \eta+t_k)}{\partial t} + \Delta G, \tag{3.90}$$

a perturbed version of the interval correction dynamics (3.89), where the perturbation is $\Delta G = \Delta_1 + \Delta_2 + \Delta_3$.

Now, the first component of the perturbation satisfies

$$\begin{aligned}
\|\Delta_1\| &= \Big\| g\left(x^{(0)}, e_z + \hat{z}_k + h\left(x^{(0)}, \eta + t_k\right), \eta + t_k; 0\right) - g\left(x^{(0)}, e_z + h\left(x^{(0)}, \eta + t_k\right), \eta + t_k; 0\right) \\
&\qquad - g\left(x^{(0)}, \hat{z}_k + h\left(x^{(0)}, \eta + t_k\right), \eta + t_k; 0\right) + g(x^{(0)}, h(x^{(0)}, \eta + t_k), \eta + t_k; 0) \Big\| \\
&= \left\| \int_{h(x^{(0)}, \eta + t_k)}^{\hat{z}_k + h(x^{(0)}, \eta + t_k)} \left(\frac{\partial g(x^{(0)}, s + e_z, \eta; 0)}{\partial z} - \frac{\partial g(x^{(0)}, s, \eta; 0)}{\partial z} \right) \mathrm{d}s \right\| \\
&\leq \left\| \int_{h(x^{(0)}, \eta + t_k)}^{\hat{z}_k + h(x^{(0)}, \eta + t_k)} M \|e_z\| \, \mathrm{d}s \right\| \\
&\leq M \|e_z\| \, \|\hat{z}_k\| ,
\end{aligned}$$

over the domain for some $M \geq 0$ since g is continuously differentiable. The second component has the bound

$$\begin{aligned}
\|\Delta_2\| &= \left\| g(x^{(0)}, z, \eta + t_k; \nu) - g(x^{(0)}, z, \eta + t_k; 0) \right\| \\
&\leq \mu L_4
\end{aligned}$$

over the domain for some $L_4 \geq 0$ since g is Lipschitz in its last argument. The third component is then similarly bounded by

$$\begin{aligned}
\|\Delta_3\| &= \left\| g\left(x, z, \eta + t_k; \nu\right) - g\left(x^{(0)}, z, \eta + t_k; \nu\right) \right\| \\
&\leq L_1 \left\| x - x^{(0)} \right\|
\end{aligned}$$

over the domain for some $L_1 \geq 0$ since g is Lipschitz in its first argument. Therefore the overall perturbation bounds

$$\|\Delta G\| \leq \left(M \|\hat{z}_k\|\right) \|e_z\| + \left\{ L_1 \left\| x - x^{(0)} \right\| + \mu L_4 \right\} \tag{3.91}$$

hold over the domain.

Step 2:

By assumption, the interval correction system (3.89) is uniformly asymptotically stable for each $x^{(0)} \in D_x$. Therefore, by the converse Lyapunov theorem [62, Theorem 4.16]

there exists a Lyapunov function V over some domain $D_V = \left\{ \hat{z}_k \in \mathbb{R}^n \;\middle|\; \|\hat{z}_k\|_2 < r \right\}$ for the dynamics that satisfies the inequalities

$$\alpha_1 \left(\|\hat{z}_k\| \right) \leq V(\eta, \hat{z}_k) \leq \alpha_2 \left(\|\hat{z}_k\| \right),$$
$$\frac{\partial V}{\partial \eta} + \frac{\partial V}{\partial \hat{z}_k} \left\{ g\left(x^{(0)}, \hat{z}_k + h\left(x^{(0)}, \eta + t_k \right), \eta + t_k; 0 \right) - \frac{\partial h(x^{(0)}, \eta + t_k)}{\partial t} \right\} \leq -\alpha_3 \left(\|\hat{z}_k\| \right),$$

and

$$\left\| \frac{\partial V}{\partial \hat{z}_k} \right\| \leq \alpha_4 \left(\|\hat{z}_k\| \right)$$

for class $\mathcal{K}$ functions α_i defined on $[0, r]$.

Step 3:

In (3.91), the perturbation ΔG in the error dynamics (3.90) has been shown to satisfy

$$\|\Delta G\| \leq \gamma(\eta) \|e_z\| + d,$$

with $\gamma(\eta) = (M \|\hat{z}_k\|) \|e_z\|$ and $d = L_1 \left\| x - x^{(0)} \right\| + \mu L_4$. Due to the asymptotic stability of the interval correction dynamics,

$$\|\hat{z}_k\| \leq \beta_1(\|\hat{z}_k(0)\|, \eta), \; \forall \; 0 \leq \eta < t_{k+1} - t_k \tag{3.92}$$

for some class $\mathcal{KL}$ function β_1. Now, $\gamma(\eta) = M\beta_1(\|\hat{z}_k(0)\|, \eta)$ and d are both non-negative, continuous, and bounded for all $0 \leq \eta \leq t_{k+1} - t_k$. Since $\left\| x - x^{(0)} \right\| = \mathcal{O}(1)$ and $e_z(0) = \mathcal{O}(1)$, μ can be chosen, dependent on r (the same r that defines D_V) and for $0 \leq \eta \leq t_{k+1} - t_k$, small enough that

$$\begin{aligned} \gamma(\eta) \|e_z\| + d &= M\beta_1(\|\hat{z}_k(0)\|, \eta) \|e_z\| \\ &\quad + L_1 \left\| x - x^{(0)} \right\| + \mu L_4 \\ &\leq \delta < \theta \alpha_3 \left(\alpha_2^{-1} \left(\alpha_1 \left(r \right) \right) \right) / \alpha_4(r), \end{aligned}$$

with $\|e_z\| < r$, $\delta \in \mathbb{R}_+$, and θ a positive constant with $\theta < 1$. Therefore, by [62, Lemma 9.3], there is a small enough $\|e_z(0)\|$ such that trajectories of the approximation error system (3.90) satisfy

$$\|e_z(\eta)\| \leq \beta_2(\|e_z(0)\|, \eta), \; \forall \; 0 \leq \eta < \bar{\eta}$$

and

$$\|e_z(\eta)\| \leq \alpha_5(\delta),\ \forall\, \bar{\eta} \leq \eta \leq t_{k+1} - t_k$$

for some class $\mathcal{KL}$ function β_2, some finite $\bar{\eta}$, and α_5 the class κ function defined by

$$\alpha_5(\delta) = \alpha_1^{-1}\left(\alpha_2\left(\alpha_3^{-1}\left(\frac{\delta\alpha_4(r)}{\theta}\right)\right)\right).$$

This gives the bound on $z(t) - h(x^{(0)}, t) - \hat{z}_k(t - t_k)$ for all $t_k \leq t < t_{k+1}$. Since (3.92) gives an asymptotically decaying bound on $\|\hat{z}_k\|$, μ can be chosen large enough that there exists a t_j with $t_k < t_j \leq t_{k+1}$ such that $\|\hat{z}_k(t - t_k)\| = \wp(1)$ for $t \geq t_j$ and thus $z(t) - h(x^{(0)}, t) = \wp(1)$ holds for all $t \in [t_j, t_{k+1})$. □

In Lemma 3.2, the Landau 'little-Oh' $\wp(1)$ bounds on the approximation error of the continuous state over an interval can be interpreted as saying that this error decreases asymptotically as μ grows large even though the reduced-order model is not quite the same as the full model and the approximation starts from different initial conditions than the true dynamics. This is a result of the assumption of uniform asymptotic stability for (3.89), which allows the continuous dynamics to eventually evolve to a known trajectory when $x^{(0)}$ is known. As described by the following lemma, tighter bounds on this approximation error can be found under the more restrictive assumption of exponential stability for (3.89).

Lemma 3.3. *Under the conditions of Lemma 3.2, if instead the errors in the initial conditions are $\mathcal{O}(\mu^{-1})$ and the interval correction system (3.89) is exponentially stable for all points $x^{(0)} \in D_x$ and their corresponding known trajectories $h\left(x^{(0)}\left(t_k^+\right), t\right)$, then the $\wp(1)$ bounds on the approximation in Lemma 3.2 are replaced by $\mathcal{O}(\mu^{-1})$ bounds.*

Proof. The proof adopts the same three-step structure as the proof of Lemma 3.2, with the following changes:

Step 1: Follows identically.

Step 2: By [62, Theorem 4.14], the conditions on the converse Lyapunov function V are satisfied with $\alpha_i\left(\|\hat{z}_k\|\right) = c_i\|\hat{z}_k\|^2$ for $i = 1, 2, 3$ and $\alpha_4\left(\|\hat{z}_k\|\right) = c_4\|\hat{z}_k\|$ for positive constants c_1–c_4.

Step 3: Since exponential stability holds, then the bound on $\|\hat{z}_k\|$ in (3.92) is of the form $\beta_1(\|\hat{z}_k(0)\|, \eta) = k\,\|\hat{z}_k(0)\|\, e^{-a\eta}$. Further, $\int_0^\eta \gamma(\tau)d\tau \leq 0 \cdot \eta + \omega$ for some non-negative constant ω. Define $a = \frac{1}{2}\frac{c_3}{c_2} > 0$ and $p = \exp\left(\frac{c_4\omega}{2c_1}\right) \geq 1$, where the c_i come from the bounds on the converse Lyapunov function V, and choose μ large enough that $e_z(0) = z(t_k) - \hat{z}_k(0) - h(x^{(0)}(t_k^+), t_k) = \mathcal{O}(\mu^{-1})$ satisfies $\|e_z(0)\| < \frac{r}{p}\sqrt{\frac{c_1}{c_2}}$ and small enough that $d < \frac{2c_1 ar}{c_4 p}$. Using the comparison method [62, Lemma 9.4], trajectories of the approximation error system (3.90) therefore satisfy the norm bound

$$\|e_z(\eta)\| \leq \sqrt{\frac{c_2}{c_1}} p\,\|e_z(0)\|\, e^{-\alpha\eta} + \frac{c_4 p}{2c_1} d \int_0^\eta e^{-a(\eta-\tau)} \mathrm{d}\tau,$$

where the first term is of $\mathcal{O}(\mu^{-1})$ for all $\eta \geq 0$ if $\|e_z(0)\| = \mathcal{O}(\mu^{-1})$, and the second term is of $\mathcal{O}(\mu^{-1})$ because d is and since the integral is bounded for all $\eta \geq 0$. This gives the bound on $z - h(x^{(0)}, t) - \hat{z}_k(t - t_k)$ for all $t_k \leq t < t_{k+1}$. Since $\|\hat{z}_k\|$ has an exponentially decaying bound in η, μ can be chosen large enough that there exists a t_j with $t_k < t_j \leq t_{k+1}$ such that $\|\hat{z}_k(t - t_k)\| = \mathcal{O}(\mu^{-1})$, giving the desired bound on $z(t) - h(x^{(0)}, t)$. □

Under the more stringent condition of exponential stability for (3.89), the Landau 'big-Oh' $\mathcal{O}(\mu^{-1})$ bounds gives a stricter statement of the rate of the approximation error's decrease as μ grows large. This is possible because exponential stability gives concrete time bounds for the evolution of z towards $h(x^{(0)}, t)$ in Step 3 of the lemma.

With Lemmas 3.2 and 3.3 in place, the validity of approximating the coupled hybrid-time system (3.84) by dynamics of the reduced-order models (3.88) and (3.89) can now be determined.

Theorem 3.5. *For the dynamics (3.84), assume that the interval correction system (3.89) is uniformly asymptotically stable for all points $x^{(0)} \in D_x$ and the corresponding known trajectories $h\left(x^{(0)}\left(t_k^+\right), t\right)$. Then, for the reduced-order models $x^{(0)}$ and $\hat{z}$ respectively characterized in (3.88) and (3.89), and any $t_f \geq t_0$, there exists a μ_0, $0 < \mu_0 < \infty$, such that for all $\mu \geq \mu_0$*

the approximations

$$\begin{aligned} x(t_k^+) &= x^{(0)}(t_k^+) + \mathcal{O}(1) \\ z(t) &= h\left(x^{(0)}\left(t_k^+\right), t\right) + \hat{z}_k(t - t_k) + \mathcal{O}(1) \end{aligned}$$

are valid for all $t \in [t_0, t_f]$. *Further, for each interval* $\mathcal{I}_k$ *between discrete updates with* $t_k < t_f$, *there is a* t_j *with* $t_k < t_j \leq t_{k+1}$ *such that the approximation*

$$z = h\left(x^{(0)}\left(t_k^+\right), t\right) + \mathcal{O}(1)$$

holds for all $t \in [t_j, t_{k+1})$.

Proof. The proof uses induction to follow the error in the approximation for x over discrete updates, with the error in the z approximation bounded over the continuous-time intervals using Lemma (3.2).

Define $e_x(t_k^+; \mu) = x(t_k^+; \mu) - x^{(0)}(t_k^+)$. Suppose for some k that $\left\|x(t_k^-) - x^{(0)}(t_k^-)\right\| = \mathcal{O}(1)$ and $\left\|z(t_k - \mu) - h\left(x^{(0)}\left(t_k^-\right), t_k - \mu\right)\right\| = \mathcal{O}(1)$. Then, under the assumption of uniform asymptotic stability of (3.89), μ can be always be chosen large enough that $\left\|z(t_k) - h\left(x^{(0)}\left(t_k^-\right), t_k^-\right)\right\| = \mathcal{O}(1)$ by Lemma (3.2). Further, after the transition

$$\begin{aligned} \left\|e_x(t_k^+; \mu)\right\| &= \left\|f\left(x\left(t_k^-\right), z(t_k), k; \nu\right) - f\left(x^{(0)}(t_k^-), h\left(x^{(0)}\left(t_k^-\right), t_k\right), k; 0\right)\right\| \\ &\leq P_1 \left\|x(t_k^-) - x^{(0)}(t_k^-)\right\| + P_2 \left\|z(t_k) - h\left(x^{(0)}\left(t_k^-\right), t_k\right)\right\| + P_4\mu \\ &= \mathcal{O}(1), \end{aligned}$$

using the Lipschitz property of f, so that $\left\|x(t_k^+) - x^{(0)}(t_k^+)\right\| = \mathcal{O}(1)$. From the initial conditions and the assumption that x_0 and z_0 are $\mathcal{O}(1)$ and Lipschitz, $\left\|x(t_1^-) - x^{(0)}(t_1^-)\right\| = \left\|x(t_0^+) - x^{(0)}(t_0^+)\right\| = \|x_0(\mu) - x_0(0)\| = \mathcal{O}(\mu)$ and $\left\|z(t_0) - \hat{z}_0(0) - h(x^{(0)}(t_0^+), t_0)\right\| = \|z_0(\mu) - z_0(0)\| = \mathcal{O}(\mu)$, and are thus both $\mathcal{O}(1)$. Therefore, μ can be chosen large enough that the approximations

$$\begin{aligned} x(t_k^+) &= x^{(0)}(t_k^+) + \mathcal{O}(1) \\ z(t) &= h(x^{(0)}(t_k^+), t) + \hat{z}_k(t - t_k) + \mathcal{O}(1) \end{aligned}$$

hold by induction for any finite number of discrete updates, and thus are valid for all $t \in [t_0, t_f]$. The bound on z for $t \in [t_j, t_{k+1})$ then comes from application of Lemma 3.2. $\square$

Again, stricter bounds on the approximation errors may be found by assuming exponential stability of the interval correction system.

Corollary 3.1. *Under the conditions of Theorem 3.5, if the interval correction system (3.89) is instead exponentially stable for all points $x^{(0)} \in D_x$ and their corresponding known trajectories $h\left(x^{(0)}\left(t_k^+\right), t\right)$, then the $\mathcal{O}(1)$ bounds on the approximation in Theorem 3.5 are replaced by $\mathcal{O}(\mu^{-1})$ bounds.*

Proof. The desired results follow identically to the proof of Theorem 3.5 by noting that 1) both $\|x_0(\mu) - x_0(0)\| = \mathcal{O}(\mu^{-1})$ and $\|z_0(\mu) - z_0(0)\| = \mathcal{O}(\mu^{-1})$ hold since x_0 and z_0 are Lipschitz, 2) the continuous-interval bounds given by Lemma 3.3 may be used instead of the bounds given by Lemma 3.2 since the stricter requirement of (3.89) being exponentially stable is met here. $\square$

Theorem 3.5 provides a certificate that (3.88) and (3.89) are good approximations of (3.84) as μ grows large, with the trajectories of the reduced-order approximations remaining asymptotically close to the trajectories of the full system. Intuitively, the error bounds grow smaller as the update period grows because the continuous-time dynamics have more time to reach their equilibrium trajectory, making the reduced-order models more accurate. Corollary 3.5 then provides stricter bounds on the approximation error by assuming exponential stability instead of asymptotic stability, as in Lemma 3.3. These results gives mathematical rigour to the intuitive notion of a separation principle between the continuous-time and discrete-time dynamics as the time between discrete updates increases.

Chapter 4

APPLICATION TO ORBIT PROPAGATION

Effective tracking of space objects requires efficient and accurate trajectory propagation algorithms that are valid across time horizons of varying lengths (because it is not necessarily known when measurements will next be available) and that are able to appropriately handle perturbation forces that are not constant in direction or magnitude (sometimes atmospheric drag dominates, while other times geopotential perturbations dominate). On the one hand, computational efficiency of the trajectory propagation algorithm is a necessary consideration not only due to the vast number of space objects to be propagated, but also because the presence of many small perturbing forces (*e.g.*, Earth-oblateness, atmospheric drag, solar perturbation, etc.) cause the equations of motion to be numerically stiff. Viable propagation methods must therefore grapple with this stiffness. On the other hand, numerical accuracy in the trajectory solution is required over long time periods to maintain custody of known objects with sparse measurements. Any approximation of the true trajectory, to deal with the numerical stiffness in the equations of motion, induces errors that can accumulate over time. It is therefore necessary to understand how quickly and to what extent these errors manifest within a given propagation method. Further complicating propagation is that, while the conservative effects on a satellite's orbit due to the two-body and geopotential perturbation forces have been well characterized and their effects rigorously understood, non-conservative forces such as atmospheric drag and solar radiation pressure are subject to parametric uncertainties that complicate analysis. To this end, trajectory propagation methods are desired that give insight into how these uncertainties manifest in position and velocity errors over time [3], without sole reliance on numerical methods (*e.g.,* Monte Carlo).

This chapter develops a new propagation technique using MMS, based on the author's

works [63, 64]. Unlike existing approaches to orbit propagation, the method developed here gives direct information about how a non-conservative perturbation affects trajectories at particular orders of the perturbation through the form of the trajectory solution. This information includes both how the perturbation manifests in specific dynamic states as well as the length of time the solution is valid for. The basic idea is to mathematically separate the effects of the perturbing acceleration that manifest on a slow timescale from the central-body gravitational effects that manifest on a fast timescale. The trajectory solution is then constructed by numerically integrating the slow timescale derivatives along with the fast timescale derivatives which are known analytically. There are three major benefits to the orbit solution determined in this chapter. First, the derived approximations have error and period of validity of known orders that are directly linked to the parameters of the perturbing force. This information is essential to effectively task sensors while retaining custody of tracked space objects. Second, the trajectories are efficient to compute as compared to straightforward integration of the equations of motion. Third, posing the orbit approximation in multiple timescale form allows an expression to be derived for the sensitivity of the trajectory to parameters of the perturbing force, yielding the desired insight into the effects of uncertainty in these parameters.

4.1 Literature Review

Approaches to the problem of propagating a perturbed satellite's trajectory can be broadly categorized as: 1) analytic, 2) semi-analytic, or 3) purely numeric [65]. Analytic methods have the benefit of allowing large time-steps when solving the equations of motion. However, there are limitations to these approaches. For example, the use of canonical transforms [66] can lead to intractable integrals or are applicable to a small subset of orbit regimes, while Lie series approaches [67, 68] can lead to recursive, implicit solutions as opposed to explicit expressions. Further, many analytic approaches are limited to small regimes of eccentricity [69] or can only be applied to restricted models of the perturbing acceleration [70, 71]. Semi-

analytic approaches separate long-period and short-period trends, allowing analytic results to be applied for the short-period effects while applying numeric methods for the long-period effects. This separation allows semi-analytic methods to generate high-accuracy trajectory approximations with low computation time as compared to pure numeric approaches [65]. Examples of semi-analytic methods include the Draper Semianalytic Satellite Theory [72], Liu and Alford's Semianalytic Theory for a Close-Earth Artificial Satellite [73], and O'Brien and Sang's Semianalytic Satellite Theory Using the Method of Multiple Scales [74]. The existing semi-analytic methods, however, treat the drag contribution as a purely numerical computation through either direct integration, Fourier decomposition, or polynomial fits. These methods therefore do not provide the explicit insight (*i.e.,* without directly propagating multiple trajectories) into the effects of differences between predicted and actual perturbation parameters on the satellite trajectory that is desired for space situational awareness.

4.2 Problem Formulation

The equations of motion of a satellite subject to a perturbing acceleration may be written in the form

$$\frac{dk}{dt} = \begin{bmatrix} \mathbf{0} \\ n(k) \end{bmatrix} + \varepsilon g_{\text{Pert.}}(k,t) \tag{4.1}$$

where k is a given orbital element set such as the Keplerian or equinoctial elements, $n(k)$ is the (state-dependent) mean angular motion (rad/s), and the parameter ε is a small, positive number common to all components of the acceleration. This parameter can be thought of as a measure of the strength of the perturbing acceleration. To see how the form (4.1) arises, consider an acceleration parametrized as $\vec{a} = \varepsilon f_v \hat{e}_v + \varepsilon f_h \hat{e}_h + \varepsilon f_n \hat{e}_n$ in km/s^2, where $\hat{e}_v$, $\hat{e}_h$, and $\hat{e}_n$ are unit vectors respectively in the direction of orbiting velocity, in the direction of angular momentum, and in the direction that completes the right-handed orthogonal coordinate frame. Gauss' variational equations then give the perturbed equations of motion

in Keplerian elements as

$$\begin{aligned}
\frac{da}{dt} &= \frac{2a^2v}{\mu}\varepsilon f_v \\
\frac{de}{dt} &= \frac{1}{v}\left(\frac{r}{a}\sin\nu\,\varepsilon f_n + 2\left(e+\cos\nu\right)\varepsilon f_v\right) \\
\frac{di}{dt} &= \frac{r\cos\theta}{h}\varepsilon f_h \\
\frac{d\Omega}{dt} &= \frac{r\sin\theta}{h\sin i}\varepsilon f_h \\
\frac{d\omega}{dt} &= \frac{1}{ev}\left(-\left(2e+\frac{r}{a}\right)\cos\nu\,\varepsilon f_n + 2\sin\nu\,\varepsilon f_v\right) - \frac{r\sin\theta\cos i}{h\sin i}\varepsilon f_h \\
\frac{dM}{dt} &= \sqrt{\frac{\mu}{a^3}} + \frac{b}{aev}\left(\frac{r}{a}\cos\nu\,\varepsilon f_n - 2\left(1+e^2\frac{r\mu}{h^2}\right)\sin\nu\,\varepsilon f_v\right),
\end{aligned} \tag{4.2}$$

where a is the semi-major axis (km), e is the eccentricity, i is the inclination angle (rad), Ω is the argument of the ascending node (rad), ω is the argument of the periapsis (rad), M is the mean anomaly (rad), v is the velocity of the satellite (km/s), r is its radius from the central body (km), $b = a/\sqrt{1-e^2}$, h is the magnitude of the orbit angular momentum (km^2/s), θ is the argument of the latitude (rad), ν is the true anomaly (rad), and μ is the gravitational coefficient (km^3/s^2) [75]. This is in the form of (4.1), as desired. Similar expressions exist for other orbital element sets such as the equinoctial elements.

In the particular case of atmospheric drag, for example, the corresponding acceleration is

$$\vec{a}_{\text{Drag}} = -\frac{AC_d}{2m}\rho\left(\vec{r}\right)\left\|\vec{v}-\vec{v}_{atm}\right\|\left(\vec{v}-\vec{v}_{atm}\right), \tag{4.3}$$

where A is the reference area of the satellite (km^2), m is the mass of the satellite (kg), C_d is the drag coefficient, $\rho(\vec{r})$ is the position-dependent atmospheric density function (kg/km^3), $\vec{v}$ is the velocity of the satellite (km/s), and $\vec{v}_{atm}$ is the velocity of the atmosphere (km/s). The perturbation parameter is defined from (4.3) by

$$\varepsilon = \frac{AC_d}{2m}\rho_0, \tag{4.4}$$

where ρ_0 is the nominal density (*e.g.,* the density at perigee of the initial instantaneous orbit). The corresponding perturbation function $g_{\text{Drag}}(k,t)$ is then written for Keplerian elements directly from (4.3) and (4.2).

In the following developments, the Keplerian element set $k = [a,\, e,\, i,\, \Omega,\, \omega,\, M]^T$ will be used as in (4.2). Note that in (4.2), a numerical divide by zero will occur for argument of perigee and mean anomaly as eccentricity deteriorates to zero. Other coordinates such as modified equinoctial elements [72] can be utilized to circumvent this problem. However, Keplerian elements are used here in order to easily demonstrate and convey the power of the MMS for orbit trajectory prediction and motion insight.

4.3 Trajectory Solutions with MMS

The perturbed satellite dynamics (4.1) exhibit multiple timescale behavior, where trajectories obey the unperturbed dynamics on a fast timescale (the satellite locally evolves according to Keplerian dynamics) but behave very differently on a slow timescale (eventually, the perturbing acceleration significantly effects the satellite's trajectory). This behaviour is a consequence of the structure of the dynamics and, as noted in Section 2.3, is associated with a secular singularity when attempting to construct an asymptotic approximation to the trajectory solution that is valid for a large time domain. In this section, MMS is therefore applied to (4.1) to overcome this challenge and construct a uniformly valid trajectory solution that rigorously incorporates the satellite's behaviour on both the slow and the fast timescales.

To this end, search for an approximation k_ε to the exact solution k of (4.1) in the form of a two-time asymptotic expansion in the perturbation parameter

$$k_\varepsilon(\eta, \tau; \varepsilon) = \sum_{i \geq 0} \varepsilon^i k^{(i)}(\eta, \tau), \tag{4.5}$$

where the fast time $\eta = t$ and the slow time $\tau = \varepsilon t$ are treated as independent (see Section 2.3 for more details). Practically, an expansion in this form is attractive because it means that, for small enough ε, higher-order terms in the series (4.5) are "well-behaved" and do not dominate the overall solution.

The procedure for generating k_ϵ is as follows:

Step 1. Expand the first derivative with (4.5) as

$$\frac{dk_\varepsilon}{dt} = \frac{\partial k_\varepsilon}{\partial \eta} + \varepsilon \frac{\partial k_\varepsilon}{\partial \tau}. \tag{4.6}$$

Step 2. Use the asymptotic expansion (4.5) and the two-time derivatives (4.6) in the perturbed equations of motion (4.1).

Step 3. Equate orders of ε to find ordered dynamic equations.

Step 4. Sequentially solve the resulting ordered dynamic equations. The ordered solutions k_i are chosen such that the resulting power series in the perturbation parameter, (4.5), is asymptotic and uniform in t; that is,

$$\lim_{\varepsilon \to 0^+} \frac{\varepsilon k_{i+1}(t, \varepsilon t)}{k_i(t, \varepsilon t)} = 0 \tag{4.7}$$

for t up to $\mathcal{O}(\varepsilon^{-1})$.

Following this process, the dynamics (4.1) are rewritten in terms of the two-time derivatives as

$$\frac{\partial k_\varepsilon}{\partial \eta} + \varepsilon \frac{\partial k_\varepsilon}{\partial \tau} = \begin{bmatrix} \mathbf{0}_{5\times 1} \\ \sqrt{\mu / k_{\varepsilon,1}^3} \end{bmatrix} + \varepsilon g_{\text{Pert.}}(k_\varepsilon, t).$$

Substituting the asymptotic series expansion (4.5) and equating orders of ε, the zeroth order equation is then found to be

$$\frac{\partial k^{(0)}}{\partial \eta} = \begin{bmatrix} \mathbf{0}_{5\times 1} \\ \sqrt{\mu / k_1^{(0)^3}} \end{bmatrix}, \tag{4.8}$$

subject to the original initial conditions $k^{(0)}(0,0) = k(0)$, while the first order equation is found as

$$\frac{\partial k^{(1)}}{\partial \eta} + \frac{\partial k^{(0)}}{\partial \tau} = \begin{bmatrix} \mathbf{0}_{5\times 1} \\ -\frac{3}{2} k_1^{(1)} \sqrt{\mu / k_1^{(0)^5}} \end{bmatrix} + g_{\text{Pert.}}(k^{(0)}, \eta), \tag{4.9}$$

subject to the initial conditions $k^{(1)}(0,0) = \mathbf{0}$.

The zeroth order equation (4.8) has solutions of the form

$$k^{(0)}(\eta,\tau) = k^{(0)}(\tau) + \begin{bmatrix} \mathbf{0}_{5\times 1} \\ \sqrt{\mu/k_1^{(0)^3}} \end{bmatrix} \eta, \tag{4.10}$$

subject to $k^{(0)}(0) = k(0)$ and where the dependence on τ will be determined by enforcing asymptoticity of $k^{(0)}$ and $\varepsilon k^{(1)}$. These asymptoticity conditions are derived next.

The first order equation (4.9) can be rewritten in state-space form as

$$\frac{\partial k^{(1)}}{\partial \eta} = \begin{bmatrix} \mathbf{0}_{5\times 1} & \mathbf{0}_{5\times 5} \\ -\frac{3}{2}\sqrt{\mu/k_1^{(0)^5}} & \mathbf{0}_{1\times 5} \end{bmatrix} k^{(1)} + \left(g_{\text{Pert.}}(k^{(0)},\eta) - \frac{\partial k^{(0)}}{\partial \tau} \right).$$

That is, as

$$\dot{k}^{(1)} = Ak^{(1)} + b(\eta) \tag{4.11}$$

where $b(\eta)$ is periodic in η with period

$$P = 2\pi\sqrt{k_1^{(0)^3}/\mu}.$$

Following [76], define the adjoint system as

$$\dot{\zeta} = -A^T\zeta.$$

Then, denoting n linearly independent and P-periodic solutions of the adjoint system by $\zeta^1, \zeta^2, \ldots, \zeta^n$, [76, Theorem 2.3.4] states that (4.11) has P-periodic solutions if and only if the orthogonality conditions

$$\int_0^P \zeta^{iT}(\eta) b(\eta) d\eta = 0$$

hold, and otherwise the solution will display secular behaviour. Now, while periodicity is required for the first five elements of the first order solution, $k_{1:5}^{(1)}$, so that they remains asymptotic to the corresponding elements of the zeroth order solution defined in (4.10), the sixth element $k_6^{(0)}$ grows linearly with time and thus linear secular growth is allowed in $k_6^{(1)}$.

Due to the separation of (4.11), for conditions on $k_{1:5}^{(1)}$ consider instead the periodicity of the system

$$\dot{k}_{1:5}^{(1)} = A_{1:5,1:5} k_{1:5}^{(1)},$$

which has the associated adjoint system

$$\dot{\zeta}_{1:5} = -\left(A_{1:5,1:5}\right)^T \zeta_{1:5}.$$

Write

$$-\left(A_{1:5,1:5}\right)^T = \mathbf{0}_{5\times 5},$$

so that

$$\zeta_{1:5}(\eta) = \zeta_{1:5}(0).$$

Choosing five linearly independent solutions based on $\zeta_{1:5}(0)$, the orthogonality conditions can then be written as

$$\int_0^P \left(g_{\text{Pert.},1:5}(k^{(0)}, \eta) - \frac{\partial k_{1:5}^{(0)}}{\partial \tau} \right) d\eta = 0. \tag{4.12}$$

With these conditions in mind, the equation for $k_6^{(1)}$ is written from (4.11) as

$$\frac{\partial k_6^{(1)}}{\partial \eta} = \underbrace{-\frac{3}{2}\sqrt{\mu/k_1^{(0)^5}}\, a_1}_{P-\text{periodic in } \eta} + g_{\text{Pert.},6}(k^{(0)}, \eta) - \frac{\partial k_6^{(0)}}{\partial \tau},$$

whose solution will be $\mathcal{O}(\eta)$ in the limit of $\eta \to \infty$ if and only if

$$\int_0^P \left(g_{\text{Pert.},6}(k^{(0)}, \eta) - \frac{\partial k_6^{(0)}}{\partial \tau} \right) d\eta = 0 \tag{4.13}$$

and $\eta = o(k_6^{(1)})$ otherwise. This is the last condition needed. The asymptoticity conditions can therefore be compactly rewritten for the slow timescale derivatives as

$$\frac{\partial k^{(0)}}{\partial \tau} = \frac{1}{P} \int_0^P \left(g_{\text{Pert.}}(k^{(0)}, \eta) \right) d\eta. \tag{4.14}$$

This is a solvability condition analogous to the Fredholm alternative discussed in Section 2.3; note the use of corresponding conditions in the method of averaging [77], which is expected to give asymptotically equivalent solutions.

The zeroth order solution can now be constructed by numerically integrating the equations

$$\frac{dk^{(0)}}{dt} = \frac{\partial k^{(0)}}{\partial \eta} + \varepsilon \frac{\partial k^{(0)}}{\partial \tau}, \tag{4.15}$$

subject to the initial conditions $k_0(0) = k(0)$, where $\partial k^{(0)}/d\eta$ is defined in (4.8) and $\partial k^{(0)}/\partial \tau$ is defined in (4.14). These expressions may be efficiently and accurately evaluated by numerical quadrature given a particular perturbation model [78]. This completes the search for the $k^{(0)}$ solution; higher-order terms are found similarly.

By construction, the zeroth order solution found by integrating (4.15) is valid for time up to order ε^{-1}. This is because the slow timescale derivative (4.14) is explicitly chosen so that the asymptoticity condition (4.7) holds for t up to $\mathcal{O}(\varepsilon^{-1})$, and thus higher-order terms are well-behaved in this time domain. In the case of atmospheric drag, with ε defined in terms of the nominal atmospheric density and all else being equal, the trajectory found using the zeroth order solution will remain a valid approximation for a longer period of time when the atmosphere is less dense. This could occur, for example, if the satellite initially has a higher altitude at perigee or if the solar conditions are more favorable (*i.e.*, leading to lower levels of atmospheric density). Over this period of validity, the solution has error of order ε. This is because the solution (4.5) has been constructed as an asymptotic expansion in the perturbation parameter, with the higher-order terms in the expansion correspondingly well-behaved, over this time domain. Thus, for the drag case, less dense atmospheric conditions directly lead to greater accuracy in the approximation. The combination of these properties has important implications for the object tracking and catalog maintenance problem. Since the propagated trajectory has known error properties, a sensor can be effectively tasked to update the object's state while it is in the sensor's observation window. Absence of consideration of these error properties leads to sensors being tasked either: 1) more often than is necessary, leading to a waste of resources; or 2) less often than is necessary, leading

to loss of object custody. It is important to note for implementation that the slow time derivatives change on the slow timescale and thus do not have to be evaluated at every integration step.

4.3.1 Specialization to Atmospheric Drag

For the particular case of the drag perturbation in Keplerian elements, the asymptoticity conditions (4.14) can be rewritten in a more explicit form. With the drag acceleration given by (4.3) and corresponding perturbation parameter defined by (4.4), the drag perturbation function $g_{\text{Drag}}(k,t)$ is then explicitly written for the Keplerian elements set $k = [a,\, e,\, i,\, \Omega,\, \omega,\, M]^T$ from Gauss' variational equations (4.2) as

$$g_{\text{Drag}}(k,t) = \begin{bmatrix} -\frac{2a^2 v v_{rel}}{\mu} F(\vec{r}) v_{rel,v} \\ -\frac{v_{rel}}{v} F(\vec{r}) \left(\frac{r}{a} \sin f \, v_{rel,n} + 2\left(e + \cos f\right) v_{rel,v} \right) \\ -\frac{r\cos\theta}{h} F(\vec{r}) v_{rel} v_{rel,h} \\ -\frac{r\sin\theta}{h\sin i} F(\vec{r}) v_{rel} v_{rel,h} \\ \frac{v_{rel}}{ev} F(\vec{r}) \left(\left(2e + \frac{r}{a}\right) \cos f \, v_{rel,n} - 2\sin f \, v_{rel,v} \right) + \frac{r\sin\theta\cos i}{h\sin i} F(\vec{r}) v_{rel} v_{rel,h} \\ \frac{b v_{rel}}{aev} F(\vec{r}) \left(-\frac{r}{a} \cos f \, v_{rel,n} + 2\left(1 + e^2 \frac{r}{p}\right) \sin f \, v_{rel,v} \right) \end{bmatrix} \tag{4.16}$$

where $F\left(\vec{r}\right) \triangleq \rho\left(\vec{r}\right)/\rho_0$ is the scaled atmospheric density, $v_{rel,v} \triangleq \langle \vec{v}_{rel},\, \hat{e}_v \rangle$, $v_{rel,n} \triangleq \langle \vec{v}_{rel},\, \hat{e}_n \rangle$, $v_{rel,h} \triangleq \langle \vec{v}_{rel},\, \hat{e}_h \rangle$, and $\langle \alpha, \beta \rangle$ denotes the inner product between any two vectors α and β.

To obtain explicit expressions for the slow timescale derivatives, substitute the specific perturbation function (4.3.1) into the general slow timescale derivative expression (4.14). Then, denoting the zeroth order states by $k^{(0)} = \left[a^{(0)},\, e^{(0)},\, i^{(0)},\, \Omega^{(0)},\, \omega^{(0)},\, M^{(0)}\right]^T$, use the *vis-a-vis* equation

$$\begin{aligned} v &= \sqrt{\mu\left(\frac{2}{r} - \frac{1}{a}\right)} \\ &= \sqrt{\frac{\mu}{a}\left(\frac{1 + e\cos E}{1 - e\cos E}\right)}, \end{aligned}$$

and the relationship

$$d\eta = \left(1 - e^{(0)} \cos E\right) \sqrt{\frac{a^{(0)^3}}{\mu}} dE$$

to find closed-form expressions. For example, the slow timescale derivative for the zeroth order semi-major axis term is found to be

$$\begin{aligned}
\frac{\partial a^{(0)}}{\partial \tau} &= -\frac{1}{P} \int_0^P \frac{2a^{(0)^2} v^{(0)} v_{rel}^{(0)}}{\mu} F(\vec{r}^{(0)}) v_{rel,v}^{(0)} d\eta \\
&= -\frac{2}{P} \frac{a^{(0)^2}}{\mu} \int_0^P \sqrt{\frac{\mu}{a^{(0)}} \left(\frac{1 + e^{(0)} \cos E}{1 - e^{(0)} \cos E}\right)} F(\vec{r}^{(0)}) v_{rel}^{(0)} v_{rel,v}^{(0)} d\eta \\
&= -\frac{2}{P} \frac{a^{(0)^3}}{\mu} \int_0^P \sqrt{1 - e^{(0)^2} \cos^2 E} F(\vec{r}^{(0)}) v_{rel}^{(0)} v_{rel,v}^{(0)} dE.
\end{aligned}$$

Following the same approach for the eccentricity, inclination, longitude of the ascending node, argument of perigee, and mean anomaly then yields the following expressions:

$$\begin{aligned}
\frac{\partial e^{(0)}}{\partial \tau} = -\frac{1}{P} \frac{a^{(0)^2}}{\mu} \sqrt{1 - e^{(0)^2}} \int_0^P v_{rel}^{(0)} \frac{\left(1 - e^{(0)} \cos E\right)^{3/2}}{\sqrt{1 + e^{(0)} \cos E}} F(\vec{r}^{(0)}) \\
\cdot \left\{ \sin E \, v_{rel,n}^{(0)} + 2 \frac{\sqrt{1 - e^{(0)^2}} \cos E}{1 - e^{(0)} \cos E} v_{rel,v}^{(0)} \right\} dE,
\end{aligned}$$

$$\frac{\partial i^{(0)}}{\partial \tau} = -\frac{1}{P} \frac{a^{(0)^2}}{\mu \sqrt{1 - e^{(0)^2}}} \int_0^P \left(1 - e^{(0)} \cos E\right)^2 \cos \theta^{(0)} F(\vec{r}^{(0)}) v_{rel}^{(0)} v_{rel,h}^{(0)} dE,$$

$$\frac{\partial \Omega^{(0)}}{\partial \tau} = -\frac{1}{P} \frac{a^{(0)^2}}{\mu \sqrt{1 - e^{(0)^2}}} \int_0^P \left(1 - e^{(0)} \cos E\right)^2 \frac{\sin \theta^{(0)}}{\sin i^{(0)}} F(\vec{r}^{(0)}) v_{rel}^{(0)} v_{rel,h}^{(0)} dE,$$

$$\begin{aligned}
\frac{\partial \omega^{(0)}}{\partial \tau} = \frac{1}{P} \frac{a^{(0)^2}}{\mu} \int_0^P \left\{ \sqrt{\frac{1 - e^{(0)} \cos E}{1 + e^{(0)} \cos E}} \frac{1}{e^{(0)}} \right. \\
\cdot \left[\left(2e^{(0)} + 1 - e^{(0)} \cos E\right) \left(\cos E - e^{(0)}\right) v_{rel,n}^{(0)} - 2\sqrt{1 - e^{(0)^2}} \sin E \, v_{rel,v}^{(0)} \right] \\
\left. + \frac{\left(1 - e^{(0)} \cos E\right)^2 \sin \theta^{(0)} \cos i^{(0)}}{\sqrt{1 - e^{(0)^2}} \sin i^{(0)}} v_{rel,h}^{(0)} \right\} F(\vec{r}^{(0)}) v_{rel}^{(0)} \, \mathrm{d}E,
\end{aligned}$$

$$\frac{\partial M^{(0)}}{\partial \tau} = \frac{1}{P}\frac{a^{(0)^2}\sqrt{1-e^{(0)^2}}}{e^{(0)}\mu}\int_0^P v_{rel}^{(0)}\sqrt{\frac{1-e^{(0)}\cos E}{1+e^{(0)}\cos E}}F(\vec{r}^{(0)})$$
$$\cdot\left\{-\left(1-e^{(0)}\cos E\right)\left(\cos E - e^{(0)}\right)\, v_{rel,n}^{(0)} + 2\frac{1-e^{(0)^3}\cos E}{\sqrt{1-e^{(0)^2}}}\sin E\, v_{rel,v}^{(0)}\right\}\mathrm{d}E.$$

This completes the specialization of the $\partial k^{(0)}/\partial\tau$ terms to the particular case of atmospheric drag.

4.3.2 Sensitivity of Trajectory to Perturbation Parameters

To understand the effects of perturbation parameter uncertainty, a measure of the trajectory's sensitivity is desired. Posing the trajectory solution in the form (4.5) has the additional benefit of allowing computation of this sensitivity without propagation of the state transition matrix. Differentiating (4.5) with respect to ε yields

$$\begin{aligned}
\frac{\partial k_\varepsilon(\eta,\tau;\varepsilon)}{\partial\varepsilon} &= \frac{\partial}{\partial\varepsilon}\left(\sum_{i\geq 0}\varepsilon^i k^{(1)}(\eta,\tau)\right)\\
&= \frac{\partial}{\partial\varepsilon}\left(k^{(0)}(\eta,\tau)+\varepsilon k^{(1)}(\eta,\tau)+\mathcal{O}\left(\varepsilon^2\right)\right)\\
&= \left\{k^{(1)}(\eta,\tau)+\varepsilon k^{(2)}(\eta,\tau)+\mathcal{O}\left(\varepsilon^2\right)\right\}\\
&\quad+\left\{\frac{\partial k^{(0)}(\eta,\tau)}{\partial\tau}+\varepsilon\frac{\partial k^{(1)}(\eta,\tau)}{\partial\tau}+\mathcal{O}\left(\varepsilon^2\right)\right\}\frac{\partial\tau}{\partial\varepsilon}\\
&\quad+\left\{\frac{\partial k^{(0)}(\eta,\tau)}{\partial\eta}+\varepsilon\frac{\partial k^{(1)}(\eta,\tau)}{\partial\eta}+\mathcal{O}\left(\varepsilon^2\right)\right\}\frac{\partial\eta}{\partial\varepsilon}\\
&= \frac{1}{\varepsilon}e_{0\text{th order}}+\frac{\partial k_\varepsilon}{\partial\tau}t+\mathcal{O}\left(\varepsilon\right).
\end{aligned} \tag{4.17}$$

The first term, $\frac{1}{\varepsilon}e_{0\text{th order}}$, is the scaled error in the zeroth order solution due to higher-order terms in (4.5) that are neglected in the zeroth-order solution. It therefore represents the effects of errors in the zeroth-order solution on the trajectory when the perturbation parameter is changed, and is well-approximated by the first order solution of (4.5). The second term, $(\partial k_\varepsilon/\partial\tau)\,t$, is the change in the trajectory due to the change in the slow timescale, τ. It is well-approximated by the zeroth order term $\left(\partial k^{(0)}/\partial\tau\right)t$, which is evaluated during

numerical integration of the zeroth order solution. Furthermore, this slow timescale term will dominate the scaled-error term for large t. The sensitivity expression (4.17) is explored for representative orbit families below, in Section 4.4.

4.3.3 Inclusion of Geopotential Perturbations

In the development of the slow time derivatives (4.14), the two-body force was implicitly considered to be the underlying source of motion on the η timescale. However, in low-Earth orbits, conservative geopotential perturbations (of which the J_2 perturbation is the largest) must be accounted for. These geopotential perturbations are well characterized and their effects understood [3]. Since they do not vary with the parameter of the non-conservative perturbation, they will be considered to be of zeroth order in ε. The fast time derivatives (4.8) are therefore calculated as

$$\frac{\partial k^{(0)}}{\partial \eta} = \begin{bmatrix} \mathbf{0}_{5\times 1} \\ \sqrt{\mu / k_1^{(0)^3}} \end{bmatrix} + \left(\frac{dk}{dt}\right)_{\text{Geopotential}}, \tag{4.18}$$

where $(dk/dt)_{\text{Geopotential}}$ are the instantaneous induced rates on the Keplerian elements due to the geopotential perturbations. These can be directly written, for example, using Lagrange's planetary equations [75]. The slow-time derivatives are adapted from (4.14) as

$$\frac{\partial k_0}{\partial \tau} = \frac{1}{\tilde{P}} \int_0^{\tilde{P}} g_{\text{Pert.}} \left(k_0 \left(s, \tau\right), s\right) ds, \tag{4.19}$$

where $\tilde{P}$ is the geopotentially-perturbed anomalistic period in seconds. That is, the perturbing function is averaged over an orbit of the geopotential-only dynamics propagated from the current zeroth-order solution. In general, the integral (4.19) must be evaluated using numerical quadrature. The geopotential-only dynamics necessary to evaluate this integral, including the necessary anomalistic period, can be found efficiently using an analytical expression or a variational integrator.

4.4 Results and Discussion

In this section, results from the orbit propagation technique developed in Section 4.3 are applied to the atmospheric drag perturbation and investigated for three representative sets of low-Earth orbits. The chosen orbit sets, defined in Table 4.1, have perigee altitudes between 431 and 629 kilometers and were chosen to be representative of a range of typical low-perigee orbits [79]. The first set represents a generic low-Earth orbit of moderate eccentricity, the second a high-eccentricity orbit that has a low altitude at perigee, and the third a low-Earth frozen orbit.

For all three sets, the error characteristics of the zeroth order MMS solution are first presented in comparison to approximations given by Escobal [80, Chapter 10.4], Vallado [65, Chapter 9], Li [70], and Dallas [81]. The approaches given by Vallado and Escobal involve numerically averaging different expressions to obtain secular drag effects, and do not rely on a particular atmospheric model. The Li method gives an analytic approximation for the drag effects but assumes an exponential drag model. The fully averaged approach given by Dallas uses numerical averaging for the drag effects and analytical averaging for geopotential effects. In these comparisons, the slow timescale derivatives in the MMS solution as well as the corresponding secular drag effects for the compared methods are evaluated once per orbit as is standard in many semi-analytical methods [72, 74]. Next, the consequences of changing this update rate are explored for the MMS solution, including the effects on computation time. Finally, the expression for the trajectory's sensitivity to changes in the drag parameter, developed in Section 4.3.2, is evaluated for each of the example orbit sets.

The simulations in this section were performed using the conditions defined in Table 4.2. Results are given both for simplified orbits where higher-order geopotential perturbations are neglected as well as for orbits where the geopotential perturbations are included. This is done to 1) illustrate the direct effects of using a reduced-order approximation, 2) facilitate an accurate comparison between the MMS solution and the other propagation methods which do not include geopotential perturbations, and 3) highlight the trends that parallel the simple

orbit case as well as those trends that differ.

Table 4.1: Sets of initial parameters for three characteristic orbits

	Initial Altitude (km)	a (km)	e	i (deg)	Ω (deg)	ω (deg)	M (deg)	P (min)
Set 1	629.2	7078	0.01	30	0	0	0	98.8
Set 2	528.0	26562	0.74	63.4	0	0	0	718.0
Set 3	431.2	6878	7.7×10^{-4}	45	0	90	0	94.6

4.4.1 Atmospheric Drag Perturbation

Considering simplified orbits that only consider the atmospheric drag perturbation, the evolution of error for the MMS solution is shown in Keplerian elements in Figure 4.1a. By construction, the zeroth order MMS solution has error of $\mathcal{O}(\varepsilon)$ and is valid for times up to $\mathcal{O}(\varepsilon^{-1})$. As expected, then, these results show that the MMS solution exhibits a low, predominantly quasi-periodic error in all Keplerian components for each orbit set. Further, the Keplerian element error for the MMS solution compares favorably to the error of the other propagation methods, shown in Table 4.3. This translates to good performance in the total magnitudes of position and velocity errors, shown for the MMS solution in Figure 4.1b. The maximum position errors over the 100 propagated orbits, as well as the total computation times for the various methods, are indicated in Table 4.4. While the MMS solution takes longer to compute in this case than the methods of Vallado, Escobal, and Li, it is more accurate than these alternate methods while remaining much faster than the exact numerical propagation. Further, it is comparable in computation time and accuracy to the Dallas method.

Table 4.2: List of orbit propagation simulation parameters

Description	Value
Satellite Mass	500 kg
Satellite Effective Area	1.0 m^2
Satellite Drag Coefficient	2.0
Atmosphere Model	Harris-Priester (*e.g.*, [82])
Geopotential Model	Pines EGM96 (36×36 field)
Numerical Integration Scheme	Explicit Runge-Kutta (4,5)
Absolute & Relative Integration Tolerances	Both 1×10^{-14}

In the two-time derivative expansion (4.6), the effects that depend on the fast timescale η are separated from those that depend on the slow timescale τ. This implies that the slow timescale derivatives change at a much slower rate than the fast timescale derivatives and do not have to be evaluated at every time step during the numerical integration. Further, from the MMS analysis the slow timescale is $\tau = \varepsilon t = (AC_d/2m)\, t$. The slow timescale derivative rate of change is therefore directly dependent on the drag parameters. It is therefore reasonable to ask how the update rate of the slow timescale derivatives in (4.15) affects the error properties and computation time of the resulting propagated trajectory. The effect of different update rates on the corresponding maximum position error and computation time is shown in Table 4.5. These results show that, in the absence of additional perturbations such as higher-order geopotential effects, the update rate has minimal effect on the resulting error even when updates only occur only intermittently due to the slow rate of change in the slow timescale derivative. Furthermore, the results show that the overall computation time falls dramatically as the time between updates increases indicating that, from an implementation

Table 4.3: Simple orbits: Maximum orbital element errors over 100 propagated orbits

	a (km) $\times 10^{-3}$	e $\times 10^{-7}$	i (rad) $\times 10^{-8}$	Ω (rad) $\times 10^{-10}$	ω (rad) $\times 10^{-6}$	M (rad) $\times 10^{-5}$
Set 1						
Vallado	2.16	15.49	2.31	48.43	76.25	22.02
Escobal	0.06	0.07	0.00	0.00	86.17	8.93
Li	3.37	1.30	2.31	48.42	76.24	30.05
Dallas	0.23	0.36	0.00	0.00	1.13	1.43
MMS	**0.05**	**0.06**	**0.00**	**1.35**	**0.72**	**0.27**
Set 2						
Vallado	10.58	1.06	2.66	4.24	0.22	17.08
Escobal	1.13	0.11	0.00	0.00	0.23	0.24
Li	136.75	9.18	2.66	4.24	0.22	242.07
Dallas	1.13	0.11	0.00	0.00	0.00	0.24
MMS	**1.08**	**0.11**	**0.01**	**0.23**	**0.00**	**0.22**
Set 3						
Vallado	12.16	240.71	22.45	7.68	2454.96	328.79
Escobal	0.16	0.37	0.00	0.00	2696.71	270.30
Li	72.64	50.30	22.45	7.68	2454.96	255.45
Dallas	0.20	0.41	0.00	0.00	82.72	8.26
MMS	**0.15**	**0.31**	**3.43**	**3.76**	**75.29**	**7.52**

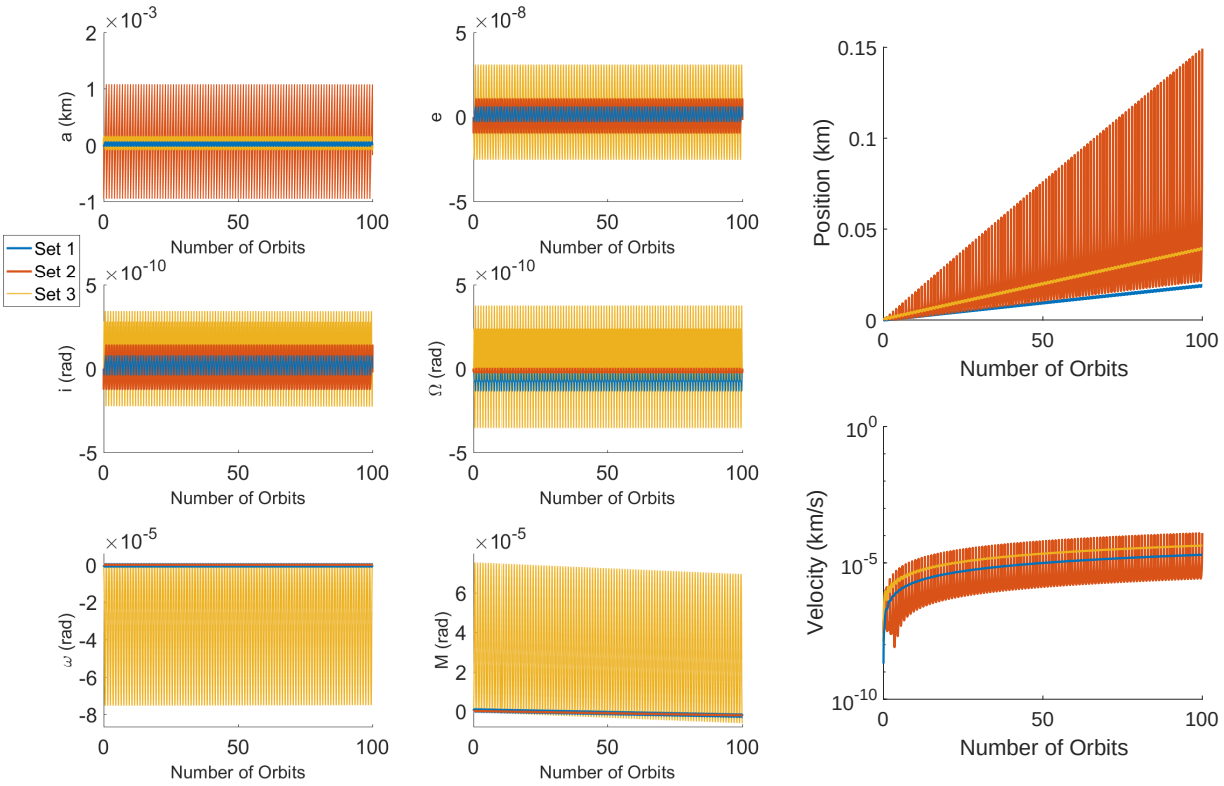

(a) (b)

Figure 4.1: Simple orbits: Difference between truth and approximate solution using MMS vs time. (a) Keplerian element errors. (b) Total magnitude of position and velocity errors.

standpoint, slow updates are permissible for dealing with pure drag effects.

An important aspect of using MMS for orbit propagation is that it gives insight into the effect of uncertainties in the parameters of the perturbing forces on an object's trajectory. To demonstrate these benefits, the trajectory sensitivity expressions derived in Section 4.3.2 are now applied to the atmospheric drag perturbation. To do so, the exact and zeroth order MMS trajectories are first propagated using the nominal density $\rho = \rho_{\text{nom}}(\vec{r})$. The density is then changed to $\rho = 1.2\rho_{\text{nom}}(\vec{r})$ and the exact trajectory computed. Finally, the trajectory sensitivity expression (4.17) is evaluated at the desired time in the trajectory and

Table 4.4: Simple Orbits: Computation Time and Maximum Error over 100 Propagated Orbits

	Time to Compute (s)			Max Position Error (m)		
	Set 1	Set 2	Set 3	Set 1	Set 2	Set 3
Exact Numerical Integration	2028	2273	1621	–	–	–
Vallado	2	5	1	1047	11736	6035
Escobal	4	10	3	35	165	72
Li	3	3	2	1614	166320	34180
Dallas	399	1292	75	40	165	62
MMS	**462**	**1931**	**274**	**19**	**149**	**39**

Table 4.5: Simple orbits: Effect of $\partial k^{(0)}/\partial \tau$ update rates on computation time and maximum error over 100 propagated orbits

	Time to Compute (s)			Max Position Error (m)		
	Set 1	Set 2	Set 3	Set 1	Set 2	Set 3
Exact Numerical Integration	2028	2273	1621	–	–	–
MMS, 0.1 Orbits/Update	4159	23066	2668	19.02	148.35	39.88
MMS, 0.25 Orbits/Update	1680	9132	1073	19.02	149.25	39.82
MMS, 1 Orbit/Update	462	1931	274	19.01	149.29	39.52
MMS, 5 Orbits/Update	100	395	57	18.99	149.28	37.94
MMS, 10 Orbits/Update	43	207	30	18.97	149.54	36.01

the approximation

$$k_{\text{Approx.},\,1.2\rho_{\text{nom}}} = k^{(0)} + \frac{\partial k_\varepsilon(\eta,\tau;\varepsilon)}{\partial \varepsilon}\,(1.2\varepsilon - 1.0\varepsilon) \tag{4.20}$$

constructed at this desired point in the orbit. The results are found in Table 4.6. As expected, the derived sensitivity function yields a good approximation in orbital element space, signified by the predicted change being of the same order of magnitude and in the same direction as the exact change for each element. This validates the sensitivity expression derived in Section 4.3.2, and demonstrates how the form of the MMS solution gives direct insight into how the drag parameters affects the trajectory solution.

Table 4.6: Simple orbits: Change in Keplerian elements after 50 orbits due to change in drag parameters

	Δa (km) $\times 10^{-2}$	Δe $\times 10^{-7}$	Δi (rad) $\times 10^{-8}$	$\Delta\Omega$ (rad) $\times 10^{-10}$	$\Delta\omega$ (rad) $\times 10^{-4}$	ΔM (rad) $\times 10^{-4}$
Set 1						
Exact	−0.16	−1.05	−0.23	4.84	0.08	0.47
Predicted	−0.16	−1.05	−0.23	4.84	0.08	0.55
Set 2						
Exact	−2.09	−2.04	−0.27	0.38	0.00	1.84
Predicted	−2.07	−2.03	−0.26	0.42	0.00	1.84
Set 3						
Exact	−1.21	4.72	−2.24	−0.42	2.45	1.69
Predicted	−1.21	4.70	−2.24	−0.42	2.46	4.15

4.4.2 Atmospheric Drag and Higher-Order Geopotential Model

For propagations including geopotential perturbations, the exact geopotential accelerations were evaluated at every step for the methods of Escobal, Vallado, and Li, while the averaged geopotential effects in the Dallas method were evaluated ten times per orbit. The corresponding evolution of error in Keplerian elements for the MMS solution is shown in Figure 4.2a, and the maximum absolute errors of each Keplerian element over 100 propagated orbits are compared for the different propagation methods in Table 4.7. The alternative propagation methods all exhibit secular drift in error in every component, leading to large errors over the propagated timespan. This is because none of these propagation methods incorporate the geopotential perturbation effects during the next orbit on the satellite's trajectory when calculating the upcoming secular effect of drag. Further, the Dallas solution propagates analytically averaged geopotential effects that ignore the significant corresponding short-period effects, leading to a large error. The MMS solution, on the other hand, exhibits relatively small, though growing, oscillatory error in most of its components except for the mean anomaly which exhibits slight secular drift. This drift in mean anomaly is expected because the order ε term, $M^{(1)}$, is allowed to grow with time by the asymptoticity conditions that are embedded in the MMS solution. This is most evident in the highly eccentric orbit of Set 2, where the drift in mean anomaly for the MMS solution is faster than the drift in the Escobal solution (which does not include any effects of drag on the mean anomaly). These trends translate to the total magnitude of position and velocity error of the solutions, the evolution of which is shown for the MMS solution in Figure 4.2b. The maximum position errors over the 100 propagated orbits, as well as the total computation times for the various methods, are indicated in Table 4.8. The MMS solution performs favorably in both respects against the other methods, except as compared to the Escobal solution error for Set 2 as was previously discussed. While the MMS solution takes longer to compute for Set 2 than the methods of Vallado, Li, and Dallas, it is more accurate for all orbits than these solutions while remaining faster than the Escobal solution and much faster than the exact numerical

propagation.

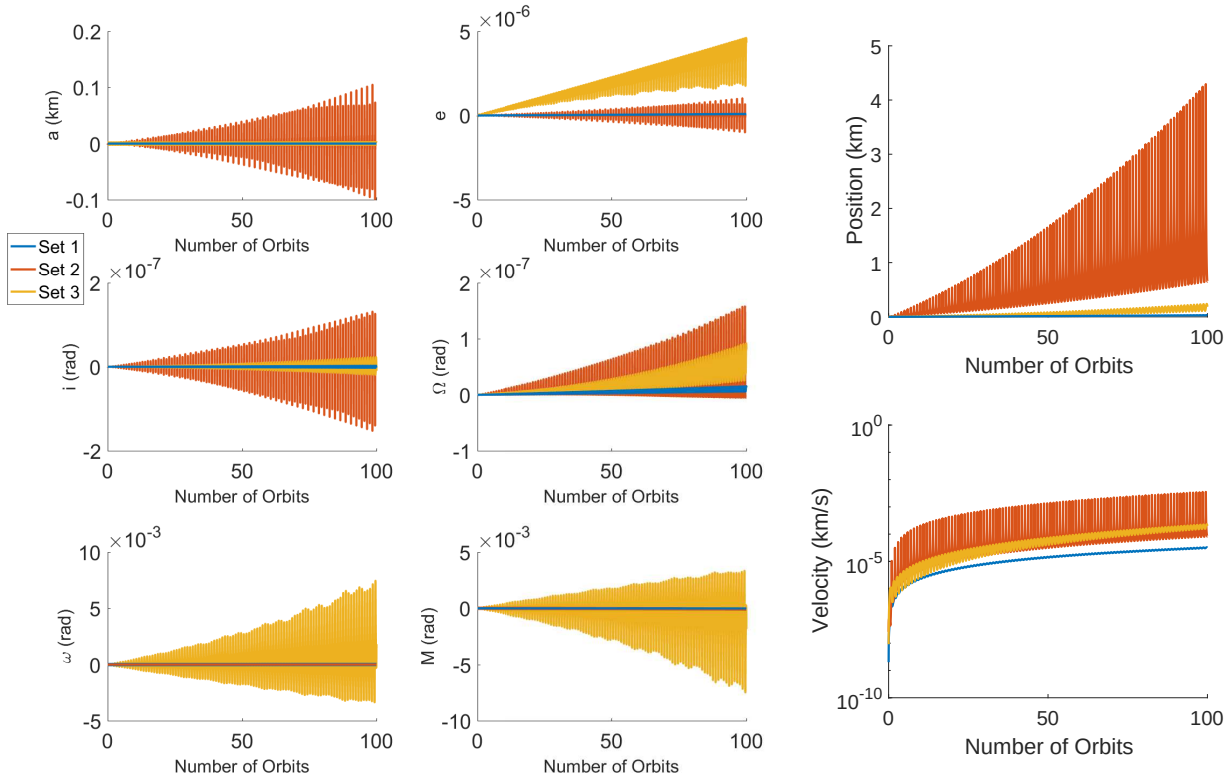

Figure 4.2: General orbits: Difference between truth and approximate solution using MMS vs time. (a) Keplerian element errors. (b) Total magnitude of position and velocity errors.

For these general orbits, the effect of different slow timescale derivative update rates on the corresponding maximum position error and computation time is shown in Table 4.9. As in the simple orbit case, longer intervals between updates of the slow time derivatives once again leads to a shorter computation time. In contrast to the simple orbit cases, however, the slow timescale update rate has a significant effect on the error solution. This indicates that propagations that use longer intervals between updates may *not* be permissible in general. While the low-eccentricity orbits have position errors that approximately double over the

range of simulated update rates, the highly eccentric Orbit 2 exhibits an order of magnitude greater error at the slowest update rate than with the fastest update rate. Further, as shown in Table 4.10, there is a corresponding trend in the maximum error of each of the Keplerian elements. These error trends occur because geopotential effects can drastically change the satellite's trajectory in between updates, leading to an inaccurate slow timescale derivative being used in the integration. Thus, even though implementing long intervals between updates is beneficial from a computation time perspective, it is undesirable for maintaining good error properties in the general case. The limiting factor for an effective slow timescale derivative update rate is how quickly the other forces, such as the geopotential perturbation, change the predicted orbit. These results imply that the update rate should be chosen based on the nominal magnitude of the non-conservative perturbation, with a larger magnitude corresponding to more frequent updates. By doing so, the errors in the evaluated slow-time derivative will be mitigated by recalculation when the errors have a more significant effect on the trajectory solution.

As in the simple orbits case, the trajectory sensitivity expression (4.17) was used to construct a predicted trajectory (4.20) for these general orbits with a twenty percent change in the nominal atmospheric density. The results are presented in Table 4.11. Here, the predicted change is close to the exact change in a, e, and M while generally under-predicting the exact change in i, ω, and Ω. This is because the differences in drag perturbations generally do not lead to orbits with meaningfully different geopotential effects in these out-of-plane elements at this order of approximation. Even in these more complicated cases, however, the results demonstrate that the form of the MMS solution gives direct, meaningful insights into how differences in the drag parameters manifests in the trajectory solution over time.

Table 4.7: General orbits: Maximum orbital element errors over 100 propagated orbits

	a (km) $\times 10^{-3}$	e $\times 10^{-6}$	i (rad) $\times 10^{-7}$	Ω (rad) $\times 10^{-7}$	ω (rad) $\times 10^{-4}$	M (rad) $\times 10^{-4}$
Set 1						
Vallado	1.74	1.82	0.74	3.11	1.23	2.09
Escobal	1.07	0.08	0.33	2.17	1.08	0.52
Li	5.05	0.74	1.56	8.94	1.30	3.61
Dallas	4879.23	2205.48	5778.45	33661.50	1261.32	1196.85
MMS	**0.07**	**0.09**	**0.02**	**0.16**	**0.06**	**0.10**
Set 2						
Vallado	274.23	2.71	4.15	3.98	0.03	1.65
Escobal	23.20	0.23	0.31	0.32	0.00	0.13
Li	4333.20	42.43	60.11	65.02	0.43	25.90
Dallas	132850.28	1253.16	2751.39	15184.39	12.15	9.56
MMS	**104.82**	**1.02**	**1.52**	**1.58**	**0.01**	**0.64**
Set 3						
Vallado	26.80	22.88	9.81	35.97	434.24	445.22
Escobal	7.29	3.03	2.18	10.38	73.65	76.75
Li	114.24	8.66	34.59	155.02	84.05	127.74
Dallas	9622.42	1034.71	6970.18	11093.56	10797.10	10773.68
MMS	**0.61**	**4.61**	**0.23**	**0.92**	**74.49**	**74.75**

Table 4.8: General Orbits: Computation Time and Maximum Error over 100 Propagated Orbits

	Time to Compute (s)			Max Position Error (m)		
	Set 1	Set 2	Set 3	Set 1	Set 2	Set 3
Exact Numerical Integration	2176	2907	2120	–	–	–
Vallado	3378	1999	5877	641	11120	7870
Escobal	3879	2839	7338	408	890	2188
Li	3586	1974	6260	1673	174533	32320
Dallas	441	1275	58	44202	200002	17286
MMS	**1168**	**2569**	**1497**	**31**	**4294**	**238**

Table 4.9: General orbits: Effect of $\partial k^{(0)}/\partial \tau$ update rates on computation time and maximum error over 100 propagated orbits

	Time to Compute (s)			Max Position Error (m)		
	Set 1	Set 2	Set 3	Set 1	Set 2	Set 3
Exact Numerical Integration	2176	2908	2120	–	–	–
MMS, 0.1 Orbits/Update	8385	32303	8291	29.38	3116.42	125.24
MMS, 0.25 Orbits/Update	3508	11737	3619	30.15	3221.77	132.26
MMS, 1 Orbit/Update	1168	2569	1497	31.44	4293.52	238.20
MMS, 5 Orbits/Update	542	712	814	45.44	12710.48	224.78
MMS, 10 Orbits/Update	463	473	748	65.24	35162.34	214.55

Table 4.10: General orbits: Effect of $\partial k^{(0)}/\partial \tau$ update rates on maximum orbital element errors over 100 propagated orbits

	a (km) $\times 10^{-4}$	e $\times 10^{-7}$	i (rad) $\times 10^{-7}$	Ω (rad) $\times 10^{-8}$	ω (rad) $\times 10^{-6}$	M (rad) $\times 10^{-5}$
Set 1						
0.1 Orbits/Update	0.68	0.96	0.02	1.43	5.50	0.94
0.25 Orbits/Update	0.70	0.96	0.02	1.47	5.52	0.96
1 Orbits/Update	0.70	0.97	0.02	1.55	5.58	0.98
5 Orbits/Update	1.08	1.08	0.04	2.28	5.91	1.21
10 Orbits/Update	1.65	1.21	0.05	3.31	6.24	1.52
Set 2						
0.1 Orbits/Update	760.24	7.38	1.09	11.78	0.79	4.62
0.25 Orbits/Update	786.62	7.64	1.12	12.14	0.82	4.77
1 Orbits/Update	1048.22	10.22	1.52	15.77	1.09	6.36
5 Orbits/Update	3118.36	30.67	4.56	45.25	3.24	18.81
10 Orbits/Update	8663.43	85.40	12.37	126.52	8.95	52.08
Set 3						
0.1 Orbits/Update	2.50	45.84	0.11	3.95	7417.69	742.67
0.25 Orbits/Update	2.62	45.87	0.12	4.27	7435.08	744.52
1 Orbits/Update	6.11	46.07	0.23	9.16	7449.27	747.47
5 Orbits/Update	5.61	45.98	0.22	8.55	7497.00	752.05
10 Orbits/Update	5.23	45.73	0.21	8.10	7544.07	756.61

Table 4.11: General orbits: Change in Keplerian elements after 50 orbits due to change in drag parameters

	Δa (km) $\times 10^{-2}$	Δe $\times 10^{-7}$	Δi (rad) $\times 10^{-8}$	$\Delta\Omega$ (rad) $\times 10^{-7}$	$\Delta\omega$ (rad) $\times 10^{-5}$	ΔM (rad) $\times 10^{-4}$
Set 1						
Exact	−0.19	−1.36	−3.27	−1.81	1.14	0.45
Predicted	−0.16	−0.92	−0.24	−0.00	0.91	0.55
Set 2						
Exact	−2.76	−2.75	4.45	0.09	0.00	2.40
Predicted	−2.18	−2.13	−0.28	0.00	0.00	1.95
Set 3						
Exact	−1.08	5.43	4.31	−13.07	4.48	3.56
Predicted	−1.18	−0.36	−2.17	−0.00	31.31	4.03

Chapter 5

APPLICATION TO NETWORKED DYNAMICAL SYSTEMS

Consensus-based systems provide an effective means of distributed information-sharing and control for networked, multi-agent systems in settings such as multi-vehicle control, formation control, swarming, and distributed estimation; see for examples [83, 84, 85, 86, 87]. In their simplest form, consensus-based systems describe linear diffusive coupling between agents in a static network. In practice, however, consensus is often coupled to nonlinear tracking and dynamic weight evolution that operate over distinct timescales. This dynamic coupling introduces several challenges for analysis. First, even if both sets of dynamics are stable when isolated, their interconnection does not guarantee the stability of the coupled dynamics. Second, the coupling hides and potentially changes the correspondence between properties of the graph and the behaviour of the consensus dynamics even if stability is maintained. It is thus unclear whether features such as reaching agreement with a given rate of convergence will be invariant when consensus is coupled with another dynamic system.

This chapter considers three specific cases of network coupling over multiple timescales, and is based on the author's works [88, 89, 35]. The first case considered is a *state-dependent graph problem,* where agents follow a fast evolving consensus dynamics whose underlying network interactions have their own slowly varying dynamics. Next, a *continuous-communication consensus tracking problem* is investigated where agents with nonlinear dynamics must "quickly" track a reference given by slow consensus dynamics. The final case is an *intermittent-communication consensus tracking problem,* where the agents can only communicate over the network intermittently to reach agreement. In each instance, singular perturbation theory is used to formulate reduced-order models that allow analysis of the coupled system based on the behavior of the individual sets of dynamics. These reduced-order

models are then used to develop quantitative bounds with respect to the underlying graph topology and to the communication rate that guarantee asymptotic stability of the coupled systems.

5.1 Literature Review

The state-dependent graph problem has been investigated from several different directions in the past. In [90] a method was proposed for maximizing the second smallest eigenvalue of the graph Laplacian when edge weights are dependent on inter-agent distances. Controllability was considered in [91] for discrete-event, finite-state distributed systems operating over a graph whose edges are dependent on relative states. On another front, a heterophilious form of opinion dynamics was analyzed in [92] where edges are strengthened between agents with disparate opinion states.

Consensus tracking problems have likewise been previously explored for specific scenarios. Tracking is an essential assumption in much of the literature on distributed robotics [93, 94], but a reference trajectory may not be immediately realizable by agents with nonlinear dynamics. One approach is therefore to design the distributed protocol for a particular set of (usually homogeneous) agent dynamics [95, 96]. Alternatively, many designers assume arbitrary levels of tracking performance, which is sometimes referred to as tracking a virtual vehicle or virtual particle [97]. This allows, for example, distributed formation controllers to be developed that approximately decouple a formation's shape and its center of mass [98].

In the network systems literature, singular perturbation theory has been primarily applied to explore timescale separation within a network caused by weak connections. For example, this approach was exploited to formulate reduced-order models for large power networks by area-aggregation [9], dynamic equivalence [99], and slow coherency [100]. Weak inter-node connections have also been characterized with respect to the graph structure in [101]. Further, singular perturbation methods have been leveraged to design favorable spectral graph properties in the partial edge design problem [102]. More recently, these methods have

been applied to the reduced-order modeling and synchronization of a network of identical linear agents that individually exhibit multiple timescale behavior and whose graph topology is fixed and undirected [103]. However, the existing works do not exploit the timescale separation that naturally arises between the network layer and the agent layer. By taking advantage of this structure, the approach detailed in this chapter is therefore adaptable to a wide set of agent dynamics and network protocols, and gives key insight into the role of important design parameters such as controller gains and communication rates in the stability of coupled consensus systems.

5.2 Notation and Background

This section describes some of the specific notation and terminology particular to networked dynamical systems that is used in this chapter; see [87] for further details.

An undirected, weighted graph $\mathcal{G}$ is made up of a node set V with cardinality $|V| = n$, an edge set E with cardinality $|E| = m$, and a positive weight set W with cardinality $|W| = m$. Associated with W is a vector of weights w under some ordering with w_{ij} referring to the weight on the edge $\{i, j\} \in E$ between nodes $i, j \in V$. The set of nodes adjacent to a given node $i \in V$ is denoted by $\mathcal{N}(i)$.

In the agreement problem, a group of dynamic agents interract with one another over a communication graph $\mathcal{G}$ while attempting to reach consensus on their states. The classical consensus dynamics define a distributive protocol to reach this goal, with each agent using only relative state information of neighboring agents. These dynamics are given in simplest form for each agent as

$$\dot{q}_i = \sum_{j \in \mathcal{N}(i)} w_{ij} \left(q_i - q_j \right),$$

where $q_i \in \mathbb{R}^p$ is the ith agent's state. Denoting the collection of agents states by $q = \left[q_1^T, \cdots, q_n^T \right]^T \in \mathbb{R}^{np}$, the consensus dynamics can be compactly represented over all agents in the graph as

$$\dot{q}(t) = -(L(\mathcal{G}) \otimes I) q(t), \tag{5.1}$$

where $L(\mathcal{G})$ is the Laplacian matrix and $\otimes$ is the Kronecker product. Assuming $w \succeq 0$, the eigenvalues $\lambda_i(\mathcal{G})$ of $L(\mathcal{G})$ are ordered as $0 = \lambda_1 \leq \lambda_2 \leq \cdots \leq \lambda_n \triangleq \lambda_{\max}$ with the associated normalized eigenvectors $v_1 \triangleq \frac{1}{n}\mathbf{1}$, $v_2, \ldots, v_n$ so that $L(\mathcal{G})\mathbf{1} = 0$. Further, the number of zero eigenvalues of $L(\mathcal{G})$ is equal to the number of connected components of $\mathcal{G}$. Together, these properties imply that under the dynamics (5.1) the agents approach the consensus subspace $\mathcal{X}_c = \left\{ q \in \mathbb{R}^{np} \,\middle|\, q_1 = q_2 = \cdots = q_n \right\}$.

5.3 State-dependent Networks

Consider the consensus dynamics with a slowly changing state-dependent network given by

$$\begin{aligned} \dot{x} &= f\left(x, z\right) \\ \varepsilon \dot{z} &= -L(\mathcal{G}_x) z, \end{aligned} \tag{5.2}$$

and illustrated in Figure 5.1. Here, $z(t) \in \mathbb{R}^n$ is the set of fast agent states, $x(t) \in D_x \subseteq \mathbb{R}^m$ is the set of slow edge states, the function $f(\cdot)$ describes the slowly varying evolution of these edge states, $\mathcal{G}_x = (V, E, W(x))$ is the undirected, weighted graph whose weights $w_{ij}(x)$ depend on the edge states, and ε is a small, positive parameter. The parameter ε can be interpreted as a uniform scaling factor for the weight functions $W(x)$. Such state-dependent networks arise, for example, when modeling social interactions with opinion dynamics [104] or when constructing distributed protocols to ensure connectivity of multiagent systems with distance-based communication links [87].

Several assumptions are now made to facilitate the subsequent analysis.

Assumption 1. *The functions $f\left(x, z\right)$ and $L(\mathcal{G}_x)$ are continuous over their respective domains.*

Assumption 2. *There is an open set $D_c \subset D_x$ over which the graph $\mathcal{G}_x$ is connected.*

Assumption 3. *There exists a positive-definite Lyapunov function $V_{slow}(x)$ in the domain $x \in D_c$ about the equilibrium set $x_{eq} \subseteq D_c$ that satisfies*

$$\frac{\partial V_{slow}}{\partial x} f\left(x, z_{\parallel}\mathbf{1}\right) \leq -\alpha_1 \Psi^2(x, z_{\parallel}),$$

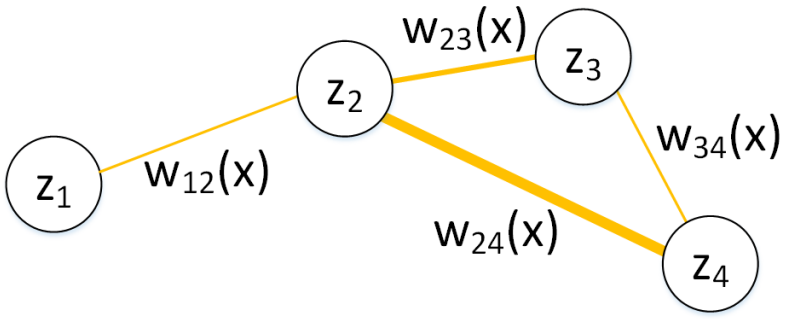

Figure 5.1: State-dependent network problem with fast agent states, z, and slow edge states, x

with $\alpha_1 > 0$, $z_\parallel \triangleq \frac{1}{n}\mathbf{1}^T z(0)$ *denoting the average of the agent states, and* $\Psi\left(x, z_\parallel\right) \in \mathbb{R}$ *a continuous scalar function that satisfies* $\Psi\left(x_{eq}, z_\parallel\right) = 0$.

Many state-dependent weight functions $W(x) = \{w_{ij}(x)\}$ fit into the class of functions described in Assumptions 1 and 2. For example, with $x_{ij} = x_j - x_i$ and $\rho_2 - \rho_1, \rho_1, \delta > 0$, these weight functions include: the Hegselmann-Krausse dynamics [104] initially introduced to describe opinion dynamics with $w_{ij}(x) = \min(\delta - \|x_{ij}\|, 0)$, the Kuramoto dynamics used to describe synchronization phenomenon in coupled oscillators [105] with scalar x_i and $w_{ij}(x) = \delta \sin(x_{ij})/x_{ij}$, connectivity maintenance dynamics which through edge tension bounds the distance between adjacent nodes [106] with $w_{ij}(x) = (2\delta - \|x_{ij}\|) / (\delta - \|x_{ij}\|)^2$, and the general class of edge functions whose weights are nonincreasing with distance described by Mesbahi [90] with $w_{ij}(x) = \delta^{(\rho_1 - \|x_{ij}\|)/(\rho_1 - \rho_2)}$. More formally, Assumption 2 ensures the applicability of reduced-order models, developed in Section 5.3.1, that characterize a separation principle between the consensus dynamics and the edge dynamics in the domain D_c. Assumption 3 then states that the isolated edge dynamics are uniformly asymptotically stable if the agents are at consensus. This assumption will be used in Section 5.3.1 to develop conditions that ensure that the graph stays connected if it starts connected.

5.3.1 Reduced-Order Models

In this section, reduced-order models are developed for the dynamics (5.2) based on the timescale separation between the slow edge states and the fast agent states as $\varepsilon \to 0^+$. To begin, note that (5.2) is not in standard singularly perturbed form. This is because the nullspace of $L(\mathcal{G}_x)$ has dimension equal to the number of connected components in the graph; hence, the solutions of $0 = -L(\mathcal{G}_x)z$ are not isolated. A separation principle between the subsystem dynamics cannot therefore be directly applied as described in Section 2.2. However, (5.2) can be placed in the standard form as follows. Define a new set of states $\left(z_\parallel, z_\perp\right)$ for the nominally fast agent dynamics, where $z_\parallel$ is the average agent state and $z_\perp \triangleq Cz$ represents the projection of the agent dynamics onto $\mathbf{1}^\perp = \left\{z \in \mathbb{R}^n \,\middle|\, z^T\mathbf{1} = 0\right\}$. The orthogonal matrix $Q = \left[v_1^T; C\right]$ then defines an explicit transformation between z and $\left(z_\parallel, z_\perp\right)$. Next, take $z_\parallel$ as an invariant parameter of the system given that

$$\begin{aligned}\frac{dz_\parallel}{dt} &= \frac{d}{dt}v_1^T z \\ &= v_1^T\left(-\frac{1}{\varepsilon}L(\mathcal{G}_x)z\right) \\ &= 0\end{aligned}$$

for $x \in D_c$ as defined in Assumption 2. The dynamics of $z_\perp$ is then

$$\begin{aligned}\frac{dz_\perp}{dt} &= \frac{\partial z_\perp}{\partial z}\frac{dz}{dt} + \frac{\partial z_\perp}{\partial x}\frac{dx}{dt} \\ &= C\left(-\frac{1}{\varepsilon}L(\mathcal{G}_x)z\right) + \frac{\partial}{\partial x}\left(Cz\right)f(x,z) \\ &= -\frac{1}{\varepsilon}CL(\mathcal{G}_x)C^T z_\perp,\end{aligned}$$

where $z_\perp \in \mathbb{R}^{n-1}$. Further, these transformed fast dynamics have the unique, isolated root $z_\perp = 0$ corresponding to the algebraic equation $0 = -CL(\mathcal{G}_x)C^T z_\perp$. The dynamics (5.2) is therefore rewritten for $x \in D_c$ in standard singularly perturbed form as

$$\begin{aligned}\dot{x} &= f\left(x, z_\perp; z_\parallel\right) \\ \varepsilon\dot{z}_\perp &= -CL(\mathcal{G}_x)C^T z_\perp,\end{aligned} \tag{5.3}$$

where $f\left(x, z_\perp; z_\parallel\right) \triangleq f\left(x, v_1 z_\parallel + C^T z_\perp\right)$.

Reduced-order models can now be written using the transformed dynamics.

Definition 5.1. The Reduced Slow System of (5.3) is

$$\dot{x}^{(0)} = f\left(x^{(0)}, \mathbf{0}; \bar{z}\right) \tag{5.4}$$

subject to $x^{(0)}(0) = x(0)$, where $\bar{z} = \mathbf{1}^T z(0)$ is the average of the agents' initial state.

Definition 5.2. The Reduced Fast System of (5.3) is

$$\frac{d}{d\eta} z_\perp^{(0)} = -CL(\mathcal{G}_{x(0)}) C^T z_\perp^{(0)} \tag{5.5}$$

subject to $z_\perp^{(0)}(0) = z_\perp(0)$, where $\eta = t/\varepsilon$ is the fast time and $\mathcal{G}_{x(0)}$ denotes that the graph is fixed at the initial conditions of x.

The Reduced Fast System describes the evolution of the agent states over a fast timescale in the limit where edge dynamics are frozen. The Reduced Slow System then describes the evolution of the edge states in the limit where the agents have reached consensus at the average of their initial conditions. The validity of these reduced-order models is certified by the following theorem.

Theorem 5.1. *Under the dynamics (5.3) and with Assumptions 1 and 2, for any finite T there exists an $\varepsilon_0 > 0$ such that, for $0 < \varepsilon < \varepsilon_0$, the approximations given by (5.4) and (5.5) satisfy*

$$\begin{aligned} x(t) &= x^{(0)}(t) + \mathcal{O}(\varepsilon) \\ z_\perp(t) &= z_\perp^{(0)}(t/\varepsilon) + \mathcal{O}(\varepsilon) \end{aligned}$$

for all $t \in [0, T]$. Further, there exists a $t_1 > 0$ such that the approximation

$$z_\perp(t) = \mathbf{0} + \mathcal{O}(\varepsilon)$$

holds for $t \in [t_1, T]$.

Proof. The asymptotic error bounds follow from Theorem 2.1 since the problem is in standard form and by noting the assumptions. □

The results of Theorem 5.1 state that the reduced-order models (5.4) and (5.5) provide valid approximations of the true dynamics (5.3) on finite time intervals provided that ε is small enough, even without the stability of the reduced slow system guaranteed by Assumption 3. In terms of the network structure, by examining the dynamics (5.3) it can be seen that a larger $\lambda_2(\mathcal{G}_x)$ makes the agent dynamics faster and thus yields a smaller effective ε in Theorem 5.1. This indicates that adding edges with positive weights to the network will tend to make the reduced-order models better approximations of the original dynamics.

5.3.2 Quantitative Stability Bounds

While Theorem 5.1 describes a qualitative separation principle between the individual subsystems in (5.3), quantitative bounds on ε that guarantee stability of the coupled system are desirable. Such bounds are necessary to certify the performance of these complex, state-dependent networks. To this end, the following theorem uses the additional information provided by Assumption 3 to construct a Lyapunov function for the full dynamics (5.3) from Lyapunov functions for the reduced systems (5.4) and (5.5) to guarantees asymptotic stability of the equilibrium.

Theorem 5.2. *Under the dynamics (5.3) and with Assumptions 1-3, if there exists a "mixing" constant $\beta > 0$ such that*

$$\frac{\partial V_{slow}}{\partial x}\left\{f\left(x, z_\perp; z_\parallel\right) - f\left(x, \mathbf{0}; z_\parallel\right)\right\} \leq \beta\Psi(x, z_\parallel)\left\|z_\perp\right\|_2$$

for all $x \in D_c$ and $z_\perp \in \mathbb{R}^{n-1}$, then the set $(x, z) = \left(x_{eq}, z_\parallel \mathbf{1}\right)$ is asymptotically stable for all $\varepsilon > 0$.

Proof. Construct a Lyapunov function $V\left(x, z_\perp; z_\parallel\right) = (1-d)\, V_{\text{slow}}\left(x; z_\parallel\right) + dV_{\text{fast}}\left(x, z_\perp; z_\parallel\right)$ with $0 < d < 1$ for the full dynamics (5.3) from the Reduced Slow System Lyapunov function

V_{slow} given by Assumption 3 and a Reduced Fast System Lyapunov function $V_{\text{fast}} = \frac{1}{2} z_\perp^T z_\perp$. The time derivative of this composite Lyapunov function is then

$$\begin{aligned}
\dot{V} &= (1-d)\left\{ \frac{dV_{\text{slow}}}{dx}\frac{dx}{dt} + \frac{dV_{\text{slow}}}{dz_\parallel}\frac{dz_\parallel}{dt} \right\} \\
&\quad + d\left\{ \frac{dV_{\text{fast}}}{dz_\perp}\frac{dz_\perp}{dt} + \frac{dV_{\text{fast}}}{dx}\frac{dx}{dt} + \frac{dV_{\text{fast}}}{dz_\parallel}\frac{dz_\parallel}{dt} \right\} \\
&= (1-d)\left\{ \frac{dV_{\text{slow}}}{dx} f\left(x, z_\perp; z_\parallel\right) + \frac{dV_{\text{slow}}}{dz_\parallel} 0 \right\} \\
&\quad + d\left\{ z_\perp^T \frac{1}{\varepsilon} g_{\text{fast}}(x, z_\perp; z_\parallel) + 0 f\left(x, z_\perp; z_\parallel\right) + 0) \right\} \\
&= (1-d)\frac{dV_{\text{slow}}}{dx} f\left(x, z_\perp; z_\parallel\right) - \frac{d}{\varepsilon} z_\perp^T C L(\mathcal{G}_x) C^T z_\perp \\
&= (1-d)\frac{dV_{\text{slow}}}{dx} f\left(x, \mathbf{0}; z_\parallel\right) + (1-d)\frac{dV_{\text{slow}}}{dx}\left\{ f\left(x, z_\perp; z_\parallel\right) - f\left(x, \mathbf{0}; z_\parallel\right) \right\} \\
&\quad - \frac{d}{\varepsilon} z_\perp^T C L(\mathcal{G}_x) C^T z_\perp,
\end{aligned}$$

using the transformed coupled state dynamics (5.3).

Now, the first term of this time derivative can be bounded by

$$\frac{\partial V_{\text{slow}}}{\partial x} f\left(x, \mathbf{0}; z_\parallel\right) \leq -\alpha_1 \Psi^2(x, z_\parallel),$$

with $\alpha_1 > 0$ using Assumption 3. The mixing constant assumption in the theorem bounds the second term by

$$\frac{\partial V_{\text{slow}}}{\partial x}\left\{ f\left(x, z_\perp; z_\parallel\right) - f\left(x, \mathbf{0}; z_\parallel\right) \right\} \quad \leq \quad \beta \Psi(x, z_\parallel) \left\| z_\perp \right\|_2,$$

with $\beta \geq 0$. A bound on the third term is found to be

$$-z_\perp^T C L(\mathcal{G}_x) C^T z_\perp \leq -\min_{x \in D_c} \lambda_2\left(\mathcal{G}_x\right) \left\| z_\perp \right\|_2^2,$$

where $\min_{x \in D_c} \lambda_2\left(\mathcal{G}_x\right) > 0$ since $\mathcal{G}_x$ is connected on D_c. The total time derivative of the composite Lyapunov function is then bounded by

$$\dot{V} \leq -\begin{bmatrix} \Psi(x, z_\parallel) & \left\| z_\perp \right\|_2 \end{bmatrix} \mathbb{K}_1 \begin{bmatrix} \Psi(x, z_\parallel) \\ \left\| z_\perp \right\|_2 \end{bmatrix},$$

where

$$\mathbb{K}_1 \triangleq \begin{bmatrix} (1-d)\,\alpha_1 & -\frac{1}{2}(1-d)\,\beta \\ -\frac{1}{2}(1-d)\,\beta & \frac{d}{\varepsilon}\min_{x\in D_c}\lambda_2(\mathcal{G}_x) \end{bmatrix}.$$

Therefore, $\dot{V} \leq 0$ if the matrix $\mathbb{K}_1$ is positive definite. Since $\operatorname{trace}\mathbb{K}_1 > 0$, this occurs if and only if

$$\begin{aligned} 0 &< \det\mathbb{K}_1 \\ &= (1-d)\,\alpha_1\frac{d}{\varepsilon}\min_{x\in D_c}\lambda_2(\mathcal{G}_x) - \frac{1}{4}(1-d)^2\,\beta^2 \end{aligned}$$

which can be rearranged to bound ε as

$$\varepsilon < \frac{d}{(1-d)}\frac{4\alpha_1\min_{x\in D_c}\lambda_2(\mathcal{G}_x)}{\beta^2}. \tag{5.6}$$

In particular, given $0 < d < 1$ there is a corresponding ε such that inequality (5.6) is satisfied. Taking the limit of $d \to 1$ then establishes that an arbitrarily large ε may be used. □

Theorem 5.2 states, perhaps surprisingly, that the coupled system (5.3) is stable for *any* $\varepsilon > 0$ if the reduced systems are individually stable and if the difference between the Reduced Slow System dynamics and the full edge state dynamics can be appropriately bounded in the domain for some mixing constant β. However, the stability basin for a particular value of ε may be arbitrarily small. This is because, as illustrated in Figure 5.2a, the level sets of the composite Lyapunov function V at a given point may not be contained within D_c as $d \to 1$ in the proof of Theorem 5.2. If this occurs, the graph in the nominally stable consensus dynamics will become disconnected and the dynamic coupling may cause the system to be unstable. For practical purposes, then, it is desirable not only that the system be stable but also that a range of desirable initial conditions are guaranteed to be contained within the equilibrium's stability basin. The following theorem gives conditions on ε that ensure this property.

Theorem 5.3. *Under the conditions of Theorem 5.2, assume that:*

1. *Associated with the domain D_c is the constant $v_c \triangleq \min_{x\in\partial D_c} V_{slow}(x)$.*

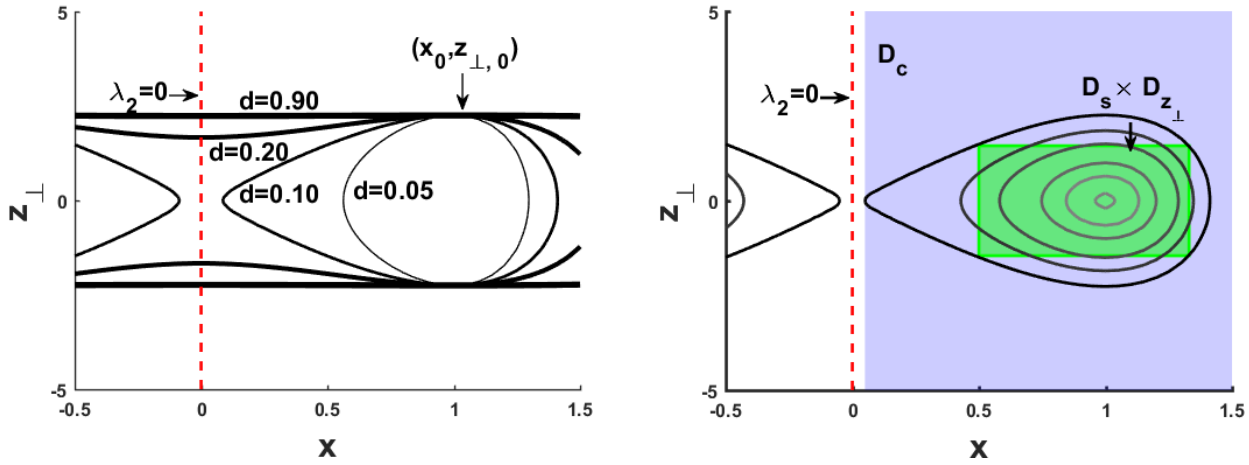

(a) (b)

Figure 5.2: Level sets of the composite Lyapunov function in Theorems 5.2 and 5.3. (a) behavior of the level sets evaluated at $(x_0, z_{\perp,0})$ as d increases. (b) Level sets are contained within the allowable domain for trajectories starting within the operating domain in Theorem 5.3.

2. *There is a sub-level set* $D_s = \left\{x \,\middle|\, V_{slow}(x) \leq v_s\right\}$ *with* $D_s \subset D_c$ *and* $x_{eq} \in D_s$ *such that* $v_s < v_c$.

3. *There is a set* $D_{z_\perp}$ *containing zero with the associated constant* $r_{z,\max} \triangleq \max_{z_\perp \in D_{z_\perp}} \|z_\perp\|_2$.

Then the set $D_s \times D_{z_\perp}$ *is within the asymptotic stability basin of the set* $(x, z_\perp) = (x_{eq}, 0)$ *for all* $0 < \varepsilon < \varepsilon^\star$, *where*

$$\varepsilon^\star = 8\frac{\alpha_1 (v_c - v_s) \min_{x \in D_c} \lambda_2 (\mathcal{G}_x)}{r_{z,\max}^2 \beta^2},$$

with α_1 *provided by Assumption 3 and* β *defined in Theorem 5.2.*

Proof. To find the sufficient bound on ε, a composite Lyapunov function is constructed so that the function's level sets are contained within the allowable domain for all initial conditions within the operating domain. This concept is illustrated in Figure 5.2b.

Begin by constructing a Lyapunov function $V = (1-d)\,V_{\text{slow}}\left(x; z_{\|}\right) + d\frac{1}{2}z_{\perp}^{T}z_{\perp}$ with $0 < d < 1$. Then, from the proof of Theorem 5.2, $\dot{V} \leq 0$ whenever (5.6) is satisfied. The particular value of d will now be chosen such that the system always starts at a level set of the composite Lyapunov function V below which the network will not become disconnected. In particular, note that the network is always connected for $x \in D_c$ but may be disconnected on its boundary ∂D_c. Therefore, the maximum allowable level set is defined by the minimum value of V_{slow} on this boundary, $(1-d)v_c$. Use this value to bound the total Lyapunov function from above:

$$(1-d)\,v_c \;>\; V\left(x, z_{\perp}; z_{\|}\right) \;=\; (1-d)\,V_{\text{slow}}\left(x; z_{\|}\right) + \frac{d}{2}z_{\perp}^{T}z_{\perp}.$$

For initial conditions within $D_s \times D_{z_\perp}$, V is closest to this upper bound if $z_{\perp}^{T}z_{\perp} = r_{z,\max}^{2}$ and $V_{\text{slow}} = v_s$. In this case, the bound becomes

$$(1-d)\,v_c > (1-d)\,v_s + \frac{d}{2}r_{z,\max}^{2}.$$

Rearranging, if

$$\frac{d}{(1-d)} < \frac{2\,(v_c - v_s)}{r_{z,\max}^{2}}$$

then initial conditions in D_s are guaranteed to start below the minimum unallowable level set. Combining this with the $\dot{V}$ inequality (5.6), if

$$\varepsilon^{\star} = 8\frac{\alpha_1\,(v_c - v_s)\min_{x\in D_c}\lambda_2\left(\mathcal{G}_x\right)}{r_{z,\max}^{2}\beta^{2}},$$

then both the maximum level set condition and the $\dot{V} < 0$ inequality condition (5.6) are satisfied for $\varepsilon < \varepsilon^{\star}$ and $\{x, z_{\perp}\} \in D_s \times D_{z_\perp}$ will asymptotically approach the equilibrium. $\square$

Theorem 5.3 provides an ε bound that guarantees that any initial conditions drawn from $D_s \times D_{z_\perp}$ will asymptotically approach the equilibrium set $(x, z) = (x_{\text{eq}}, 0)$. It does *not* state that trajectories will stay within $D_s \times D_{z_\perp}$ on their way to the equilibrium set. Instead, this theorem provides a guarantee that the edge states x will remain within the smallest level set of V_{slow} defined by the boundary of D_c. Practically speaking, this theorem provides conditions to ensure that if the state-dependent graph starts connected then it will remain connected with the agents approaching consensus.

5.3.3 Example

Consider the dynamics (5.2) with $z \in \mathbb{R}^n$, and $x \in \mathbb{R}^m$ composed of states x_{ij} corresponding to edge $\{i,j\} \in E$. The particular dynamics defined for every edge is

$$f_{ij}(x_{ij}, z) = 1 - x_{ij}^2 - |z_i - z_j|,$$

and the weights $w_{ij}(x) = x_{ij}/n$. These dynamics satisfy Assumption 1, and Assumption 2 for the set $D_c \triangleq \left\{x \in \mathbb{R}^m \,\middle|\, 0.05 \leq x_{ij} \leq 1.25\right\}$. Therefore, by Theorem 5.1 a separation principle is guaranteed between the fast consensus dynamics and the slow edge dynamics for small enough ε. Further, the corresponding reduced-order models, based on the isolated subsystem dynamics, have trajectory errors of $\mathcal{O}(\varepsilon)$. This result is depicted in Figure 5.3, which shows how the reduced-order models (5.4) and (5.5) become more accurate as ε decreases.

In order to find a bound on ε that guarantees that the coupled system (5.3) (equivalently (5.2)) is stable from a set of possible initial conditions, take $V_{\text{slow}}(x) = \frac{1}{4}\sum_{\{i,j\}\in E}\left(1 - x_{ij}^2\right)^2$. Then

$$\frac{\partial V_{\text{slow}}}{\partial x} f\left(x, z_\parallel \mathbf{1}\right) = -\sum_{\{i,j\}\in E} \left(\left(1 - x_{ij}^2\right)\sqrt{x_{ij}}\right)^2,$$

so Assumption 3 is satisfied with $\alpha_1 = 1$ and $\Psi(x) = \sqrt{\sum_{\{i,j\}\in E}\left(\left(1 - x_{ij}^2\right)\sqrt{x_{ij}}\right)^2}$. Further,

$$\begin{aligned}
\frac{\partial V_{\text{slow}}}{\partial x}\left\{f\left(x, z_\perp; z_\parallel\right) - f\left(x, \mathbf{0}; z_\parallel\right)\right\} &= -\sum_{\{i,j\}\in E}\left(1 - x_{ij}^2\right) x_{ij}\left\{\left(1 - x_{ij}^2 - |z_{i,1} - z_{j,1}|\right) - \left(1 - x_{ij}^2\right)\right\} \\
&= \sum_{\{i,j\}\in E}\left(1 - x_{ij}^2\right) x_{ij}\,|z_{i,1} - z_{j,1}| \\
&\leq \sum_{\{i,j\}\in E}\left(1 - x_{ij}^2\right)\sqrt{x_{ij}}\sqrt{x_{ij,\max}}\,|z_{i,1} - z_{j,1}| \\
&\leq \sqrt{x_{\max}}\sum_{\{i,j\}\in E}\left|\left(1 - x_{ij}^2\right)\sqrt{x_{ij}}\right|\,|z_{i,1} - z_{j,1}| \\
&\leq \sqrt{x_{\max}}\sqrt{\sum_{\{i,j\}\in E}\left(\left(1 - x_{ij}^2\right)\sqrt{x_{ij}}\right)^2}\sqrt{\sum_{\{i,j\}\in E}\left(z_{i,1} - z_{j,1}\right)^2} \\
&= \sqrt{x_{\max}}\Psi(x)\sqrt{\sum_{\{i,j\}\in E}\left(z_{i,1} - z_{j,1}\right)^2},
\end{aligned}$$

by use of the Schwartz inequality. With $D(\mathcal{G})$ the incidence matrix of the graph $\mathcal{G}$,

$$\begin{aligned}\sqrt{\sum_{\{i,j\}\in E}\left(z_{i,1}-z_{j,1}\right)^2} &= \sqrt{\left(D(\mathcal{G})z\right)^T\left(D(\mathcal{G})z\right)}\\ &= \left\|D(\mathcal{G})z\right\|_2\\ &= \left\|D(\mathcal{G})\left(\frac{1}{n}\mathbf{1}z_{\|}+C^Tz_{\perp}\right)\right\|_2\\ &= \left\|D(\mathcal{G})C^Tz_{\perp}\right\|_2\\ &\leq \left\|D(\mathcal{G})C^T\right\|_2\left\|z_{\perp}\right\|_2\\ &= \left\|D(\mathcal{G})\right\|_2\left\|z_{\perp}\right\|_2,\end{aligned}$$

and the inequality becomes

$$\frac{\partial V_{\text{slow}}}{\partial x}\left\{f\left(x,z_{\perp};z_{\|}\right)-f\left(x,\mathbf{0};z_{\|}\right)\right\}\leq\sqrt{x_{\max}}\left\|D(\mathcal{G})\right\|_2\Psi(x)\left\|z_{\perp}\right\|_2.$$

The additional assumption in Theorem 5.2 is therefore satisfied with $\beta=\sqrt{x_{\max}}\left\|D(\mathcal{G})\right\|_2$. Assuming a cycle graph on 5 nodes, then $n=m=5$,

$$\min_{x\in D_c}\lambda_2\left(\mathcal{G}_x\right)=\lambda_2\left(\mathcal{G}_{x=0.05}\right)=1.38\times10^{-2},$$

and $\left\|D(\mathcal{G})\right\|_2^2=3.618$. From the definition of D_c, $x_{\max}=1.25$ and the constant v_c is found as

$$v_c=\min_{x\in\partial D_c}V_{\text{slow}}(x)=1.25.$$

With $D_s\triangleq\left\{x\in\mathbb{R}^m\,\middle|\,0.25\leq x_{ij}\leq1.25\right\}$, the constant v_s is found as

$$v_s=\max_{x\in\partial D_s}V_{\text{slow}}(x)=1.10.$$

If the initial state $z(0)$ of the agents satisfy $\left\|z\right\|_\infty\leq1$, then take $D_{z_\perp}=\left\{z_\perp\in\mathbb{R}^4\,\middle|\,\left\|C^Tz_\perp\right\|_\infty\leq1\right\}$

so that

$$\begin{aligned} r_{z,\max}^2 &= \max_{z_\perp \in D_{z_\perp}} \|z_\perp\|_2^2 \\ &= \max_{z \in D_z} \|Cz\|_2^2 \\ &\leq \left(\|C\|_2 \max_{z \in D_z} \|z\|_2 \right)^2 \\ &= \left(\max_{z \in D_z} \|z\|_2 \right)^2 \\ &= \left(\|\mathbf{1}_{5\times 1}\|_2 \right)^2 \\ &= 5. \end{aligned}$$

Therefore, by Theorem 5.3, the initial conditions $(x(0), z(0)) \in D_s \times D_{z_\perp}$ are guaranteed to be within the stability basin of (5.3) for all (positive) ε less than

$$\begin{aligned} \varepsilon^\star &= 8 \frac{\alpha_1 \left(v_c - v_s\right) \min_{x \in D_c} \lambda_2 \left(\mathcal{G}_x\right)}{r_{z,\max}^2 \beta^2} \\ &= 7.39 \times 10^{-4}. \end{aligned}$$

In fact, Figure 5.3 shows that the derived bound is conservative for this example. Additional simulations indicate that the system may be stable for $\varepsilon < 6.10 \times 10^{-2}$. However, guarantees are not available with this higher "experimental bound" for all initial conditions in $D_s \times D_{z_\perp}$. Furthermore, the separation principle is lost for these larger ε values as the subsystems' characteristic timescales become commingled, leading to a loss of the well-understood behavior of the consensus dynamics for the agent states.

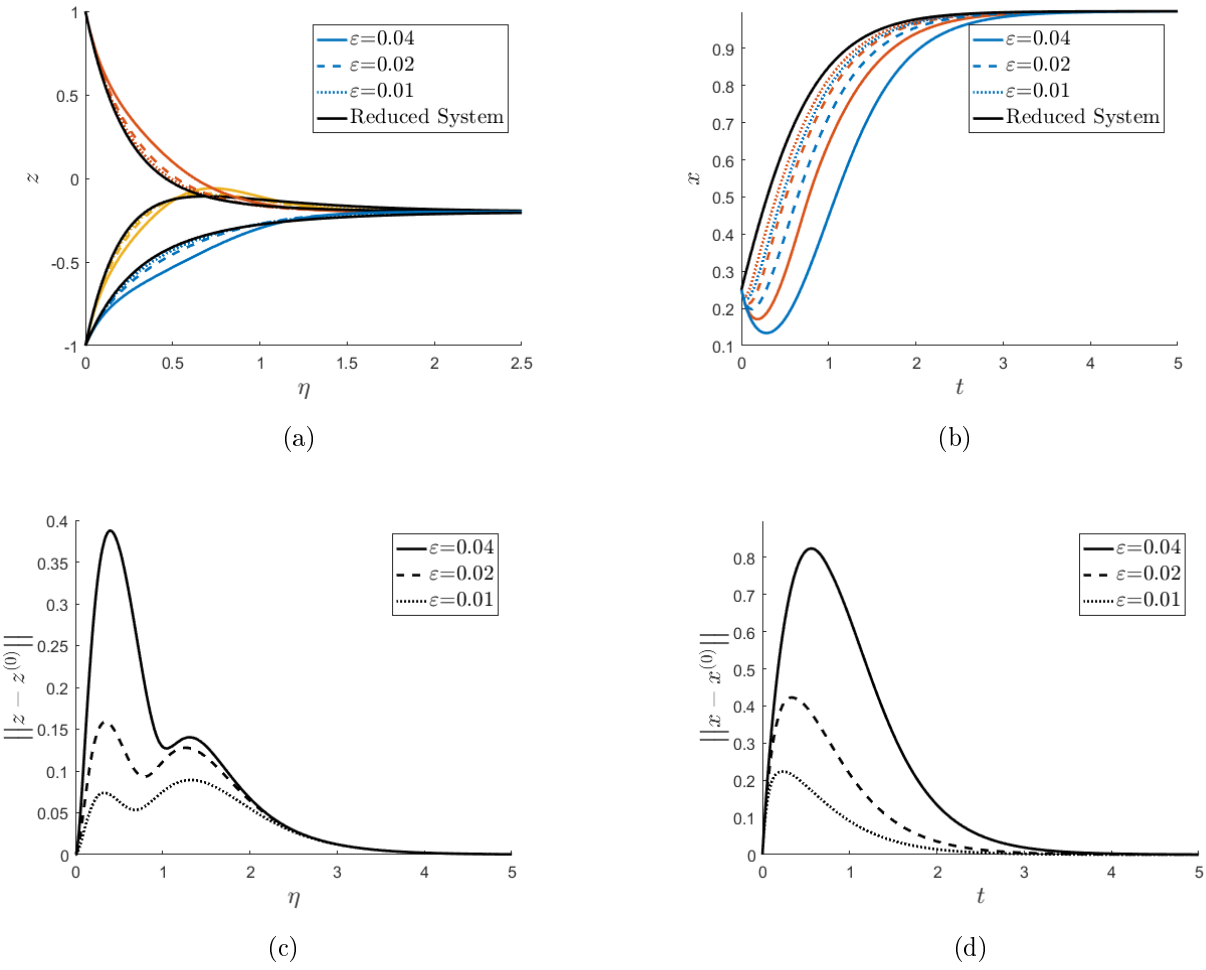

Figure 5.3: Comparison of state evolution for different ε values in the example of Section 5.3.3. (a) Agent state trajectories. (b) Edge state trajectories. (c) Norm of agent error trajectories. (d) Norm of edge error trajectories.

5.4 Consensus Tracking with Continuous Communication

Consider the consensus tracking dynamics with continuous communication given by

$$\begin{aligned} \dot{x} &= -(L(\mathcal{G}) \otimes I)(I \otimes M)\, z \;\; = -(L(\mathcal{G}) \otimes M) z \\ \varepsilon \dot{z} &= g(x, z), \end{aligned} \tag{5.7}$$

and illustrated in Figure 5.4. Here, $z = \left[z_1^T \cdots z_n^T\right]^T$ is the collection of true agent states $z_i(t) \in D_z \subset \mathbb{R}^{p+p_0}$, $x = \left[x_1^T \cdots x_n^T\right]^T$ is the collection of tracked virtual consensus reference states $x_i(t) \in D_x \subset \mathbb{R}^p$, $g(x, z) = \left[g_1(x_1, z_1)^T \cdots g_n(x_n, z_n)^T\right]^T$ is the collection of tracking dynamics $g_i(x_i, z_i)$, $\mathcal{G}$ is a connected graph, and ε is a small, positive parameter. It is assumed that the agreement states are encoded in the first p elements of z_i, namely $[I,\, \mathbf{0}]z_i \triangleq M z_i \subset \mathbb{R}^p$, and the remaining non-agreement states represented by $[\mathbf{0},\, I]z_i \triangleq M_0 z_i \subset \mathbb{R}^{p_0}$. In this context, the parameter ε naturally arises from control gains embedded in the fast tracking dynamics. Inherent in the formulation of (5.7) is the assumption of continuous communication between agents, which gives rise to the correspondingly continuous evolution of the reference states, x. This assumption is reasonable, for example, when the communication occurs quickly and at a high bandwith. Of course, inter-agent communication is not always guaranteed to occur quickly, and such a scenario is investigated in Section 5.5.

To aid the subsequent analysis, consider the following assumptions.

Assumption 4. *The function $g_i(x_i, z_i)$ is continuously differentiable and has a unique, isolated zero, namely $z_i = h_i(x_i) = \begin{bmatrix} x_i^T & \mathbf{0}^T \end{bmatrix}^T = M^T x_i$ with $h(x) = \left[h_1(x_1)^T \cdots h_n(x_n)^T\right]^T = (I \otimes M^T)x$ the collection of these zeros.*

Assumption 5. *Defining the error term $\hat{z}_i = z_i - h_i(x_i)$ and $\hat{z} = \left[\hat{z}_1^T \cdots \hat{z}_n^T\right]^T$, there exists a positive-definite Lyapunov function $V_{fast,i}(\hat{z}_i)$ in the domains D_x and D_z containing $(x_i, z_i) = \left(x_i, M^T x_i\right)$ such that, for all $z_i \in D_z$ and $x_i \in D_x$,*

$$\frac{\partial V_{fast,i}}{\partial \hat{z}_i} g_i(x_i, \hat{z}_i + h_i(x_i)) \leq -\alpha_2 \Phi_i^2(\hat{z}_i),$$

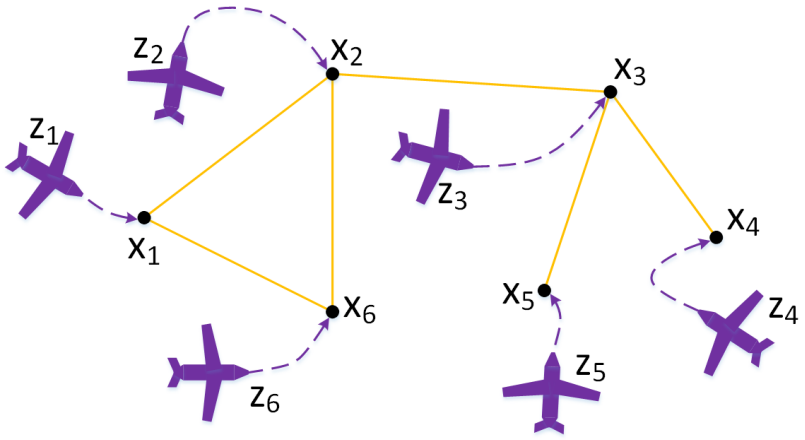

Figure 5.4: Consensus tracking problem with fast agent states, z, and slow virtual consensus states, x

where $\alpha_2 > 0$ *and* $\Phi_i(\hat{z}_i)$ *is a continuous scalar function with* $\Phi_i(0) = 0$. *Associated with the collections of individual Lyapunov functions* $V_{fast,i}(\hat{z}_i)$ *and functions* $\Phi_i(\hat{z}_i)$ *are the functions* $V_{fast}(\hat{z}) = \sum_{i=1}^{n} V_{fast,i}(\hat{z}_i)$ *and* $\Phi^2(\hat{z}) = \sum_{i=1}^{n} \Phi_i^2(\hat{z}_i)$.

Assumption 4 states that the isolated tracking dynamics has a unique equilibrium, ensuring that the reduced-order models which will be developed in Section 5.4.1 are well-posed. The equilibrium for the agreement states is the reference command, x_i, while the equilibrium for the non-agreement states is assumed to be zero. Assumption 5 then states that this equilibrium is uniformly asymptotically stable for a fixed reference command, a common assumption for tracking dynamics. The assumed Lyapunov function for these isolated dynamics will be used to develop conditions that ensure stability of the coupled system (5.7) in Section 5.4.2.

5.4.1 Reduced-Order Models

This section provides reduced-order models for the dynamics (5.7) based on the timescale separation between the slow evolution of the consensus dynamics and the fast evolution of

the agents' tracking dynamics as $\varepsilon \to 0^+$. By Assumptions 4 and 5, the dynamics (5.7) are in standard singularly perturbed form. Therefore, as described in Section 2.2, reduced-order models that describe the evolution of the individual subsystems over their characteristic timescales can be directly defined as follows.

Definition 5.3. The Reduced Slow System of (5.7) is

$$\dot{x}^{(0)} = -(L(\mathcal{G}) \otimes I)x^{(0)} \tag{5.8}$$

subject to $x^{(0)}(0) = x(0)$.

Definition 5.4. The Reduced Fast System of (5.7) is

$$\frac{d}{d\eta} z^{(0)} = g(\hat{x}, z^{(0)} + h(\hat{x})), \tag{5.9}$$

subject to $z^{(0)}(0) = z(0)$, where $\eta = t/\varepsilon$ is the fast time and $\hat{x} = x(0)$ is considered a fixed parameter.

The Reduced Fast System describes the evolution of the agent states over a fast timescale in the limit where the reference trajectory is fixed. The Reduced Slow System then describes the evolution of the consensus-based reference trajectory in the limit where the agents perfectly track the given reference command. The validity of these reduced-order models is certified by the following theorem.

Theorem 5.4. *Under the dynamics (5.7) and with Assumptions 4 and 5, for any finite T there exists an $\varepsilon_0 > 0$ such that, for $0 < \varepsilon < \varepsilon_0$, the approximations given by (5.8) and (5.9) satisfy*

$$\begin{aligned} x(t) &= x^{(0)}(t) + \mathcal{O}(\varepsilon) \\ z(t) &= (I \otimes M^T)x^{(0)}(t) + z^{(0)}(t/\varepsilon) + \mathcal{O}(\varepsilon) \end{aligned}$$

for all $t \in [0, T]$. Further, there exists a $t_1 > 0$ such that the approximation

$$z(t) = (I \otimes M^T)x^{(0)}(t) + \mathcal{O}(\varepsilon)$$

holds for $t \in [t_1, T]$.

Proof. The asymptotic error bounds follow from Theorem 2.1 since the problem is in standard form and by noting the assumptions. □

The results of Theorem 5.4 state that, on finite time intervals, the reduced-order models (5.8) and (5.9) provide good approximations of the true dynamics (5.7) when ε is small enough. With regard to the network structure, by examining the dynamics (5.7) it can be seen that a smaller $\lambda_{\max}(\mathcal{G})$, which is correlated with the maximum node degree, makes the consensus dynamics slower relative to the fast agent dynamics, yielding a smaller effective ε and thus tending to make the reduced-order models better approximations of the true dynamics.

5.4.2 Quantitative Stability Bounds

The qualitative separation principle described by Theorem 5.4 implies that, for small enough ε, the tracking dynamics can in general be designed separately from the network dynamics. For any particular manifestation and implementation of these dynamics, however, quantitative bounds on ε are required that certify the stability of the coupled system (5.7). Such bounds are now described by the following theorem, which constructs a Lyapunov function for the full dynamics from Lyapunov functions for the reduced systems to guarantee asymptotic stability of the consensus subspace.

Theorem 5.5. *Under the dynamics (5.7) and with Assumptions 4 and 5, if there exists "mixing" constants $\beta_1, \beta_3, \gamma_2 \geq 0$ such that*

1. $-x_\perp^T (L(\mathcal{G}) \otimes M)\hat{z} \leq \beta_1 \left\|x_\perp\right\|_2 \Phi(\hat{z})$
2. $\frac{\partial V_{fast}}{\partial \hat{z}} \left(L(\mathcal{G}) \otimes M^T\right) \left((I \otimes M)\,\hat{z} + x_\perp\right) \leq \beta_3 \left\|x_\perp\right\|_2 \Phi(\hat{z}) + \gamma_2 \Phi(\hat{z})^2$

for all $x \in D_x$ and $z \in D_z$, where $\hat{z} = z - h(x)$ and $x_\perp \triangleq x - \frac{1}{n}(\mathbf{1}\mathbf{1}^T \otimes I)x$, then the consensus subspace is asymptotically stable for all $0 < \varepsilon < \varepsilon^\star$, where

$$\varepsilon^\star = \frac{\alpha_2}{\gamma_2 + \frac{\beta_1 \beta_3}{\lambda_2(\mathcal{G})}}$$

and α_2 is defined in Assumption 5.

Proof. Construct a Lyapunov function $V = (1-d)\,V_{\text{slow}}(x) + dV_{\text{fast}}(x,z)$, with $0 < d < 1$ for the full dynamics from a Reduced Slow System Lyapunov function $V_{\text{slow}} = \frac{1}{2}x^T x$ and the Reduced Fast System Lyapunov function V_{fast} given in Assumption 5. Using

$$\begin{aligned}\frac{d\hat{z}}{dx} &= \frac{d}{dx}\left(z - h(x)\right)\\ &= \frac{d}{dx}\left(z - \left(I \otimes M^T\right)x\right)\\ &= -\left(I \otimes M^T\right),\end{aligned}$$

the time derivative of this composite Lyapunov function is then found to be

$$\begin{aligned}\dot{V} = &\ (1-d)\,x^T\frac{dx}{dt} + d\left\{\frac{dV_{\text{fast}}}{d\hat{z}}\frac{d\hat{z}}{dz}\frac{dz}{dt} + \frac{dV_{\text{fast}}}{d\hat{z}}\frac{d\hat{z}}{dx}\frac{dx}{dt}\right\}\\ = &\ -(1-d)\,x^T(L(\mathcal{G})\otimes I)x - (1-d)\,x^T(L(\mathcal{G})\otimes M)\hat{z}\\ &+ d\frac{1}{\varepsilon}\frac{dV_{\text{fast}}}{d\hat{z}}g(x,\hat{z}+h(x))\\ &+ d\frac{dV_{\text{fast}}}{d\hat{z}}\left(I\otimes M^T\right)(L(\mathcal{G})\otimes M)\left(\hat{z}+h(x)\right).\end{aligned}$$

Now, the first term of this time derivative is bounded by

$$-x^T(L(\mathcal{G})\otimes I)x \le -\lambda_2(\mathcal{G})x_\perp^T x_\perp,$$

where $x_\perp = x - x_\parallel$, the difference between the state x and its average component in each dimension $x_\parallel \triangleq \frac{1}{n}(\mathbf{1}\mathbf{1}^T \otimes I)x$. The second component is bounded as

$$\begin{aligned}-x^T(L(\mathcal{G})\otimes M)\hat{z} &= -\left(x_\perp + x_\parallel\right)^T(L(\mathcal{G})\otimes M)\hat{z}\\ &= -x_\perp^T(L(\mathcal{G})\otimes M)\hat{z}\\ &\le \beta_1\left\|x_\perp\right\|_2\Phi(\hat{z}),\end{aligned}$$

using the theorem's first assumption, while the third component is bounded by

$$\begin{aligned}\frac{dV_{\text{fast}}}{d\hat{z}}g(x,\hat{z}+h(x)) &= \sum_{i=1}^{n}\frac{\partial V_{\text{fast},i}}{\partial\hat{z}_i}g_i(x_i,\hat{z}_i+h_i(x_i))\\ &\le -\sum_{i=1}^{n}\alpha_2\Phi_i^2(\hat{z}_i)\\ &= -\alpha_2\Phi^2(\hat{z}),\end{aligned}$$

using Assumption 5. The last term is bounded by

$$\begin{aligned}\frac{dV_{\text{fast}}}{d\hat{z}}\left(I\otimes M^T\right)\left(L(\mathcal{G})\otimes M\right)\left(\hat{z}+h(x)\right) &= \frac{dV_{\text{fast}}}{d\hat{z}}\left(L(\mathcal{G})\otimes M^TM\right)\left(\hat{z}+h(x)\right)\\ &\leq \beta_3\left\|x_\perp\right\|_2\Phi(\hat{z})+\gamma_2\Phi(\hat{z})^2,\end{aligned}$$

using the mixed-product property of the Kronecker product and the theorem's second assumption. The total time derivative of the composite Lyapunov function is then bounded by

$$\dot{V}\leq -\begin{bmatrix}\left\|x_\perp\right\|_2 & \Phi(\hat{z})\end{bmatrix}\mathbb{K}_2\begin{bmatrix}\left\|x_\perp\right\|_2\\ \Phi(\hat{z})\end{bmatrix},$$

where

$$\mathbb{K}_2\triangleq\begin{bmatrix}(1-d)\lambda_2(\mathcal{G}) & -\frac{1}{2}\left\{(1-d)\,\beta_1+d\beta_3\right\}\\ -\frac{1}{2}\left\{(1-d)\,\beta_1+d\beta_3\right\} & d\alpha_2/\varepsilon-d\gamma_2\end{bmatrix}.$$

Therefore, if the matrix $\mathbb{K}_2$ is positive definite then $\dot{V}<0$ when $x\neq x_\parallel$ and $\hat{z}\neq 0$. Since $\operatorname{trace}\mathbb{K}_2>0$, this occurs if and only if

$$0 \;<\; \det\mathbb{K}_2 \;=\; d(1-d)\lambda_2(\mathcal{G})\Big(\frac{\alpha_2}{\varepsilon}-\gamma_2\Big)-\frac{1}{4}\{(1-d)\,\beta_1+d\beta_3\}^2$$

In particular, given $0<d<1$ there is a corresponding ε such that this inequality is satisfied.

To find the value of d that maximizes ε while guaranteeing $\dot{V}<0$ when $x\neq x_\parallel$ and $\hat{z}\neq 0$, note that the above inequality can be viewed geometrically as a condition on a parabola in $s\triangleq d/(1-d)$:

$$\beta_3^2s^2+\left[2\beta_1\beta_3-4\lambda_2(\mathcal{G})\Big[\frac{\alpha_2}{\varepsilon}-\gamma_2\Big]\right]s+\beta_1^2<0 \tag{5.10}$$

The parabola has zeros at

$$s\big|_{\text{zeros}}=\frac{1}{2\beta_3^2}\left(-\left[2\beta_1\beta_3-4\lambda_2(\mathcal{G})\Big[\frac{\alpha_2}{\varepsilon}-\gamma_2\Big]\right]\pm\sqrt{\left[2\beta_1\beta_3-4\lambda_2(\mathcal{G})\Big[\frac{\alpha_2}{\varepsilon}-\gamma_2\Big]\right]^2-4\beta_1^2\beta_3^2}\right), \tag{5.11}$$

and is non-negative at $s=d=0$ and at $s=\infty\Leftrightarrow d=1$. The parabola therefore has negative values, leading to $\dot{V}<0$, when the zeros are real. This occurs for

$$\varepsilon<\varepsilon_{\text{crit}}\triangleq\frac{\alpha_2}{\gamma_2+\frac{\beta_1\beta_3}{\lambda_2(\mathcal{G})}},$$

which is associated with $s_{\text{crit}} = (d/(1-d))_{\text{crit}} = \beta_1/\beta_3$. Taking $\varepsilon^\star = \varepsilon_{\text{crit}}$ then provides the result. □

The result of Theorem 5.5 is a sufficient bound on ε that guarantees the convergence of the consensus tracking dynamics. The bound is improved as the speed of the tracking dynamics is increased (α_2 becomes larger), and is diminished as the mixing constants β_1, β_3, and γ_2 grow larger. These results are guaranteed for initial conditions within an unspecified neighborhood of the consensus subspace. In many cases, however, stability guarantees are desired from a particular range of starting conditions. To this end, the following theorem gives bounds on ε that guarantee that a given set of initial conditions is within the equilibrium's basin of attraction.

Theorem 5.6. *Under the conditions of Theorem 5.5, assume that:*

1. *Associated with the domain $D_x \times D_z$ is the constant $v_z \triangleq \min_{(x,z)\in\partial(D_x\times D_z)} V_{fast}(z-h(x))$.*

2. *There is a sub-level set $D_o = \left\{(x,z) \in D_x \times D_z \,\middle|\, V_{fast}(z-h(x)) \leq v_o\right\}$ with $D_o \subset D_x \times D_z$ and $\left(x_{\|}, h(x_{\|})\right) \in D_o$ such that $v_o < v_u$.*

Then the consensus subspace $\mathcal{X}_c$ is asymptotically stable from initial conditions $(x,z) \in D_o$ for all $0 < \varepsilon < \varepsilon^\star$, where

$$\varepsilon^\star = \begin{cases} \frac{\alpha_2}{\gamma_2 + \frac{\beta_1\beta_3}{\lambda_2(\mathcal{G})}}, & \frac{\beta_1}{\beta_3} > \frac{\zeta}{2} \\ \frac{\alpha_2}{\gamma_2 + \frac{\left(\zeta\beta_3^2 + 2\beta_1\beta_3\right)^2}{8\lambda_2(\mathcal{G})\beta_3^2\zeta}}, & \text{otherwise} \end{cases},$$

with $r_{x,\max} \triangleq \max_{x\in D_x} \|x\|_2$ and $\zeta \triangleq r_{x,\max}^2/(v_z - v_o)$.

Proof. To find the sufficient bound on ε, a composite Lyapunov function is constructed so that the function's level sets are contained within the allowable domain for all initial conditions within the operating domain.

As in Theorem 5.5, construct the composite Lyapunov function as $V = (1-d)\,\frac{1}{2}x^T x + dV_{\text{fast}}(\hat{z})$, with $0 < d < 1$. Now, the question is how to choose d (and therefore ε) such that

a desired domain of stability is maintained. Intuitively, the key is to never let the agent states out of the domain where the tracking dynamics are guaranteed to work. Therefore, the maximum allowable level set is defined by the minimum value of V_{fast} on its boundary, dv_z. So, bound the total Lyapunov function from above by

$$dv_z \;>\; V(x,z) \;=\; (1-d)\,\frac{1}{2}x^T x + dV_{\text{fast}}(x,z)\,.$$

The Lyapunov function is closest to the bound if $x^T x = r_{x,\max}^2$, so the system is guaranteed to start below the maximum allowable level set if

$$\frac{d}{(1-d)} > \frac{r_{x,\max}^2}{2\,(v_z - v_o)}. \tag{5.12}$$

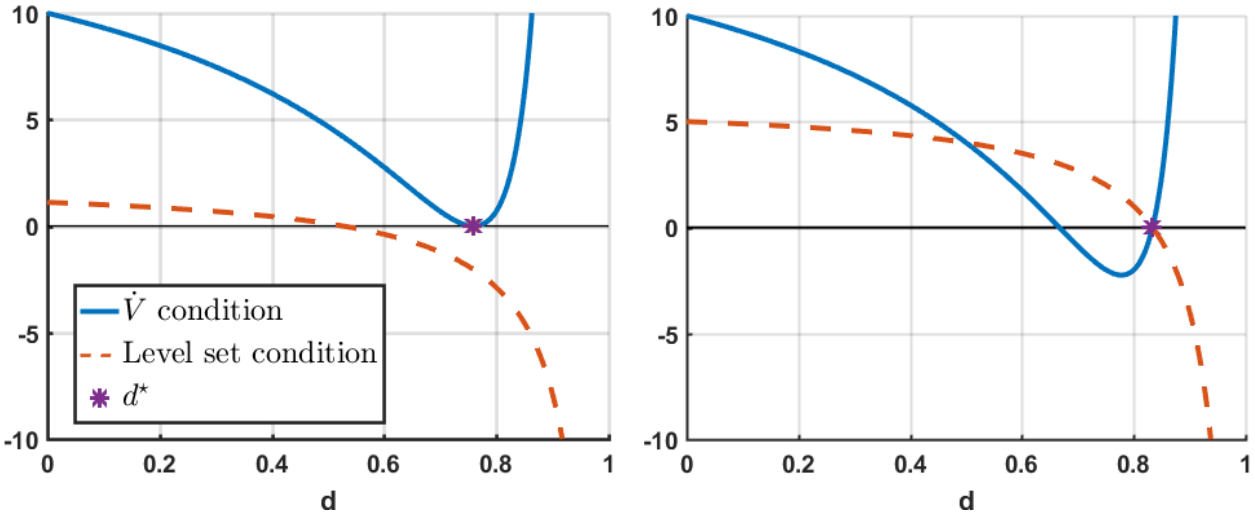

(a) (b)

Figure 5.5: The two cases for the level set and $\dot{V}$ conditions in the proof of Theorem 5.6. (a) Case 1. (b) Case 2.

Now, from Theorem 5.5, $\dot{V} < 0$ if the parabola inequality (5.10) is satisfied . This occurs for $\varepsilon < \varepsilon_{\text{crit}}$ at the associated point $(d/(1-d))_{\text{crit}}$. There are two cases to consider. In the first case, the level set condition (5.12) holds for a minimum $d/(1-d)$ less than $(d/(1-d))_{\text{crit}}$,

and the bound on ε may be taken as $\varepsilon_1^\star = \varepsilon_{\text{crit}}$ since both the level set and the $\dot{V}$ condition will hold at $(d/(1-d))_{\text{crit}}$. Otherwise, the second case holds where the minimum level set value is to the right of $(d/(1-d))_{\text{crit}}$ and ε must be set smaller so that the parabola has a lower minima and both conditions are satisfied at the same value of $d/(1-d)$. These two cases are visualized in Figure 5.5. In the second case, set the right-hand zero of the parabola to occur at

$$\frac{d}{1-d} = \frac{r_{x,\max}^2}{2\left(v_z - v_o\right)}. \tag{5.13}$$

That is, at the smallest value of $d/(1-d)$ given by the level set condition so that there is overlap between the intervals where (5.12) and (5.10) are satisfied. Using (5.13) in the equation for the parabola zeros (5.11) yields

$$\frac{r_{x,\max}^2}{2\left(v_z - v_o\right)} = \frac{1}{2\beta_3^2}\left(-\left[2\beta_1\beta_3 - 4\lambda_2(\mathcal{G})\left[\frac{\alpha_2}{\varepsilon} - \gamma_2\right]\right] + \sqrt{\left[2\beta_1\beta_3 - 4\lambda_2(\mathcal{G})\left[\frac{\alpha_2}{\varepsilon} - \gamma_2\right]\right]^2 - 4\beta_1^2\beta_3^2}\right).$$

This equation is satisfied by

$$\varepsilon_2^\star = \frac{\alpha_2}{\gamma_2 + \left(\zeta\beta_3^2 + 2\beta_1\beta_3\right)^2 / \left(8\lambda_2(\mathcal{G})\beta_3^2\zeta\right)},$$

where $\zeta = r_{x,\max}^2/(v_z - v_o)$. The overall bound for ε is therefore found dependent on the case as

$$\varepsilon^\star = \begin{cases} \varepsilon_1^\star, & \text{if } \frac{\beta_1}{\beta_3} > \frac{\zeta}{2} \\ \varepsilon_2^\star, & \text{otherwise} \end{cases},$$

with

$$d^\star = \max\left\{\frac{\beta_1}{\beta_1 + \beta_3}, \frac{r_{x,\max}}{r_{x,\max} + 2\left(v_z - v_o\right)}\right\}$$

as the associated value of d. □

In Theorem 5.6, two cases are presented for the upper bound $\varepsilon^\star$. In the first case, the desired set of initial conditions are found to be within the neighborhood guaranteed by the results of Theorem 5.5, yielding the same bound. In the second case, however, a different

composite Lyapunov function must be chosen to ensure that the state trajectories stay within $D_x \times D_z$, yielding a different corresponding bound. The stability bounds in Theorem 5.5 and 5.6 can be further related to graph-based features when Assumption 5 admits a special Lyapunov function. This is summarized in the following corollary.

Corollary 5.1. *For the dynamics and assumptions of Theorem 5.5 with Assumption 5 satisfied by* $V_{fast} = \hat{z}^T (M \otimes I)^T Q (M \otimes I) \hat{z} + W(M_0 \hat{z})$ *for* $0 \preceq Q \preceq qI$*, some positive semidefinite function* $W(\cdot) \in \mathbb{R}^{d_0} \to \mathbb{R}$*, and* $\Phi(\hat{z})^2 = \hat{z}^T \left(M^T M \otimes I\right) \hat{z}$*, then the upper bound on* ε *that guarantees stability is*

$$\varepsilon^\star = \frac{\alpha_2}{\lambda_{max}(\mathcal{G}) q \left(1 + \frac{\lambda_{max}(\mathcal{G})}{\lambda_2(\mathcal{G})}\right)}.$$

If the assumptions of Theorem 5.6 are additionally applied, then the upper bound is further refined as

$$\varepsilon^\star = \begin{cases} \frac{\alpha_2}{\lambda_{\max}(\mathcal{G}) q \left(1 + \frac{\lambda_{\max}(\mathcal{G})}{\lambda_2(\mathcal{G})}\right)}, & \text{if } \frac{1}{q} > \frac{\zeta}{2} \\ \frac{\alpha_2}{\lambda_{\max}(\mathcal{G}) \left(q + \frac{(\zeta q + 2)^2}{8\zeta} \frac{\lambda_{\max}(\mathcal{G})}{\lambda_2(\mathcal{G})}\right)}, & \text{otherwise} \end{cases},$$

with $r_{x,\max} \triangleq \max_{x \in D_x} \|x\|_2$ *and* $\zeta \triangleq r_{x,\max}^2 / (v_z - v_o)$.

Proof. Theorems 5.5 and 5.6 are satisfied with use of the Cauchy-Schwarz inequality using $\beta_1 = \lambda_{\max}(\mathcal{G})$ and $\beta_3 = \gamma_2 = \lambda_{\max}(\mathcal{G}) q$. □

It is clear from Corollary 5.1 that a larger value of $\varepsilon^\star$ occurs when the ratio $\lambda_{\max}(\mathcal{G})/\lambda_2(\mathcal{G})$ is close to unity while, analogously to the qualitative results of Theorem 5.4, $\lambda_{\max}(\mathcal{G})$ is small. Together, these trends indicate that regular graphs and expander graphs will give particularly large stability bounds. Further, with the additional assumptions of Theorem 5.6 in place, these results show the quantitative effect on the ε bound of different sets of initial conditions.

5.4.3 Example

Consider the consensus tracking problem

$$\dot{x}_i = - \sum_{j \in \mathcal{N}(i)} (y_i - y_j),$$

where $x = \left[x_1^T, \ldots, x_n^T\right]^T \in \mathbb{R}^{2n}$ is the vector of desired planar positions of the agents and $y = \left[y_1^T, \ldots, y_n^T\right]^T \in \mathbb{R}^{2n}$ is the vector of true positions. For unicycle-type robots, an agent's bearing state can be written as $\psi_i = \text{atan2}(y_i) + \pi - \theta_i$ with atan2$(\cdot)$ the four-quadrant inverse tangent, which encodes the angle between the vehicle principle axis θ_i and the position vector y_i and over all agents forms the vector $\psi = [\psi_1, \ldots, \psi_n]^T \in \mathbb{R}^n$. Under control adapted from [107] and with $z_i = [y_i, \psi_i]^T$, the closed-loop dynamics of the ith agent may then be written in the form (5.7) as

$$\varepsilon \dot{z}_i = \begin{bmatrix} -\cos^2 \psi_i \, (y_i - x_i) \\ -\left(\frac{k_\alpha}{k_d}\right) \psi_i \end{bmatrix}, \tag{5.14}$$

where $\varepsilon = 1/k_d$ and where $k_d, k_\alpha > 0$ are the controller gains. Assigning $\hat{z}_i = z_i - h_i(x_i) = z_i - M^T x_i$, then the Lyapunov function

$$\begin{aligned} V_{\text{fast},i}(\hat{z}_i) &= \frac{1}{2} \hat{z}_i^T \left(M^T M\right) \hat{z}_i + \frac{1}{2} \hat{z}_i M_0^T M_0 \hat{z}_i \\ &= \frac{1}{2} (y_i - x_i)^T (y_i - x_i) + \frac{1}{2} \psi_i^2 \end{aligned}$$

defined for each agent satisfies

$$\begin{aligned} \frac{\partial V_{\text{fast},i}}{\partial \hat{z}_i} g_i(x_i, \hat{z}_i + h_i(x_i)) &= -\cos^2 \psi_i \, (y_i - x_i)^T (y_i - x_i) - (k_\alpha / k_d) \, \psi_i^2 \\ &\leq -(y_i - x_i)^T (y_i - x_i) - \left(\frac{k_\alpha}{k_d} - (y_i - x_i)^T (y_i - x_i) \right) \psi_i^2 \\ &= -\hat{z}_i^T \left(M^T M\right) \hat{z}_i - \left(\frac{k_\alpha}{k_d} - \hat{z}_i^T \left(M^T M\right) \hat{z}_i \right) \psi_i^2. \end{aligned}$$

Restricting the domain to $k_\alpha / k_d > \hat{z}_i^T \left(M^T M\right) \hat{z}_i$, Corollary 5.1 is satisfied with $\alpha_2 = n$ and $Q = \frac{1}{2} I$. For an eight node pseudo-barbell network with $w_{ij} = 1$ for all edges, $\lambda_2 = 0.29$ and $\lambda_{\max} = 4.90$. The consensus subspace $\mathcal{X}_c$ is therefore asymptotically stable for all $0 < 1/k_d < \varepsilon^\star$ where

$$\begin{aligned} \varepsilon^\star &= \frac{2n}{\lambda_{\max}(\mathcal{G}) \left(1 + \frac{\lambda_{\max}(\mathcal{G})}{\lambda_2(\mathcal{G})}\right)} \\ &= 0.18. \end{aligned}$$

Results can be seen in Figure 5.6 for various values of ε, showing that the system is asymptotically stable for $\varepsilon < \varepsilon^\star$ while for slow tracking with $\varepsilon = 0.6$ the asymptotic stability is lost.

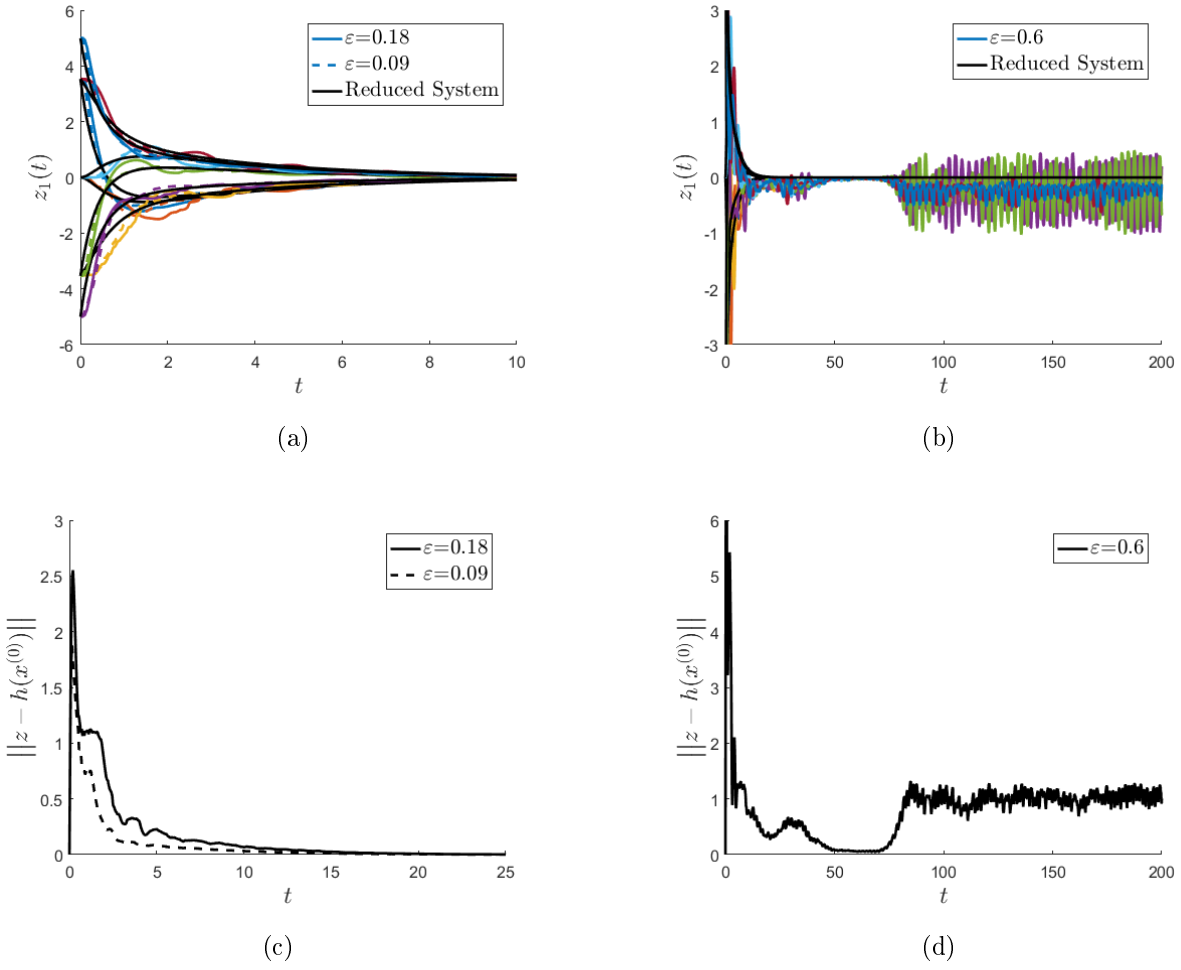

Figure 5.6: Comparison of agent evolution for different ε values in the example of Section 5.4.3. (a) Agent state trajectories for $\varepsilon < \varepsilon^\star$. (b) Agent state trajectories for slow tracking. (c) Norm of agent error trajectories for $\varepsilon < \varepsilon^\star$. (d) Norm of agent error trajectory for slow tracking.

5.5 Consensus Tracking with Intermittent Communication

Consider the leader-follower consensus tracking dynamics with intermittent communication given by

$$\begin{aligned} x^+ &= (K(\mathcal{G}) \otimes M)z + \begin{bmatrix} r_{\text{ref}} \\ \mathbf{0} \end{bmatrix}, && t = t_k \\ \dot{z} &= g(x, z, t; \nu), && t \neq t_k, \end{aligned} \tag{5.15}$$

and for which one particular manifestation is shown, for example, in Figure 5.7. Here, $z = \begin{bmatrix} z_1^T \cdots z_n^T \end{bmatrix}^T$is the collection of true agent states $z_i(t) \in D_z \subset \mathbb{R}^{p+p_0}$, $x = \begin{bmatrix} x_1^T \cdots x_n^T \end{bmatrix}^T$ is the collection of tracked virtual consensus reference states $x_i(t) \in D_x \subset \mathbb{R}^p$, $g(x, z, t) = \begin{bmatrix} g_1(x_1, z_1, t)^T \cdots g_n(x_n, z_n, t)^T \end{bmatrix}^T$ is the collection of tracking dynamics $g_i(x_i, z_i, t)$, $\mathcal{G}$ is a connected graph,

$$K(\mathcal{G}) \triangleq \begin{bmatrix} \mathbf{0}_{1\times n} \\ [I_n - \Delta L(\mathcal{G})]_{2:n,\, 1:n} \end{bmatrix}$$

is the discretized leader-follower Laplacian with step size Δ [87], $r_{\text{ref}} \in \mathbb{R}^p$ is the leader's reference input, and $t_k \in \{t_0, t_1, \ldots\}$ are the distinct communication times with $\nu \triangleq 1/(t_k - t_{k-1})$ measuring the current update rate. The differences between communication times are assumed to be lower bounded by $t_k - t_{k-1} \geq \mu > 0$. As in the continuous-time consensus tracking problem of Section 5.4, the first p elements of z_i, namely $[I, \mathbf{0}]z_i \triangleq Mz_i \subset \mathbb{R}^p$, encode the agreement states and the remaining elements, $[\mathbf{0}, I]z_i \triangleq M_0 z_i \subset \mathbb{R}^{p_0}$, the non-agreement states. In contrast to the continuous-communication problem of Section 5.4, however, the dynamics given by (5.15) assume that inter-agent communication occurs only intermittently. This assumption leads to the use of a discrete protocol for the reference states, x, and is natural when communication power or bandwith is limited.

The following will be assumed in the ensuing analysis.

Assumption 6. *The vector field $g(r, z, t; \nu)$ is Lipschitz in its arguments and has a Lipschitz derivative in its second argument for all $r \in D_x$ and $z \in D_z$.*

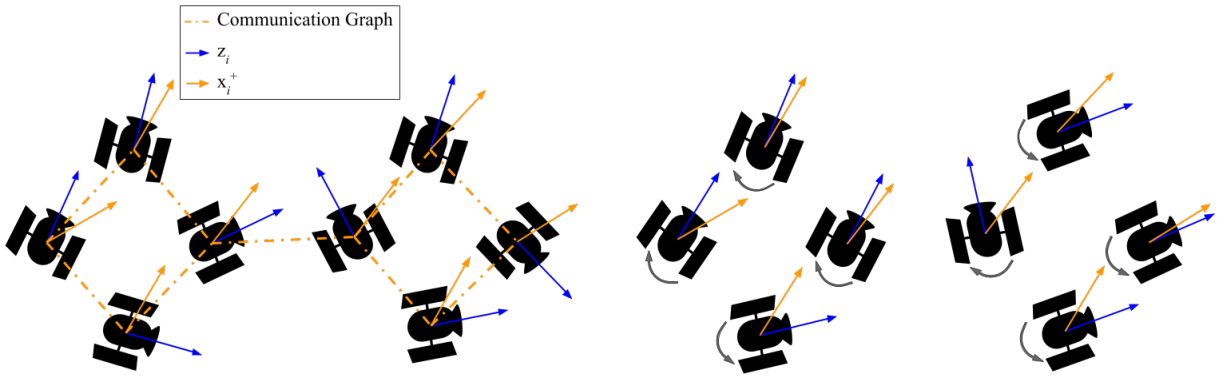

(a) (b)

Figure 5.7: Distributed attitude consensus for a network of satellites with intermittent communication with fast agent states, z, and slow virtual consensus states, x. (a) The set of reference attitudes updates distributively at time t_k over a barbell-like graph. (b) Each satellite's attitude evolves toward its reference attitude between discrete updates.

Assumption 7. *The isolated tracking dynamics defined by* $\dot{z} = g(r, z, t; 0)$ *are uniformly asymptotically stable about* $z_{\text{eq}} = (I \otimes M^T)r$ *for all fixed* $r \in D_x$.

Assumption 8. *Defining the error term* $\hat{z}_i = z_i - M^T x_i$ *and* $\hat{z} = \left[\hat{z}_1^T \cdots \hat{z}_n^T\right]^T$, *each vector field* g_i *can be written as*

$$g_i\left(x_i, z_i, t; \nu\right) = A_i \hat{z}_i + \tilde{g}_i\left(x_i, z_i, t; \nu\right),$$

where $A_i \in \mathbb{R}^{p \times p}$ *and* $\tilde{g}_i$ *is bounded over* D_x *and* D_z *as*

$$\left\|\tilde{g}_i\left(x_i, z_i, t; \nu\right)\right\|^2 \leq \hat{z}_i^T R_i \hat{z}_i + \nu \hat{z}_i^T E_i \hat{z}_i$$

with R_i, $E_i \in \mathbb{R}^{p \times p}$.

Assumption 6 allows trajectories of the tracking dynamics to remain close to one another given small differences in the initial conditions and reference commands (*e.g.*, [62, Chapter 3]). Assumption 7 then states that the isolated tracking dynamics have agreement

states that are stable about the fixed reference command and non-agreement states that are stable about zero. Together, these conditions ensure that the reduced-order models which will be developed in Section 5.5.1 are well-posed. Assumption 8 then restricts the class of nonlinearities in the tracking dynamics. Nonlinearities of these types are standard in the interconnected systems literature and cover a wide class of practical systems including the attitude dynamics of precision-pointing spacecraft [8, Chapter 6] and multimachine power systems [108, 109]. This assumption will be used in Section 5.5.2 to help develop quantitative bounds on the update rates that ensures stability of the coupled system (5.15).

5.5.1 Reduced-Order Models

This section provides reduced-order models for the dynamics (5.15) based on the timescale separation between the slow evolution of the consensus dynamics and the fast evolution of the agents' tracking dynamics as $\mu \to \infty$. With Assumptions 6 and 7, and following the analysis described in Section 3.4.2, reduced-order models that describe the evolution of the individual subsystems over their characteristic timescales can be defined as follows.

Definition 5.5. The Decision System of (5.15) is

$$x^{(0)}\left(t_k^+\right) = (K(\mathcal{G}) \otimes I)x^{(0)}(t_k^-) + \begin{bmatrix} r_{\text{ref}} \\ \mathbf{0} \end{bmatrix}, \tag{5.16}$$

subject to $x^{(0)}(0) = x(0)$.

Definition 5.6. Define the kth time interval between discrete communication instances as $\mathcal{I}_k \triangleq \left\{t \in \mathbb{R} \,\middle|\, t_k \leq t < t_{k+1}\right\}$ and the elapsed time within this interval as $\eta \triangleq t - t_k$. The Interval Correction System of (5.15) is then defined separately for each interval $\mathcal{I}_k$ as

$$\dot{\hat{z}}_k(\eta) = g\left(x^{(0)}(t_k^+), \hat{z}_k(\eta) + (I \otimes M^T)x^{(0)}(t_k^+), \eta + t_k; 0\right) \tag{5.17}$$

subject to $\hat{z}_0(0) = z(0) - (I \otimes M^T)x^{(0)}(0)$ for the first interval and $\hat{z}_k(0) = (I \otimes M^T)\left\{x^{(0)}\left(t_k^-\right) - x^{(0)}\left(t_k^+\right)\right\}$ otherwise, and where $x^{(0)}$ is the state vector of the decision system defined in (3.88).

The Decision System (5.16) describes the reduced-order behaviour of the isolated discrete-time network dynamics with the continuous-time agent dynamics perfectly tracking their state-dependent equilibrium. Note that the system is purely discrete. The Interval Correction System then describes the evolution of the isolated continuous agent dynamics towards the equilibrium trajectory between each set of consecutive discrete updates. The initial conditions are based on the state vector $x^{(0)}$ of the Decision System alone; they are independent of the state of the interval correction system on any previous intervals. The validity of these reduced-order models is certified by the following theorem.

Theorem 5.7. *Under the dynamics (5.15) and with Assumptions 6 and 7, for any $t_f \geq 0$ there exists a μ_0, $0 < \mu_0 < \infty$, such that for all $\mu \geq \mu_0$ the approximations given by (5.16) and (5.17) satisfy*

$$\begin{aligned} x(t_k^+) &= x^{(0)}(t_k^+) + \mathcal{O}(1) \\ z(t) &= (I \otimes M^T)x^{(0)}(t_k^+) + \hat{z}_k(t - t_k) + \mathcal{O}(1) \end{aligned}$$

for all $t \in [t_0, t_f]$. Further, for each interval $\mathcal{I}_k$ between discrete updates with $t_k < t_f$, there is a t_j with $t_k < t_j \leq t_{k+1}$ such that the approximation

$$z(t) = (I \otimes M^T)x^{(0)}\left(t_k^+\right) + \mathcal{O}(1)$$

holds for all $t \in [t_j, t_{k+1})$.

Proof. With Assumptions 6 and 7 in place, the asymptotic error bounds follow since the problem satisfies the conditions of Theorem 3.5. □

The results of Theorem 5.7 state that, over a finite number of network updates, the reduced-order models (5.16) and (5.17) provide good approximations of the true dynamics (5.15) when μ is large enough. Practically speaking, this theorem provides qualitative conditions under which it is reasonable for the networked decision dynamics to be designed separately from the agents' tracking dynamics.

5.5.2 Quantitative Stability Bounds

Given the qualitative results of Theorem 5.7 and the fact that the reduced-order Decision System is stable for appropriate choice of Δ, it is reasonable to ask under what conditions the coupled dynamics (5.15) is stable. If the reduced-order discrete-time Decision System (5.16) is designed assuming that the continuous-time agent dynamics are always at their state-dependent equilibrium, then too-frequent updates may lead to instability of the coupled dynamics (5.15). This is because at the time of the next update the continuous-time states will not have had a chance to reach their new equilibrium and may in fact have initially moved away from this equilibrium due to non-minimum phase behaviour [10, Chapter 6]. This section therefore details an approach to find sufficient lower bounds on μ above which the full system is guaranteed to be stable.

In order to analyze the coupled system's stability, begin by rewriting (5.15) in terms of the error coordinates $\tilde{x} \triangleq x - \mathbf{1} \otimes r_{\text{ref}}$ and $\tilde{z} \triangleq z - (I \otimes M^T)x = z - (I \otimes M^T)\tilde{x} - (\mathbf{1} \otimes M^T r_{\text{ref}})$. The discrete $\tilde{x}$ dynamics are then

$$
\begin{aligned}
\tilde{x}^+ &= x^+ - \mathbf{1} \otimes r_{\text{ref}} \\
&= (K(\mathcal{G}) \otimes M)z + \begin{bmatrix} r_{\text{ref}} \\ \mathbf{0} \end{bmatrix} - \mathbf{1} \otimes r_{\text{ref}} \\
&= (K(\mathcal{G}) \otimes M)\left(\tilde{z} + (I \otimes M^T)\tilde{x} + (\mathbf{1} \otimes M^T r_{\text{ref}})\right) + \begin{bmatrix} r_{\text{ref}} \\ \mathbf{0} \end{bmatrix} - \mathbf{1} \otimes r_{\text{ref}} \\
&= (K(\mathcal{G}) \otimes M)\tilde{z} + (K(\mathcal{G}) \otimes I)\tilde{x} + (K(\mathcal{G})\mathbf{1} \otimes r_{\text{ref}}) + \begin{bmatrix} r_{\text{ref}} \\ \mathbf{0} \end{bmatrix} - \mathbf{1} \otimes r_{\text{ref}} \\
&= (K(\mathcal{G}) \otimes M)\tilde{z} + (K(\mathcal{G}) \otimes I)\tilde{x} + \begin{bmatrix} 0 \\ \mathbf{1} \otimes r_{\text{ref}} \end{bmatrix} + \begin{bmatrix} r_{\text{ref}} \\ \mathbf{0} \end{bmatrix} - \mathbf{1} \otimes r_{\text{ref}} \\
&= (K(\mathcal{G}) \otimes M)\tilde{z} + (K(\mathcal{G}) \otimes I)\tilde{x},
\end{aligned}
$$

using the mixed-product property of the Kronecker product and the fact that $K(\mathcal{G})\mathbf{1} = [0,\, \mathbf{1}^T]^T$. Now, after a discrete update the agents' reference trajectories change due to the

updated value of the discrete network state vector, x, and $\tilde{z}$ is thus correspondingly updated as

$$\begin{aligned}
\tilde{z}^+ &= z - (I \otimes M^T)x^+ \\
&= \left\{\tilde{z} + (I \otimes M^T)\tilde{x} + (\mathbf{1} \otimes M^T r_{\text{ref}})\right\} - \left\{(I \otimes M^T)\tilde{x}^+ + (\mathbf{1} \otimes M^T r_{\text{ref}})\right\} \\
&= \tilde{z} + (I \otimes M^T)\tilde{x} - (I \otimes M^T)\tilde{x}^+ \\
&= \tilde{z} + (I \otimes M^T)\tilde{x} - (I \otimes M^T)\left\{(K(\mathcal{G}) \otimes M)\tilde{z} + (K(\mathcal{G}) \otimes I)\tilde{x}\right\} \\
&= \tilde{z} + (I \otimes M^T)\tilde{x} - (K(\mathcal{G}) \otimes M^T M)\tilde{z} - (K(\mathcal{G}) \otimes M^T)\tilde{x} \\
&= \left(I - (K(\mathcal{G}) \otimes M^T M)\right)\tilde{z} + \left((I - K(\mathcal{G})) \otimes M^T\right)\tilde{x} \\
&\triangleq F_z \tilde{z} + F_x \tilde{x}.
\end{aligned}$$

Finally, in between updates the $\tilde{z}$ dynamics are

$$\begin{aligned}
\dot{\tilde{z}} &= \dot{z} \\
&= g\left(x, \tilde{z} + h(x,t), t; \nu\right) \\
&= \text{diag}\{A_i\}\tilde{z} + \tilde{g}\left(x, \tilde{z}, t; \nu\right) \\
&\triangleq A\tilde{z} + \tilde{g}\left(x, \tilde{z}, t; \nu\right),
\end{aligned}$$

with

$$\begin{aligned}
\left\|\tilde{g}\left(x, \tilde{z}, t; \nu\right)\right\|^2 &\leq \tilde{z}^T \text{diag}\{R_i\}\tilde{z} + \nu \tilde{z}^T \text{diag}\{E_i\}\tilde{z} \\
&\triangleq \tilde{z}^T R \tilde{z} + \nu \tilde{z}^T E \tilde{z}
\end{aligned}$$

by Assumption 8. Therefore, the error dynamics are summarized as

$$\begin{aligned}
\tilde{x}^+ &= (K(\mathcal{G}) \otimes M)\tilde{z} + (K(\mathcal{G}) \otimes I)\tilde{x}, && t = t_k \\
\tilde{z}^+ &= F_z \tilde{z} + F_x \tilde{x}, && t = t_k \\
\dot{\tilde{z}} &= A\tilde{z} + \tilde{g}\left(x, \tilde{z}, t; \nu\right), && t \neq t_k.
\end{aligned} \tag{5.18}$$

With these formulations in place, the following theorem gives quantitative bounds on μ that guarantee stability of the composite system.

Theorem 5.8. *For the dynamics (5.15) under Assumptions 6 and 8, if for some $\mu^\star$ there are matrices $P_1, P_2 > 0$ and positive scalars d_{ij}, β,κ, such that the LMIs*

$$\Phi \leq 0,\ \Omega \leq 0,\ \Psi \leq 0$$

hold with

$$\Phi \triangleq \begin{bmatrix} (K(\mathcal{G})\otimes I)^T P_1 (K(\mathcal{G})\otimes I) - d_{11}P_1 & (K(\mathcal{G})\otimes I)^T P_1 (K(\mathcal{G})\otimes M) \\ * & (K(\mathcal{G})\otimes M)^T P_1 (K(\mathcal{G})\otimes M) - d_{12}P_2 \end{bmatrix},$$

$$\Omega \triangleq \begin{bmatrix} \kappa P_2 + P_2 A + A^T P_2 + \beta R + (\beta/\mu^\star)E & P_2 \\ * & -\beta I \end{bmatrix},$$

and

$$\Psi \triangleq \begin{bmatrix} -d_{21}P_1 + F_x^T P_2 F_x & F_x^T P_2 F_z \\ * & -d_{22}P_2 + F_z^T P_2 F_z \end{bmatrix},$$

and such that

$$\rho\left(\begin{bmatrix} d_{11} & d_{12}e^{-\kappa\mu^\star} \\ d_{21} & d_{22}e^{-\kappa\mu^\star} \end{bmatrix}\right) \leq 1$$

where $\rho(\cdot)$ denotes the spectral radius of a matrix, then the dynamics (5.15) reach consensus about $(x_{\text{eq}},\, z_{\text{eq}}) = \left(\mathbf{1}\otimes r_{ref},\, \mathbf{1}\otimes M^T r_{ref}\right)$ for all $\mu \geq \mu^\star$.

Proof. The proof follows by construction of a vector Lyapunov function and analysis of the corresponding comparison system. To begin, assume the vector Lyapunov function $U(t) = [V_1(t),\, V_2(t)]^T$ (see [110, Chapter 2], for example) for the error dynamics (5.18) with $V_1 = \tilde{x}^T P_1 \tilde{x}$, $V_2 = \tilde{z}^T P_2 \tilde{z}$, and $P_i > 0$. Further assume that the LMIs are satisfied for some $\mu^\star_{\text{LMI}}$. Since μ comes into the LMIs through a positive semi-definite matrix, the LMIs are also satisfied for all $\mu \geq \mu^\star_{\text{LMI}}$. In the following, the collection of error states will be denoted by $q \triangleq \left[\tilde{x}^T,\, \tilde{z}^T\right]^T$.

For V_1 , calculating the derivative for $t \in \mathcal{I}_k$ yields

$$\begin{aligned} \dot{V}_1 &= 2\tilde{x}^T P_1 \dot{\tilde{x}} \\ &= 0, \end{aligned}$$

since $\tilde{x}$ only changes at the discrete jumps. Over jumps,

$$\begin{aligned} V_1^+ &= \tilde{x}^{+T} P_1 \tilde{x}^+ \\ &= \left((K(\mathcal{G}) \otimes M)\tilde{z} + (K(\mathcal{G}) \otimes I)\tilde{x}\right)^T P_1 \left((K(\mathcal{G}) \otimes M)\tilde{z} + (K(\mathcal{G}) \otimes I)\tilde{x}\right) \\ &= q^T \begin{bmatrix} (K(\mathcal{G}) \otimes I)^T P_1 (K(\mathcal{G}) \otimes I) & (K(\mathcal{G}) \otimes I)^T P_1 (K(\mathcal{G}) \otimes M) \\ * & (K(\mathcal{G}) \otimes M)^T P_1 (K(\mathcal{G}) \otimes M) \end{bmatrix} q. \end{aligned}$$

Adding and subtracting $d_{11}V_1$ and $d_{12}V_2$, where $d_{11}, d_{12} \geq 0$, this can be further arranged as $V_1\left(t_k^+\right) = q^T \Phi q + d_{11}V_1 + d_{12}V_2$. Since $\Phi \leq 0$, the inequality

$$V_1\left(t_k^+\right) \leq d_{11}V_1\left(t_k^-\right) + d_{12}V_2\left(t_k^-\right)$$

therefore holds.

For V_2, the derivative along trajectories for $t \in \mathcal{I}_k$ satisfies

$$\begin{aligned} \dot{V}_2 &= 2\tilde{z}^T P_2 \dot{\tilde{z}} \\ &= 2\tilde{z}^T P_2 \left\{A\tilde{z} + \tilde{g}\left(x, \tilde{z}, t; \nu\right)\right\} \\ &\leq 2\tilde{z}^T P_2 \left\{A\tilde{z} + \tilde{g}\left(x, \tilde{z}, t\nu\right)\right\} + \beta\left(\tilde{z}^T R \tilde{z} + \mu \tilde{z}^T E \tilde{z} - \|\tilde{g}\|^2\right) + (\kappa V_2 - \kappa V_2) \end{aligned}$$

where $\kappa, \beta \geq 0$, since $\|\tilde{g}\|^2 \leq \tilde{z}^T R \tilde{z} + \mu \tilde{z}^T E \tilde{z}$. This can be rearranged as

$$\dot{V}_2 \leq \begin{bmatrix} \tilde{z} \\ \tilde{g} \end{bmatrix}^T \Omega \begin{bmatrix} \tilde{z} \\ \tilde{g} \end{bmatrix} - \kappa V_2,$$

and therefore

$$\dot{V}_2 \leq -\kappa V_2$$

holds since $\Omega \leq 0$. Over jumps, similarly to the V_1^+ case,

$$\begin{aligned} V_2^+ &= \tilde{z}^{+T} P_2 \tilde{z}^+ \\ &= \left\{F_z \tilde{z} + F_x \tilde{x}\right\}^T P_2 \left\{F_z \tilde{z} + F_x \tilde{x}\right\} \\ &= q^T \begin{bmatrix} F_x^T P_2 F_x & F_x^T P_2 F_z \\ * & F_z^T P_2 F_z \end{bmatrix} q \\ &= q^T \Psi q + d_{21}V_1 + d_{22}V_2 \end{aligned}$$

where $d_{21}, d_{22} \geq 0$. Thus,

$$V_2(t_k^+) \leq d_{21} V_1(t_k^-) + d_{22} V_2(t_k^-)$$

holds since $\Psi \leq 0$.

The vector Lyapunov function $U(t)$ has been shown to satisfy

$$\dot{U} \preceq \underbrace{\begin{bmatrix} 0 & 0 \\ 0 & -\kappa \end{bmatrix}}_{B} U$$

and

$$U\left(t_k^+\right) \preceq \underbrace{\begin{bmatrix} d_{11} & d_{12} \\ d_{21} & d_{22} \end{bmatrix}}_{D} U\left(t_k^-\right),$$

where $v \preceq u$ implies $v_i \leq u_i$ for all i. A comparison system for the dynamics is therefore

$$\begin{aligned} u(t_k^+) &= Du(t_k^-) \\ \dot{u} &= Bu, \end{aligned} \tag{5.19}$$

subject to $u(t_0) = U(t_0)$. It follows from [110, Theorem 2.11] that the stability properties of the zero solution of (5.19) imply the corresponding stability properties of the error dynamics (5.18), or equivalently the stability of the original dynamics (5.15) about $(x_{\text{eq}}, z_{\text{eq}})$.

To analyze stability of (5.19), construct the state evolution of u at $t \in \mathcal{I}_k$ as

$$\begin{aligned} u(t) &= e^{B(t-t_k)} \prod_{i=1}^{k} D e^{B(t_i - t_{i-1})} u(t_0) \\ &= e^{B(t-t_k)} \prod_{i=1}^{k} \tilde{D}(t_i - t_{i-1}) u(t_0), \end{aligned}$$

where $\tilde{D}$ is explicitly calculated as

$$\tilde{D}(t_i - t_{i-1}) = \begin{bmatrix} d_{11} & d_{12} e^{-\kappa(t_i - t_{i-1})} \\ d_{21} & d_{22} e^{-\kappa(t_i - t_{i-1})} \end{bmatrix}. \tag{5.20}$$

Now, $\|u(t)\|$ is bounded if each $\tilde{D}$ has spectral radius of at most one. Therefore, choosing $\mu^\star \geq \mu^\star_{\text{LMI}}$ such that $\max\left|\lambda\left(\tilde{D}(\mu^\star)\right)\right| \leq 1$, and noting that $\max\left|\lambda\left(\tilde{D}(\mu)\right)\right|$ is monotonic in μ, the original system (5.15) is stable about $(x_{\text{eq}}, z_{\text{eq}})$ for all $\mu \geq \mu^\star$. □

The results of Theorem 5.8 yield stability bounds for the hybrid-time system. The matrices in the LMIs are slack matrices that allow a simpler comparison system to be analyzed in the proof instead of the original dynamics. This comparison system is based on Lyapunov functions for the individual continuous-time and discrete-time dynamics. Examining the conditions of the theorem, if the continuous evolution of the tracking dynamics $\tilde{z}$ defined in (5.18) is faster or more stable then the $\Omega \leq 0$ condition will tend to be satisfied for a larger κ. This will then lower the necessary $\mu^\star$ since the spectral radius condition is monotonic in κ. Analogously to the continuous-time consensus tracking case, it can also be seen that there is a tradeoff on the $\mu^\star$ bound between the maximum and minimum spectral values of the network dynamics. In particular, a larger maximum singular value of $K(\mathcal{G})$ tends to raise the necessary values of d_{11} and d_{12} that satisfy the $\Phi \leq 0$ condition, thereby increasing the necessary $\mu^\star$ to satisfy the spectral radius condition. Similarly, a smaller minimum singular value of $K(\mathcal{G})$ tends to increase the maximum singular values of F_x and F_z and therefore raise the necessary values of d_{21} and d_{22} that satisfy the $\Psi \leq 0$ condition, again resulting in a larger $\mu^\star$ that satisfies the spectral radius condition. Of course, the acquired bounds may be conservative since they are based on particular Lyapunov functions. However, the outlined approach can be easily adapted if more information, such as more appropriate Lyapunov functions, are known for the reduced-order models.

It is interesting to note that the approach used in Theorem 5.8 can be directly extended to analyze the stability of a more general class of systems. Consider dynamics of the form

$$\begin{aligned} x^+ &= Kx + \tilde{f}\left(x, \tilde{z}, t_k; \nu\right), && t = t_k, \\ \dot{z} &= g\left(x, z, t; \nu\right), && t \neq t_k, \end{aligned} \tag{5.21}$$

where the the z dynamics have a unique equilibrium $z = h(x,t)$ when x is fixed. Then, defining the error state $\tilde{z} = z - h(x,t)$ and $q = [x^T,\, \tilde{z}^T]^T$, assume that $\tilde{f}$ is bounded over D_x

and D_z as

$$\left\|\tilde{f}\right\|^2 \leq q^T \begin{bmatrix} J_{11} & J_{12} \\ J_{12}^T & J_{13} \end{bmatrix} q + \mu q^T \begin{bmatrix} E_{11} & E_{12} \\ E_{12}^T & E_{13} \end{bmatrix} q \triangleq q^T J_1 q + \mu q^T E_1 q,$$

and that the vector field g can be written as

$$g\left(x, \tilde{z} + h(x,t), t; \mu\right) - \frac{\partial h(x,t)}{\partial t} = A\tilde{z} + \tilde{g}\left(x, \tilde{z}, t; \nu\right),$$

where $\tilde{g}$ is bounded over D_x and D_z as

$$\left\|\tilde{g}\left(x, \tilde{z}, t, \mu\right)\right\|^2 \leq \tilde{z}^T R \tilde{z} + \mu q^T \begin{bmatrix} E_{21} & E_{22} \\ E_{22}^T & E_{23} \end{bmatrix} q \triangleq \tilde{z}^T R \tilde{z} + \mu q^T E_2 q,$$

for J_{11}, E_{11}, $E_{21} \in \mathbb{R}^{n_x \times n_x}$, J_{12}, E_{12}, $E_{22} \in \mathbb{R}^{n_x \times n_z}$, and J_{13}, E_{13}, $E_{23}, R \in \mathbb{R}^{n_z \times n_z}$. Further assume that the jump in the $\tilde{z}$ states after a discrete update

$$\Delta h \triangleq h\left(x, t_k\right) - h\left(f\left(x, \tilde{z} + h(x, t_k), k; \nu\right), t_k\right)$$

is bounded over D_x and D_z as

$$\|\Delta h\|^2 \leq q^T \begin{bmatrix} J_{21} & J_{22} \\ J_{22}^T & J_{23} \end{bmatrix} q \triangleq q^T J_2 q,$$

with $J_{21} \in \mathbb{R}^{n_x \times n_x}$, $J_{22} \in \mathbb{R}^{n_x \times n_y}$, and $J_{23} \in \mathbb{R}^{n_y \times n_y}$. Then the following theorem provides bounds on the minimum time between updates, μ, which guarantee the stability of (5.21).

Theorem 5.9. *For the dynamics (5.21), if for some $\mu^\star$ there are matrices $P_1, P_2 > 0$ and positive scalars d_{ij}, β, γ_i, κ_i, such that the LMIs*

$$\Phi \leq 0,\ \Omega \leq 0,\ \Psi \leq 0$$

hold with

$$\Phi \triangleq \begin{bmatrix} -d_{11}P_1 + K^T P_1 K + \gamma_1 J_{11} + (\gamma_1/\mu^\star) E_{11} & \gamma_1 J_{12} + (\gamma_1/\mu^\star) E_{12} & K^T P_1 \\ * & -d_{12}P_2 + \gamma_1 J_{13} + (\gamma_1/\mu^\star) E_{13} & 0 \\ * & * & -\gamma_1 + P_1 \end{bmatrix},$$

$$\Omega \triangleq \begin{bmatrix} -\kappa_1 P_1 + (\beta/\mu^\star) E_{21} & (\beta/\mu^\star) E_{22} & 0 \\ * & \kappa_2 P_2 + P_2 A + A^T P_2 + \beta R + (\beta/\mu^\star) E_{23} & P_2 \\ * & * & -\beta I \end{bmatrix},$$

and

$$\Psi \triangleq \begin{bmatrix} -d_{21} P_1 + \gamma_2 J_{21} & \gamma_2 J_{22} & 0 \\ * & -d_{22} P_2 + P_2 + \gamma_2 J_{23} & P_2 \\ * & * & -\gamma_2 I + P_2 \end{bmatrix},$$

and such that

$$\rho\left(\begin{bmatrix} d_{11} + \frac{d_{12}\kappa_1}{\kappa_2}\left(1 - e^{-\kappa_2\mu^\star}\right) & d_{12} e^{-\kappa_2\mu^\star} \\ d_{21} + \frac{d_{22}\kappa_1}{\kappa_2}\left(1 - e^{-\kappa_2\mu^\star}\right) & d_{22} e^{-\kappa_2\mu^\star} \end{bmatrix}\right) \leq 1$$

where $\rho(\cdot)$ denotes the spectral radius of a matrix, then the dynamics (5.21) are stable about zero for all $\mu \geq \mu^\star$.

Proof. The proof follows the vector Lyapunov approach outlined in Theorem 5.8 for an assumed vector Lyapunov function $U(t) = [V_1(t),\, V_2(t)]^T$ with $V_1 = x^T P_1 x$, $V_2 = \tilde{z}^T P_2 \tilde{z}$, and $P_i > 0$. Again, the LMIs are satisfied for all $\mu \geq \mu^\star_{\text{LMI}}$ since μ comes into the LMIs through a positive semi-definite matrix.

For V_1, time derivatives between discrete updates yield $\dot{V}_1 = 0$. Over jumps,

$$\begin{aligned} V_1^+ &= f\left(x, \tilde{z} + h, k; \mu\right)^T P_1 f\left(x, \tilde{z} + h, k; \mu\right) \\ &= \left(Kx + \tilde{f}\right)^T P_1 \left(Kx + \tilde{f}\right) \\ &\leq \begin{bmatrix} q \\ \tilde{f} \end{bmatrix}^T \Phi \begin{bmatrix} q \\ \tilde{f} \end{bmatrix} + d_{11} V_1 + d_{12} V_2 \\ &\leq d_{11} V_1 + d_{12} V_2 \end{aligned}$$

since $0 \leq \gamma_1 \left[q^T J_1 q + \nu q^T E_1 q - \left\|\tilde{f}\right\|^2\right]$ and because $\Phi \leq 0$.

For V_2, time derivatives between discrete updates satisfy

$$\begin{aligned}\dot{V}_2 &= 2\tilde{z}^T P_2 \left(A\tilde{z} + \tilde{g}\left(x, \tilde{z}, t, \mu\right)\right) \\ &\leq \begin{bmatrix} q \\ \tilde{g} \end{bmatrix}^T \Omega \begin{bmatrix} q \\ \tilde{g} \end{bmatrix} + \kappa_1 V_1 - \kappa_2 V_2 \\ &\leq \kappa_1 V_1 - \kappa_2 V_2,\end{aligned}$$

using $0 \leq \beta\left(\tilde{z}^T R \tilde{z} + \nu q^T E_2 q - \|\tilde{g}\|^2\right)$ and the fact that $\Omega \leq 0$. Over jumps, similarly to the V_1^+ case,

$$\begin{aligned}V_2\left(t_k^+\right) &= \left\{\tilde{z} + \Delta h\right\}^T P_2 \left\{\tilde{z} + \Delta h\right\} \\ &\leq \begin{bmatrix} q \\ \Delta h \end{bmatrix}^T \Psi \begin{bmatrix} q \\ \Delta h \end{bmatrix} + d_{21} V_1 + d_{22} V_2 \\ &\leq d_{21} V_1 + d_{22} V_2\end{aligned}$$

since $0 \leq \gamma_2 \left[q^T J_2 q - \|\Delta h\|^2\right]$ and $\Psi \leq 0$.

Therefore, the vector Lyapunov U satisfies

$$\dot{U} \preceq \underbrace{\begin{bmatrix} 0 & 0 \\ \kappa_1 & -\kappa_2 \end{bmatrix}}_{B} U$$

and

$$U\left(t_k^+\right) \preceq \underbrace{\begin{bmatrix} d_{11} & d_{12} \\ d_{21} & d_{22} \end{bmatrix}}_{D} U\left(t_k^-\right)$$

where $\preceq$ denotes a component-wise inequality, and a comparison system for the dynamics is

$$\begin{aligned}u(t_k^+) &= Du(t_k^-) \\ \dot{u} &= Bu,\end{aligned} \tag{5.22}$$

subject to $u(t_0) = U(t_0)$. It follows from [110, Theorem 2.11] that the stability properties of the zero solution of (5.22) imply the corresponding stability properties of (5.21). The state

evolution of u is constructed as

$$u(t) = e^{B(t-t_k)} \prod_{i=1}^{k} \tilde{D}(t_i - t_{i-1}) u(t_0),$$

where

$$\tilde{D}(t_i - t_{i-1}) = \begin{bmatrix} d_{11} & d_{12} e^{-\kappa(t_i - t_{i-1})} \\ d_{21} & d_{22} e^{-\kappa(t_i - t_{i-1})} \end{bmatrix}. \tag{5.23}$$

So, $\|u(t)\|$ is bounded if each $\tilde{D}$ has spectral radius of at most one. Noting that as $\mu \to \infty$,

$$\lim_{\mu \to \infty} \lambda \left(\tilde{D}(\mu) \right) = \left(d_{11} + \frac{d_{12}\kappa_1}{\kappa_2}, 0 \right)$$

the condition is feasible if $d_{11} + d_{12}(\kappa_1/\kappa_2) \leq 1$. Therefore, choosing $\mu^\star \geq \mu^\star_{\text{LMI}}$ such that $\max \left| \lambda \left(\tilde{D}(\mu^\star) \right) \right| \leq 1$, and noting that $\max \left| \lambda \left(\tilde{D}(\mu) \right) \right|$ is monotonic in μ, the original system (5.21) is stable for all $\mu \geq \mu^\star$. □

5.5.3 Example

Consider a group of satellites communicating intermittently over a network to distributively reach consensus on their attitude as illustrated in Figure 5.7, where the ith satellite's attitude is represented by the Modified Rodrigues Parameters (MRPs) $\sigma_i \in \mathbb{R}^3$. Further assume that one satellite, the leader, has knowledge of the desired attitude σ_{desired} for the group. A distributed protocol for the ith satellite's reference attitude is then provided by the discrete leader-follower dynamics

$$\sigma^+_{\text{ref},i} = \begin{cases} \sigma_{\text{desired}}, & i = 1 \\ \sigma_i + \Delta \sum_{j \in \mathcal{N}(i)} (\sigma_i - \sigma_j), & i \neq 1 \end{cases},$$

on the satellites' undirected communication graph, $\mathcal{G}$, where Δ is a fixed step size. Under appropriate closed loop control [75, Chapter 8], the ith satellite's attitude error kinematics are described by

$$\frac{d}{dt} \begin{bmatrix} \hat{\sigma}_i \\ \dot{\sigma}_i \end{bmatrix} = \begin{bmatrix} \mathbf{0} & I_3 \\ -c_{i,1} I_3 & -c_{i,2} I_3 \end{bmatrix} \begin{bmatrix} \hat{\sigma}_i \\ \dot{\sigma}_i \end{bmatrix} + \begin{bmatrix} \mathbf{0} \\ \tilde{g}_i(\hat{\sigma}_i, \dot{\sigma}_i, t) \end{bmatrix},$$

where $\hat{\sigma}_i = \sigma_i - \sigma_{\text{ref},i}$, and where $\tilde{g}_i$ accounts for the nonlinear effects of imperfect actuation in the control. This is a tracking controller that stabilizes to $h_i(x,t) = \left[\sigma_{\text{ref},i}^T,\, \mathbf{0}_{1\times 3}\right]^T$ when $\sigma_{\text{ref},i}$ is fixed.

The discrete evolution of the satellites' reference attitudes, $x = \left[\sigma_{\text{ref},1}^T \cdots \sigma_{\text{ref},n}^T\right]^T$, and continuous evolution of their true states, $z = \left[\sigma_1^T,\, \dot{\sigma}_1^T,\, \cdots,\, \sigma_n^T,\, \dot{\sigma}_n^T\right]^T$, can be equivalently written as the coupled system

$$\begin{aligned} x^+ &= (K(\mathcal{G}) \otimes M) z + \begin{bmatrix} \sigma_{\text{desired}} \\ \mathbf{0}_{3(n-1)\times 1} \end{bmatrix}, && t = t_k \\ \dot{z} &= A\left(z(t) - \begin{bmatrix} x\left(t_k^+\right) \\ \mathbf{0}_{3n\times 1} \end{bmatrix}\right) + \tilde{g}\left(x, z, t\right), && t \neq t_k \end{aligned} \tag{5.24}$$

where

$$A \triangleq \operatorname{diag}\left\{ \begin{bmatrix} \mathbf{0}_{3\times 3} & I_3 \\ -c_{i,1} I_3 & -c_{i,2} I_3 \end{bmatrix} \right\},$$

and

$$\tilde{g}\left(x, z, t\right) \triangleq [\mathbf{0}^T,\, \tilde{g}_1(\hat{\sigma}_1, \dot{\sigma}_1, t)^T,\, \cdots, \mathbf{0}^T,\, \tilde{g}_n(\hat{\sigma}_n, \dot{\sigma}_n, t)^T]^T.$$

With the satellite and network parameters defined in Table 5.1, the dynamics (5.24) are of the form (5.15) and satisfy the conditions of Theorem 5.7. Therefore, the corresponding reduced-order models given by (5.16) and (5.17) hold for this system. As shown in Figures 5.8a and 5.8b, these reduced-order models become good approximations of the true dynamics as the minimum time μ between discrete updates increases.

To find a bound on μ that guarantees stability, note that Assumptions 7 and 6 are satisfied for the values in Table 5.1 and by assuming that $R \leq (0.01)^2 \otimes I$. The LMIs and spectral radius inequality in Theorem 5.8 are then satisfied using the constants defined in Table 5.2, providing the bound $\mu^\star = 33$ time units. As expected, Figure 5.8c shows that the hybrid-time system is stable when $\mu = 33$. However, the bound given by any particular combination

of parameters that satisfy Theorem 5.8 may be conservative. For these particular initial conditions, Figure 5.8d demonstrates that the satellites exhibit unstable oscillations in their attitudes when $\mu = 10$ time units. In this particular case, the instability is due to a resonance phenomenon where the distributed decisions on new reference attitudes are made when satellites have overshot their previous reference attitudes. For large enough μ, however, the satellites' attitudes settle closer to their individual references which allows the discrete leader-follower consensus protocol to evolve in a stable fashion as designed. This example illustrates the potential danger of too-frequent communication updates even for systems where the discrete network dynamics and continuous agent dynamics are stable when isolated.

Table 5.1: Simulation parameters for the example of Section 5.5.3

Parameter	Value
$c_{i,1}$	1
$c_{i,2}$	0.4
Δ	0.4
$\mathcal{G}$	Barbell-like graph shown in Figure 5.7

Table 5.2: Values of constants that satisfy Theorem 5.8 for the example of Section 5.5.3

Parameter	Value
P_1	I
P_2	Solution to $P_2A + AP_2 + I = 0$
d_{11}	0.9750
d_{12}	28.5469
d_{21}	16.1391
d_{22}	10.0091
β	310.9920
κ	0.3016
$\mu^\star$	**33**

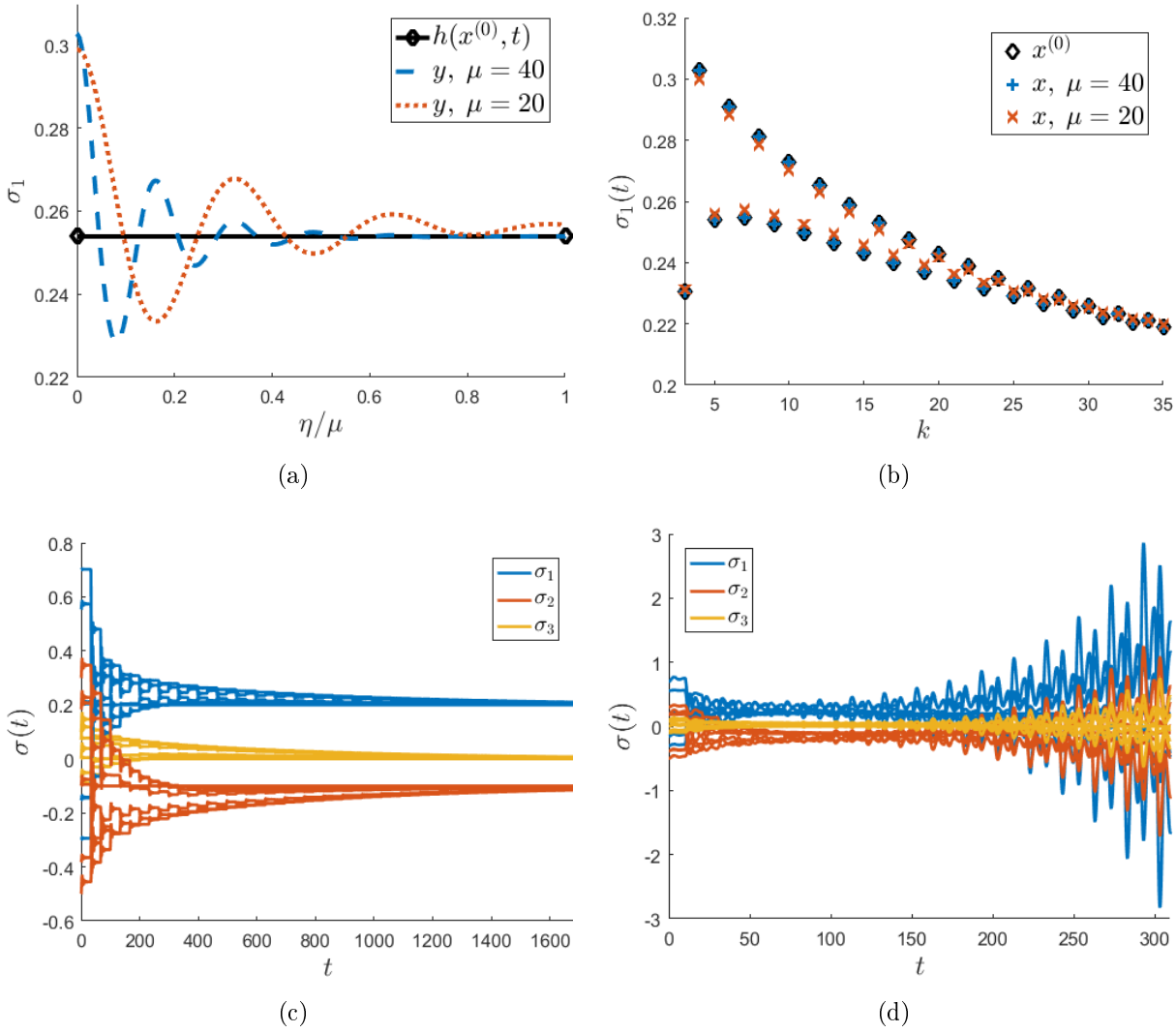

Figure 5.8: Comparison of state evolution for different μ values in the example of Section 5.5.3. (a) Trajectories of a particular satellite's first MRP within a normalized interval between communication instants. (b) Evolution of a particular satellite's first MRP reference command. (c) Evolution of all 8 satellites' attitudes when $\mu = 33 = \mu^\star$. (d) Evolution of all 8 satellites' attitudes when $\mu = 10 < \mu^\star$.

Chapter 6

CONCLUSIONS AND FUTURE WORK

The research detailed in this dissertation has focused on advancing and applying multiple scale methods to complex dynamical systems.

First, a generalized multi-scale analysis method was developed in Chapter 3 for reduced-order modeling of systems where multiple timescales arise due to heterogeneous time dependency. It was first shown how this approach extends classical multiple timescale approaches to systems that depend on a combination of continuous time and/or discrete clocks. The generalized approach was then applied to discrete, multirate systems and to hybrid-time systems. In both cases, the approach demonstrated how discrete clock rates can cause multiple timescale behaviour in these systems, and this behaviour was exploited to formulate reduced-order models. Further, these developed approximations were shown to satisfy asymptotic error bounds for both these classes of systems, and their efficacy was demonstrated by several numerical examples.

Next, in Chapter 4, MMS was applied to the problem of propagating satellite trajectories subject to non-conservative perturbing forces. The developed trajectory solution takes advantage of the timescale separation between the fast effects of central-body gravitation and the slow effects of the perturbation. Importantly, the resulting approximations have known error properties that are dependent on the nominal parameters of the perturbation. Comparisons with previous propagation methods illustrated these error properties for the case of atmospheric drag and confirmed the accuracy and computational efficiency of the approach for a range of representative low-Earth orbits. Further, an expression was developed for the trajectory's sensitivity to different perturbation parameters by exploiting the multiple timescale form of the trajectory solution. Simulations verified that this approach gives

accurate insight into the effects of uncertainties in the parameters of the non-conservative perturbation, even in the presence of high-order geopotential effects.

Finally, Chapter 5 investigated three problems in networked dynamical systems. In the first case, a set of fast consensus dynamics was considered where the edge weights had their own slowly varying dynamics. The second case examined a problem where fast agents attempt to track reference trajectories given by slow consensus dynamics, assuming that communication over the network is continuous. The third case then explored a similar consensus tracking problem where the communication between agents was instead assumed to occur only intermittently. In each case, reduced-order models were formulated based on the natural timescale separation between the agent dynamics and the network dynamics. It was then shown how stability properties of these reduced-order models can be used to develop quantitative bounds on the graph topology and on the communication rate that guarantee stability of the full systems. Numerical examples illustrated the effectiveness of the reduced-order models and demonstrated how violation of the derived quantitative bounds can cause instability in the various scenarios.

There are several avenues for possible future research that stem from this work. One possible direction is to investigate how other update rules governing discrete updates, besides the clock-based rules considered here, may also cause multi-scale behaviour. For example, reduced-order models similar to those developed in Section 3.4.2 may apply if discrete updates occur instead when the norm of the tracking error, $\|z - h(x,t)\|$, is below some bound ε. With regard to orbit propagation applications, it would be interesting to explore how trajectory sensitivity expressions could be derived in the presence of several non-conservative perturbations. This avenue is especially important for orbital regimes beyond low-Earth orbit where the nominal magnitudes of various perturbing forces are comparable. For applications in networked dynamical systems, one possibility for future work is to extend these results to directed graphs, which can help reflect sensing asymmetries for heterogeneous agents. Another potential extension is to relax the condition on a connected graph to consider graphs whose union over some time interval is connected. A third area of possible research

is to use these methods to investigate the control of networks, for instance in cases where a node is taken over by a malicious agent.

BIBLIOGRAPHY

[1] W. C. Baldwin, S. Hostetler, and W. N. Felder, "Mathematical Models of Emergence in Complex Systems-of-systems," in *INCOSE International Symposium*, 2013.

[2] "NASA Space Technology Roadmaps and Priorities Revisited," National Research Council, Washington, D.C., Tech. Rep., 2016.

[3] *Continuing Kepler's Quest – Assessing Air Force Space Command's Astrodynamics Standards.* National Academies Press, 2012.

[4] B. Sedghi, "Control design of hybrid systems via dehybridization," Ph.D. dissertation, Ecole Polytechnique Federale De Lausanne, 2003.

[5] P. Naghshtabrizi, J. P. Hespanha, and A. R. Teel, "On the robust stability and stabilization of sampled-data systems: A hybrid system approach," in *45th IEEE Conference on Decision and Control (CDC).* IEEE, 2006, pp. 4873–4878.

[6] A. Jentzen, F. Leber, D. Schneisgen, A. Berger, and S. Siegmund, "An improved maximum allowable transfer interval for Lp-Stability of networked control systems," *IEEE Transactions on Automatic Control*, vol. 55, no. 1, pp. 179–184, 2010.

[7] P. Hänggi and M. Borkovec, "Reaction-rate theory: fifty years after Kramers," *Reviews of Modern Physics*, vol. 62, no. 2, pp. 251–341, 1990.

[8] D. D. Siljak, *Large-Scale Dynamical Systems.* Elsevier, 1978.

[9] G. M. Peponides and P. V. Kokotovic, "Weak Connections, Time Scales, and Aggregation of Nonlinear Systems," *IEEE Transactions on Automatic Control*, vol. 28, no. 6, pp. 729—-735, 1983.

[10] A. Narang-Siddarth and J. Valasek, *Nonlinear Time Scale Systems in Standard and Nonstandard Forms.* SIAM, 2014.

[11] P. Kokotovic, H. Khali, and J. O'Reilly, *Singular Perturbation Methods in Control: Analysis and Design.* SIAM, 1999.

[12] D. S. Naidu and A. J. Calise, "Singular perturbations and time scales in guidance and control of aerospace systems - A survey," *Journal of Guidance, Control, and Dynamics*, vol. 24, no. 6, pp. 1057–1078, 2001.

[13] H. Ashley, "Multiple Scaling in Flight Vehicle Dynamic Analysis – A Preliminary Look," in *Proceedings of the AIAA Guidance, Control, and Dynamics Conference*, no. 670560. AIAA, 1967.

[14] P. A. Lagerstrom and J. K. Kevorkian, "Earth-to-Moon Trajectories in the Restricted Three-Body Problem," *Journal de Mecanique*, vol. 2, pp. 189–218, 1963.

[15] T. T. Johnson, J. Green, S. Mitra, R. Dudley, and R. S. Erwin, "Satellite Rendezvous and Conjunction Avoidance : Case Studies in Verification of Nonlinear Hybrid Systems," pp. 1–15.

[16] R. E. O'Malley, *Historical Developments in Singular Perturbations*. Springer, 2014.

[17] D. S. Naidu, *Singular Perturbation Methodology in Control Systems*. Peter Peregrinus Ltd., 1988.

[18] K. Mease, "Multiple time-scales in nonlinear flight mechancis: Diagnosis and modeling," *Applied Mathematics and Computation*, vol. 164, no. 2, 2005.

[19] D. S. Naidu and A. K. Rao, *Singular perturbation analysis of discrete control systems*. Springer-Verlag Berlin, 1985, vol. 1154.

[20] R. Bouyekhf and A. El Moudni, "On analysis of discrete singularly perturbed nonlinear systems: Application to the study of stability properties," *Journal of the Franklin Institute*, vol. 334B, no. 2, pp. 199–212, 1997.

[21] R. Goebel, R. G. Sanfelice, and A. R. Teel, "Hybrid Dynamical Systems: Robust Stability and Control for Systems that Combine Continuous-Time and Discrete-Time Dynamics," *IEEE Control Systems Magazine*, no. April, pp. 28–93, 2009.

[22] W. Wang, A. R. Teel, and D. Nešić, "Analysis for a class of singularly perturbed hybrid systems via averaging," *Automatica*, vol. 48, no. 6, pp. 1057–1068, 2012.

[23] D. Bainov and V. Covachev, *Impulsive Differential Equations with a Small Parameter*. World Scientific Publishing Co. Pte. Ltd., 1994.

[24] W. H. Chen, G. Yuan, and W. X. Zheng, "Robust stability of singularly perturbed impulsive systems under nonlinear perturbation," *IEEE Transactions on Automatic Control*, vol. 58, no. 1, pp. 168–174, 2013.

[25] W. Wang, "Averaging and Singular Perturbation Methods for Analysis of Dynamical Systems with Disturbances," Ph.D. dissertation, University of Melbourne, Department of Electrical and Electronic Engineering, 2011.

[26] I. Kolmanovsky and N. H. McClamroch, "Hybrid feedback laws for a class of cascade nonlinear control systems," *IEEE Transactions on Automatic Control*, vol. 41, no. 9, pp. 1271–1282, 1996.

[27] C. R. C. Rui, I. Kolmanovsky, and N. McClamroch, "Hybrid control for stabilization of a class of cascade nonlinear systems," in *1997 American Control Conference*, vol. 5, 1997, pp. 2800–2804.

[28] J. Kevorkian and J. D. Cole, *Multiple Scale and Singular Perturbation Methods*, ser. Applied Mathematical Sciences. New York, NY: Springer New York, 2012, vol. 114.

[29] B. Mudavanhu, R. E. O'Malley, and D. B. Williams, "Working with multiscale asymptotics," *Journal of Engineering Mathematics*, vol. 53, no. 3-4, pp. 301–336, dec 2005.

[30] F. C. Hoppensteadt and W. L. Miranker, "Multitime methods for systems of difference equations," *Studies in Applied Mathematics*, vol. 56, 1977.

[31] R. Subramanian and A. Krishnan, "Non-linear discrete time systems analysis by multiple time perturbation techniques," *Journal of Sound and Vibration*, vol. 63, no. 3, pp. 325–335, 1979.

[32] W. T. van Horssen and M. C. ter Brake, "On the multiple scales perturbation method for difference equations," *Nonlinear Dynamics*, vol. 55, no. 4, pp. 401–418, jun 2008.

[33] M. Rafei and W. T. Van Horssen, "Solving systems of nonlinear difference equations by the multiple scales perturbation method," *Nonlinear Dynamics*, vol. 69, no. 4, pp. 1509–1516, feb 2012.

[34] M. Rafei, "On asymptotics for difference equations," Ph.D. dissertation, Mazandaran University, 2012.

[35] A. Awad and A. Narang-Siddarth, "On Timescale Separation in Networked Systems with Intermittent Communication," *Journal of Dynamic Systems, Measurement, and Control (In Review)*, 2017.

[36] S. Hilger, "Ein Maßkettenkalkül mit Anwendung auf Zentrumsmannigfaltigkeiten," Ph.D. dissertation, Univ. Würzburg, Würzburg, Germany, 1988.

[37] M. Bohner and G. S. Guseinov, "Partial differentiation on time scales," *Dynamic Systems and Applications*, vol. 13, pp. 351–379, 2004.

[38] M. Bohner and S. G. Georgiev, *Multivariable Dynamic Calculus on Time Scales.* Springer, 2016.

[39] M. Z. Sarikaya, N. Aktan, H. Yildirim, and K. Ilarslan, "Partial Δ-differentiation for multivariable functions on n-dimensional time scales," *Journal of Mathematical Inequalities*, vol. 3, no. 2, pp. 277–291, 2009.

[40] J. Seiffertt and D. C. Wunsch, "Backpropagation and ordered derivatives in the time scales calculus." *IEEE Transactions on Neural Networks*, vol. 21, no. 8, pp. 1262–9, aug 2010.

[41] M. Bohner and A. Peterson, *Dynamic Equations on Time Scales.* Birkhauser, 2001.

[42] V. Lakshmikantham and A. Vatsala, "Hybrid systems on time scales," *Journal of Computational and Applied Mathematics*, vol. 141, pp. 227–235, 2002.

[43] A. A. Ramos, "Stability of Hybrid Dynamic Systems: Analysis and Design," Ph.D. dissertation, Baylor University, 2009.

[44] V. Lupulescu and A. Zada, "Linear impulsive dynamic systems on time scales," *Electronic Journal of Qualitative Theory of Differential Equations*, no. 11, pp. 1–30, 2010.

[45] A. H. Nayfeh, *Perturbation methods.* WILEY-VCH, 2004.

[46] J. Hinchman, M. Clark, J. Hoffman, B. Hulbert, and C. Snyder, "Towards Safety Assurance of Trusted Autonomy in Air Force Flight Critical Systems," 2010.

[47] D. Glasson, "Development and applications of multirate digital control," *Control Systems Magazine, IEEE*, vol. 3, no. 4, pp. 2–8, 1983.

[48] G. J. Balas, "Flight Control Law Design: An Industry Perspective," *European Journal of Control*, vol. 9, no. 2-3, pp. 207–226, 2003.

[49] G. Kranc, "Input-output analysis of multirate feedback systems," *Automatic Control, IRE Transactions on*, vol. 3, no. 1, pp. 21–28, 1957.

[50] T. C. Coffey and I. J. Williams, "Stability analysis of multiloop, multirate sampled systems." *AIAA Journal*, vol. 4, no. 12, pp. 2178–2190, 1966.

[51] A. F. Kleptsyn, V. S. Kozyakin, and M. Krasnosel'skii, "Effect of small synchronization errors on stability of complex systems-II." *Automation and Remote Control*, vol. 45, no. 3, pp. 309–314, 1984.

[52] V. S. Ritchey and G. F. Franklin, "A Stability Criterion for Asynchronous Multirate Linear Systems," *IEEE Transactions on Automatic Control*, vol. 34, no. 5, pp. 529–535, 1989.

[53] A. Bhaya and P. R. Medeiros, "On the stability of asynchronous multirate linear systems," in *36th IEEE Conference on Decision and Control*, vol. 3, no. December. IEEE, 1997, pp. 2041–2042.

[54] C. Lorand and P. H. Bauer, "Distributed discrete-time systems with synchronization errors: models and stability," *Circuits and Systems II: Express Briefs, IEEE Transactions on*, vol. 52, no. 4, pp. 208–212, 2005.

[55] S. P. Gordon, "On converses to the stability theorems for difference equations," *SIAM Journal on Control*, vol. 10, no. 1, pp. 76–81, 1972.

[56] W. M. Haddad and V. S. Chellaboina, *Nonlinear Dynamics and Control: A Lyapunov-based Approach*. Princeton University Press, 2008.

[57] S. H. Strogatz, *Nonlinear Dynamics and Chaos: With Applications To Physics, Biology, Chemistry, And Engineering*. Westview Press, 2001.

[58] D. G. Feingold and R. S. Varga, "Block Diagonally Dominant Matrices and Generalizations of the Gerscgorin Circle Theorem," *Pacific Journal of Mathematics*, vol. 12, no. 4, 1962.

[59] S. Elaydi, *An Introduction to Difference Equations*, 3rd ed. Springer, 2005.

[60] W. Minkina, "Non-linear models of temperature sensor dynamics," *Sensors and Actuators A: Physical*, vol. 30, pp. 209–214, 1992.

[61] R. G. Sanfelice and A. R. Teel, "On singular perturbations due to fast actuators in hybrid control systems," *Automatica*, vol. 47, no. 4, pp. 692–701, 2011.

[62] H. K. Khalil, *Nonlinear Systems*, 3rd ed. Prentice Hall, 2001.

[63] A. Awad, A. Narang-Siddarth, and R. Weisman, "The Method of Multiple Scales for Orbit Propagation with Atmospheric Drag," in *AIAA Guidance, Navigation, and Control (GNC) Conference*, San Diego, California, 2016.

[64] ——, "Method of Multiple Scales for Orbit Propagation with Nonconservative Forces," *Journal of Guidance, Control, and Dynamics*, vol. 40, no. 6, 2017.

[65] D. A. Vallado, *Fundamentals of Astrodynamics and Applications*, 4th ed. Microcosm Press, 2013.

[66] D. Brouwer and G.-I. Hori, "Theoretical Evaluation of Atmospheric Drag Effects in the Motion of an Artificial Satellite," *The Astronomical Journal*, vol. 66, no. 1290, pp. 193–225, 1961.

[67] F. Delhaise, "Analytical treatment of air drag and earth oblateness effects upon an artificial satellite," *Advances in Space Research*, vol. 14, no. 5, pp. 69–72, may 1994.

[68] R. Barrio and J. Palacian, "High-order averaging of eccentric artificial satellites perturbed by the Earth's potential and air-drag terms," *Proceedings of the Royal Society of London. Series A: Mathematical, Physical and Engineering Sciences*, vol. 459, pp. 1517–1534, 2003.

[69] F. Hoots, "A Short Efficient Analytical Satellite Theory," *Journal of guidance, control, and dynamics*, vol. 5, no. 2, pp. 194–199, 1982.

[70] L.-s. Li, "Perturbation Effects of Quadratic Drag on the Orbital Elements of a Satellite in a Central Force Field," *The Journal of the Astronautical Sciences*, vol. 58, no. 1, pp. 23–33, 2011.

[71] V. Martinusi, L. Dell'Elce, and G. Kerschen, "Analytic propagation of near-circular satellite orbits in the atmosphere of an oblate planet," *Celestial Mechanics and Dynamical Astronomy*, vol. 123, no. 1, 2015.

[72] D. Danielson, C. Sagovac, B. Neta, and L. Early, "Semianalytic satellite theory," 1995.

[73] J. Liu and R. Alford, "Semianalytic Theory for a Close-Earth Artificial Satellite," *Journal of Guidance and Control*, vol. 3, no. 4, pp. 304–311, 1980.

[74] R. T. O'Brien and J. Sang, "Semianalytic Satellite Theory Using the Method of Multiple Scales," in *AIAA/AAS Astrodynamics Specialist Conference and Exhibit*, no. August, 2004.

[75] H. Schaub and J. L. Junkins, *Analytical Mechanics of Space Systems*. AIAA, 2003.

[76] M. Farkas, *Periodic Motions*, ser. Applied mathematical sciences. Springer-Verlag, 1994, vol. 104.

[77] J. a. Sanders, F. Verhulst, and J. Murdock, *Averaging Methods in Nonlinear Dynamical Systems*. Springer, 2007.

[78] H. Engels, *Numerical quadrature and cubature*. Academic Press, 1980.

[79] J. R. Wertz, *Mission geometry: orbit and constellation design and management: spacecraft orbit and attitude systems*. Microcosm Press, 2001, vol. 1.

[80] P. R. Escobal, *Methods of Orbit Dertermination*. John Wiley & Sons, 1965.

[81] S. Dallas and I. Khan, "The singly averaged differential equations of satellite motion for e greater than or equal to 0 and less than 1," in *AIAA/AAS Astrodynamics Conference*, 1976.

[82] O. Montenbruck and E. Gill, *Satellite Orbits: Models, Methods and Applications*. Springer Science & Business Media, 2012.

[83] R. Olfati-Saber, J. A. Fax, and R. M. Murray, "Consensus and cooperation in networked multi-agent systems," *Proc. IEEE*, vol. 95, no. 1, pp. 215–233, 2007.

[84] H. G. Tanner, G. J. Pappas, and V. Kumar, "Leader-to-Formation Stability," *IEEE Transactions on Robotics and Automation*, vol. 20, no. 3, pp. 443–455, 2004.

[85] A. Jadbabaie, J. Lin, and A. S. Morse, "Coordination of groups of mobile autonomous agents using nearest neighbor rules," *IEEE Transactions on Automatic Control*, vol. 48, no. 6, pp. 988–1001, 2003.

[86] Y. Hatano and M. Mesbahi, "Agreement over random networks," *IEEE Transactions on Automatic Control*, vol. 50, no. 11, pp. 1867–1872, 2005.

[87] M. Mesbahi and M. Egerstedt, *Graph Theoretic Methods in Multiagent Networks*. Princeton University Press, 2010.

[88] A. Awad, A. Chapman, E. Schoof, A. Narang-Siddarth, and M. Mesbahi, "Time-scale Separation on Networks: Consensus, Tracking, and State-dependent Interactions," in *54th IEEE Conference on Decision and Control*, Osaka, Japan, 2015.

[89] ——, "Time-Scale Separation in Networks: State-Dependent Graphs and Consensus Tracking," *IEEE Transactions on Control of Network Systems (In Revision)*, 2017.

[90] Y. Kim and M. Mesbahi, "On maximizing the second smallest eigenvalue of a state-dependent graph Laplacian," *IEEE Transactions on Automatic Control*, vol. 51, no. 1, pp. 116–120, 2006.

[91] M. Mesbahi, "On state-dependent dynamic graphs and their controllability properties," *IEEE Transactions on Automatic Control*, vol. 50, pp. 387–392, 2005.

[92] S. Motsch and E. Tadmor, "Heterophilious dynamics enhances consensus," *SIAM Review*, vol. 56, no. 4, pp. 577–621, 2014.

[93] N. Michael, M. M. Zavlanos, V. Kumar, and G. J. Pappas, "Distributed Multi-Robot Task Assignment and Formation Control," *IEEE International Conference on Robotics and Automation*, vol. 1, pp. 128–133, 2008.

[94] E. Schoof, A. Chapman, and M. Mesbahi, "Bearing-compass formation control: A human-swarm interaction perspective," in *American Control Conference*, 2014, pp. 3881–3886.

[95] S.-J. Chung, U. Ahsun, and J.-J. E. Slotine, "Application of Synchronization to Formation Flying Spacecraft: Lagrangian Approach," *Journal of Guidance, Control, and Dynamics*, vol. 32, no. 2, pp. 512–426, 2009.

[96] Z. Li, W. Ren, X. Liu, and M. Fu, "Consensus of multi-agent systems with general linear and lipschitz nonlinear dynamics using distributed adaptive protocols," *IEEE Transactions on Automatic Control*, vol. 58, no. 7, pp. 1786–1791, 2013.

[97] M. Egerstedt and X. Hu, "Formation constrained multi-agent control," *IEEE Transactions on Robotics and Automation*, vol. 17, no. 6, pp. 3961–3966, 2001.

[98] S. Mastellone, D. M. Stipanovic, and M. W. Spong, "Multi-agent formation control and trajectory tracking via singular perturbation," in *16th IEEE International Conference on Control Applications*, 2007.

[99] J. H. Chow and J. R. Winkelman, "Singular perturbation analysis of large-scale power systems," *International Journal of Electrical Power and Energy Systems*, vol. 12, no. 2, pp. 117–126, 1990.

[100] D. Romeres, F. Dorfler, and F. Bullo, "Novel Results on Slow Coherency in Consensus and Power Networks," in *2013 European Control Conference*, 2013.

[101] E. Bıyık and M. Arcak, "Area aggregation and time-scale modeling for sparse nonlinear networks," *Systems and Control Letters*, vol. 57, no. 2, pp. 142–149, 2008.

[102] S. Roy, Y. Wan, and A. Saberi, "On time-scale designs for networks," *International Journal of Control*, vol. 82, no. 7, pp. 1313–1325, jul 2009.

[103] J. B. Rejeb, I.-C. Morarescu, and J. Daafouz, "Synchronization in networks of linear singularly perturbed systems," in *American Control Conference (ACC)*, 2016.

[104] R. Hegselmann and U. Krause, "Opinion dynamics and bounded confidence," *Simulation*, vol. 5, no. 3, pp. 1–33, 2002.

[105] F. A. Rodrigues, T. K. D. Peron, P. Ji, and J. Kurths, "The Kuramoto model in complex networks," *Phys. Rep.*, vol. 610, pp. 1–98, 2016.

[106] M. Ji and M. Egerstedt, "Distributed coordination control of multiagent systems while preserving connectedness," *IEEE Transactions on Robotics*, vol. 23, no. 4, pp. 693–703, 2007.

[107] M. Aicardi, G. Casalino, A. Bicchi, and A. Balestrino, "Closed Loop Steering of Unicycle-like Vehicles via Lyapunov Techniques," *IEEE Robotics & Automation Magazine*, pp. 27–35, 1995.

[108] A. I. Zečević and D. D. Šiljak, "Control design with arbitrary information structure constraints," *Automatica*, vol. 44, no. 10, 2008.

[109] A. Sghaier Tlili, "Linear Matrix Inequality Robust Tracking Control Conditions for Nonlinear Disturbed Interconnected Systems," *Journal of Dynamic Systems, Measurement, and Control*, vol. 139, no. 6, 2017.

[110] W. M. Haddad, V. S. Chellaboina, and S. G. Nersesov, *Impulsive and Hybrid Dynamical Systems : Stability, Dissipativity, and Control*. Princeton University Press, 2014.